Reactions on Mineral Dust

Courtney R. Usher,[†,‡] Amy E. Michel,[‡] and Vicki H. Grassian*[,†,‡,§]

Department of Chemistry, Department of Chemical and Biochemical Engineering, and Center for Global and Regional Environmental Research, University of Iowa, Iowa City, Iowa 52242

Received May 7, 2003

Contents

* Author to whom correspondence should be addressed [telephone (319) 335-1392; fax (319) 353-1115; e-mail vicki-grassian@uiowa.edu].
† Department of Chemistry.
‡ Center for Global and Regional Environmental Research.
§ Department of Chemical and Biochemical Engineering.

1. Introduction

In recent years, there has been a great deal of interest in the heterogeneous chemistry of trace atmospheric gases on aqueous and solid-phase particles present in the troposphere (see reviews 1−11). An understanding of these reactions is critical as they affect a multitude of atmospheric processes. For example, particulates can alter the chemical balance of the atmosphere by providing a reactive substrate or medium on and in which reactions can occur. The thermodynamic and optical properties of atmospheric particles may also be altered as their chemical composition changes during these reactions. In turn, climate forcing by atmospheric particles through absorption and scattering of solar radiation will depend on its chemical history. Climate forcing by particulates is currently recognized as one of the greatest uncertainties in global climate models.[12−14] Although there are a variety of particulates present in the atmosphere, this review will focus on mineral dust and its role in altering atmospheric processes. To better understand the heterogeneous reactions that can occur, some aspects of the physical and chemical properties of mineral dust, known transport processes, environmental implications, and the first atmospheric chemistry models that included heterogeneous reactions are summarized in this introductory section.

10.1021/cr020657y CCC: $44.00
Published on Web 11/12/2003

Courtney R. Usher was born in 1976 and has lived most of her life in Iowa City, IA. She received her B.S. degree in chemistry from the University of Northern Iowa in 1998. For graduate school, she returned to her hometown, studying heterogeneous reactions of mineral dust particles with sulfur dioxide and ozone at the University of Iowa. She completed her Ph.D. in 2003 under the supervision of Prof. Vicki H. Grassian and is currently carrying out postdoctoral research in the laboratory of Prof. Daniel Strongin at Temple University in Philadelphia.

Amy E. Michel received her B.S. degree in chemistry from Ursinus College in 1996 and her Ph.D. from the University of Colorado in 2001 under the direction of Prof. John W. Birks and Prof. Kathy L. Rowlen. Her doctoral research focused on atomic force microscopy investigations of carbonaceous materials. After her graduate studies, she worked as a postdoctoral researcher in Prof. Vicki H. Grassian's laboratory at the University of Iowa, where she examined ozone reactions on mineral dust. Currently, she is an Assistant Professor of Chemistry at the University of Puget Sound in Tacoma, WA.

Vicki H. Grassian received her B.S. degree in chemistry from the State University of New York at Albany. From there, she did her graduate studies at Rensealaer Polytechnic Institute (M.S., 1982) and the University of California—Berkeley (Ph.D., 1987). At Berkeley, she was advised by Prof. Earl Muetterties and Prof. George Pimentel. Following her Ph.D., she was a postdoctoral scientist at Colorado State University (1988) and a research associate at the University of California—Berkeley (1989). In 1990, she went to the University of Iowa as an Assistant Professor. Prof. Grassian is currently a full professor of chemistry and holds a joint appointment in the Department of Chemical and Biochemical Engineering. At the University of Iowa, she has received a faculty-scholar award and a distinguished achievement award. Her research interests are in the areas of heterogeneous atmospheric chemistry, environmental remediation, catalysis, and environmental molecular surface science. In 2003, she received a special two-year creativity extension from the National Science Foundation in support of her research.

1.1. Background

Historically, most attention within the scientific community and popular press has been given to pollutant anthropogenic particles due to their direct impact on visibility, respiratory distress, and climate effects. However, formation of anthropogenic particles is a relatively new feature of Earth's ecosystem as these particles have been an issue only since the industrial revolution. In contrast, mineral aerosol particles have been around for a much longer period of time, which is confirmed with the presence of mineral dust in ice core samples (see Kohlfeld and Harrison[15] and references therein). It has not been until the past 30 years that the role of mineral aerosol in the atmosphere and climate change has received any attention from the scientific community. It is our intent to review the present understanding of heterogeneous reactions on mineral dust in the troposphere. This review mainly addresses mineral dust from deserts or semiarid areas as these regions are the most important dust sources on a global scale. Volcanic dust represents another source of mineral-containing particles. Road dust and dust from industrial and agricultural processes are also important in determining chemistry on a local scale, especially in the polluted troposphere.

For more detailed information concerning the properties, transport, and environmental impact of mineral dust, the reader is directed to several sources in a multitude of books, articles, and reviews that specifically focus on these individual aspects of mineral dust. Pye offers a comprehensive treatise on the physical properties of aeolian dust, transport and deposition mechanisms, and environmental effects, in particular, terrestrial and oceanic deposition.[16] Goudie and Middleton review research pertaining to Saharan dust storms and their impact on the environment.[17] In several articles and reviews, Prospero describes the transport of North African dust and the effects of oceanic deposition.[18−21] Duce examines the research on the sources, mass, and number particle size distributions, transport, and deposition of mineral aerosol.[22] Reviews explaining the potential climatic effects of atmospheric aerosols include articles by Andreae,[23] Duce,[22] Buseck and Posfai,[24] Buseck et al.,[25] and Haywood and Boucher.[12]

1.2. Mineral Dust Properties

1.2.1. Composition

Mineral aerosols are soil particles that have been mobilized by strong wind currents and entrained into

Table 1. Abundance of Major Elements in the Upper Continental Crust and Major Elements as Oxides in the Continental Crust (Based on Data Reported by Wedepohl[26])

element	%	oxide	%
Si	30.348	SiO_2	61.5
Al	7.744	Al_2O_3	15.1
Fe	3.089	Fe_2O_3	6.28
Ca	2.945	CaO	5.5
Na	2.567	Na_2O	3.2
Mg	1.351	MgO	3.7
K	2.865	K_2O	2.4
Ti	0.3117	TiO_2	0.68
Ba	0.0668	BaO	0.0584
Mn	0.0527	MnO	0.1

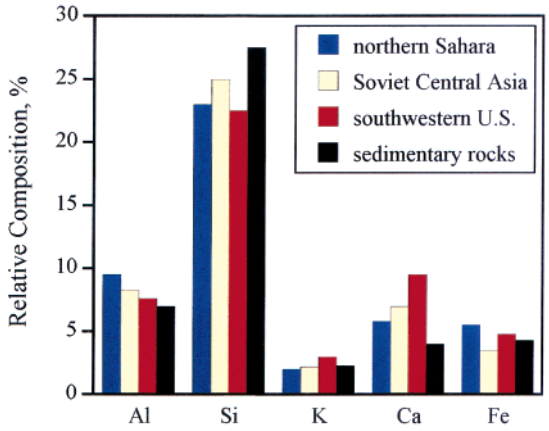

Figure 1. Relative elemental concentrations of major constituents in mineral aerosol from various source locations. (Reprinted with permission from *Atmospheric Environment, 27A*, pp 2539−2544; L. Gomes and D. A. Gilette, A comparison of characteristics of aerosol from dust storms in central Asia with soil-derived dust from other regions. Copyright 1993 Elsevier.)

the atmosphere. Because these particles are eroded soils, their chemical composition is similar, if not identical, to that of crustal rock.[17] The abundance of the major elements and oxides found in the continental crust is displayed in Table 1.[26] The Earth's crust is dominated by silicon and aluminum oxides. Multiple studies (see review by Goudie and Middleton[17] and references therein) on the elemental content of windblown dust originating from various locations around the world report that mineral dust is approximately 60% SiO_2 and 10−15% Al_2O_3. The percentages of other oxides, such as Fe_2O_3, MgO, and CaO, are slightly more varied and dependent on source location. As is seen in Figure 1, airborne mineral dust that has been collected around the globe has fairly small variations in elemental content.

Despite the similar chemical compositions of various dusts, the mineralogy of dust particles can be quite varied. Common minerals found in aerosolized dust include quartz, feldspars, micas, chlorite, kaolinite, illite, smectite, palygorskite, calcite, dolomite, gypsum, halite, opal, and mixed-layer clays.[16] See Table 2 for the general formulas of these minerals found in airborne dust.[27,28] Although halite (or NaCl) and other salts derived from the sea are technically minerals from a geological viewpoint, they will not be addressed in this review as the focus here will be on rock-forming minerals.

Table 2. Chemical Formulas for Common Clays and Minerals in Dust[a]

mineral	formula
calcite	$CaCO_3$
chlorite	$A_{5-6}Z_4O_{10}(OH)_8$[b]
corundum	α-Al_2O_3
dolomite	$CaMg(CO_3)_2$
feldspars	WZ_4O_8[c]
gypsum	$CaSO_4 \cdot 2H_2O$
halite	NaCl
hematite	α-Fe_2O_3
illite	$(K,H_3O)(Al,Mg,Fe)_2(Si,Al)_4O_{10}[(OH)_2,H_2O]$
kaolinite	$Al_4Si_4O_{10}(OH)_8$
magnesite	$MgCO_3$
montmorillonite (smectite)	$(Na,Ca)_{0.33}(Al,Mg)_2Si_4O_{10}(OH)_2 \cdot nH_2O$
mica	$W(X,Y)_{2-3}Z_4O_{10}(OH,F)_2$[d]
opal	$SiO_2 \cdot nH_2O$
palygorskite	$(Mg,Al)_2Si_4O_{10}(OH) \cdot 4H_2O$[e]
quartz	SiO_2

[a] From refs 27 and 28. [b] Typically A = Al, Fe, Li, Mg, Mn, and/or Ni; Z = Al, B, Si, and/or Fe. [c] Typically W = Na, K, Ca, and/or Ba; Z = Si and/or Al. [d] Typically W = K or Na; X and Y = Al, Mg, Fe^{2+}, Fe^{3+}, and Li; Z = Si and Al. [e] From ref 28.

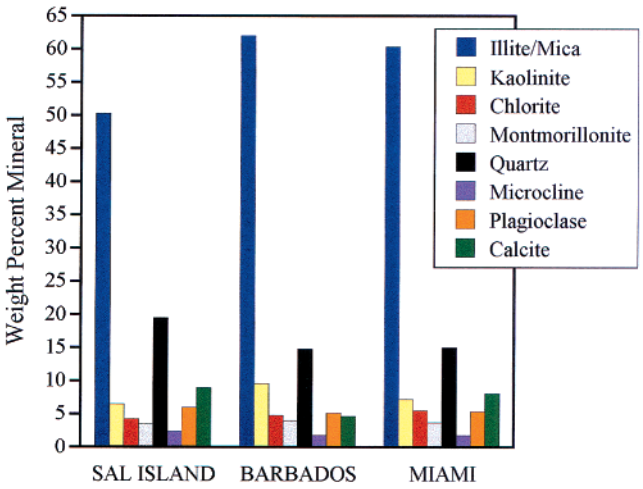

Figure 2. Mineralogical composition of North African dust transported to the Cape Verde Islands, Barbados, and Miami, FL. (Reprinted with permission from *Marine Geology, 37*, pp 295−321; R. A. Glaccum and J. M. Prospero, Saharan aerosols over the tropical North Atlantic—mineralogy. Copyright 1980 Elsevier.)

Quartz is often found in mineral dust distributions around the world as a result of the large abundance of SiO_2 in continental rock. Within a given size distribution of transported aerosol, the larger, coarser particles are typically composed of quartz, feldspars, and carbonates, and the smaller, finer particles are often clays or micas. As the dust is transported farther away from a source region, the overall composition tends to become enriched with clays as the larger quartz particles fall out of the atmosphere via gravitational settling. To demonstrate the preferential settling of quartz compared to clays, Figure 2 shows the relative mineral composition of aerosol transported from North Africa and collected in Sal Island in the Cape Verde Islands, Barbados, and Miami, FL.[29] The Sal Island sample had a greater relative percentage of quartz compared to the Barbados and Miami samples collected over 3800 and 5900 km away, respectively. Moreover, the illite and

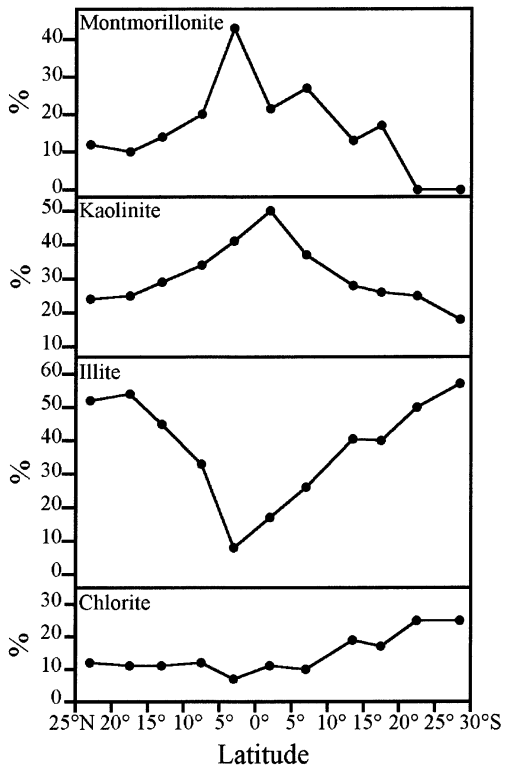

Figure 3. Regional differences in mineralogy dependent on latitude. (Reprinted with permission from *Marine Geology*, *13*, pp 91−106; R. Chester, H. Elderfield, J. J. Griffin, L. R. Johnson, and R. C. Padgham, Eolian dust along the eastern margins of the Atlantic Ocean. Copyright 1972 Elsevier.)

kaolinite clay contents became enriched as the dusts traveled a greater distance. Although not as common, there are reports of extremely large silica particles (>75 μm) having been found over 10000 km from their source, which is unexplainable with current transport mechanisms but is thought to be the result of multiple high-powered currents that provided lift to the large particles throughout their transport.[30]

In addition to having a size dependence, the relative mineralogy of these aerosols is also dependent on source region. Mineral aerosols originating from North Africa have a slightly different elemental content from Asian dust and, therefore, different mineral contents and properties. For instance, Asian dusts tend to be grayish in color, whereas dusts from African regions have more brown, yellow, and red tones, which is due in large part to the higher iron (hematite) content in African soils[31] (also apparent in Figure 1). Furthermore, even the mineral content of dust originating within the Saharan Desert varies regionally, and differences are observed whether a plume came from the northern, western, central, or southern region of the desert.[32] Investigations report that dust from the northern Sahara is abundant in illite,[33,34] as well as carbonates, chlorite, palygorskite, and montmorillonite,[35] whereas the southern Sahara and Sahel regions contain more kaolinite[33−35] and hematite.[36] Regional variations in mineralogy as a function of latitude within North Africa are demonstrated in Figure 3. Understanding the variations in regional mineral content will help to provide insight into the chemical reactivity of these particles in the atmosphere.

1.2.2. Chemical Tracers

The variations in mineralogy help researchers identify mineral aerosol from other aerosols and to trace the source area of airborne dusts detected in locations far from the source (see Schütz[37] and references therein). Often elemental enrichment factors are calculated in which the composition of various elements within an ambient aerosol sample is compared to the abundance of a reference element found in mineral aerosol.[37−41] Because this is a relative comparison, it is important that a reference element is chosen which is present in both the sample and reference aerosol (often the composition of crustal rock is used as a reference), has little contribution from pollution sources, and can easily be sampled and analyzed.[41]

One element that is commonly used to identify mineral aerosol from an aerosol population is aluminum.[41−44] Particulate aluminum is most often due to aluminosilicate minerals originating from crustal material. Additionally, the Si/Al ratio will change depending on the mineral. For example, crustal rock has a Si/Al ratio between 3.41 and 4.02, whereas the ratio for clays ranges from 1.04 for kaolinite to 2.07 for smectite.[16] Iron content is sometimes used as a tracer for dust,[41,44] as is calcium.[43,45] The elemental content of mineral dust is typically measured though bulk analysis by X-ray fluorescence (XRF) or proton-induced X-ray emission (PIXE) methods; however, aerosol time-of-flight mass spectrometry (ATOFMS)[46] and electron microscopy,[24,25] both transmission (TEM) and scanning (SEM) methods, have also been used to characterize individual dust particles.

The clay signature of mineral aerosol may also identify where airborne dust originated. As explained previously, different regions contain different mineral contents. Caquineau et al. explain that clays may be utilized as tracers in one of two ways.[34] First, an aerosol distribution may be examined for a specific mineral. For example, soils in the northern Saharan Desert are commonly enriched with palygorskite (see references in Pye,[16] Molinaroli,[32] and Goudie and Middleton[17]), so detection of this mineral increases the probability that it came from a northern region. The other method relies on evaluating the ratio of various clays in order to determine fractionation patterns. As previously mentioned, the mineralogical content in the Saharan Desert varies with latitude, so evaluation of the ratio of illite to kaolinite can provide insight into the regional source.[34] Dust samples have also been traced by the kaolinite-to-chlorite ratio.[32,47]

Finally, naturally occurring isotopes have been used as markers to identify the source region of transported mineral dust. Researchers have used isotopic concentrations of neodymium and strontium to evaluate mineral particles trapped in ice cores,[15,48,49] snow deposits,[47] deep-sea sediments,[15,50,51] and deposited soils.[15,52−54] The natural isotopic concentration of oxygen (see references in Pye[16]) has also been used to evaluate aeolian dusts deposited into soils,[52,55] oceans, and ice cores.[56]

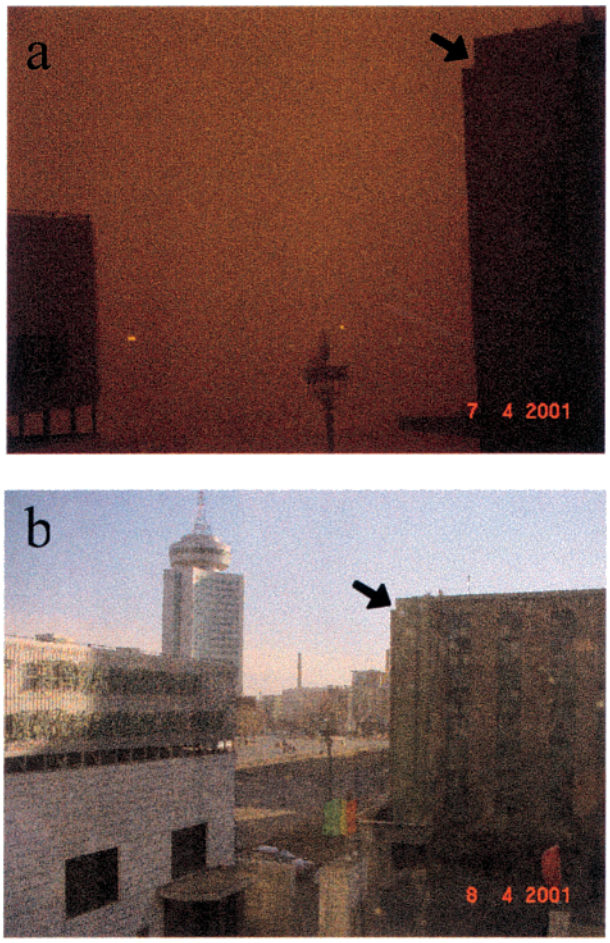

Figure 4. Photographs of the streets of Baichen, China, (a) during a dust storm on April 7, 2001, and (b) after the storm on April 8. An arrow was superimposed on both pictures as a point of reference. (Photographs were taken by and are courtesy of Zev Levin.)

1.2.3. Dust Events, Entrainment, and Transport

Dust events predominantly originate in arid or semiarid environments, which account for ~33% of the total world land area.[22] In fact, the northern hemisphere generates ~90% of the global airborne mineral dust, where it is also deposited.[22] Most frequent "dust storm" occurrences are in the region starting on the west coast of North Africa and extending through the Middle East into Central Asia. These events can be quite large and often greatly reduce visibility. Figure 4 displays two photographs that demonstrate a tremendous reduction in visibility during and after an extremely large dust storm that swept through Baichen, China, in April 2001.

One of the most prominent features of these mineral dust events is the long-distance global transport of dust storms originating from these regions. This extensive transport often occurs in horizontally layered plumes and can persist for days to a week over thousands of kilometers. The transatlantic transport of Saharan dust to North America has been a well-studied phenomenon (see reviews[18,20,22] and recent articles[21,44,57]). Additionally, Saharan dust has been transported in extreme westerly, northerly, and easterly directions and detected in South America,[43,58−60] northern Europe,[61,62] and the Middle East,[63−65] respectively. Meanwhile, Asian dust has been transported eastward to continental North America[66−71] and Hawaii.[54,72−78]

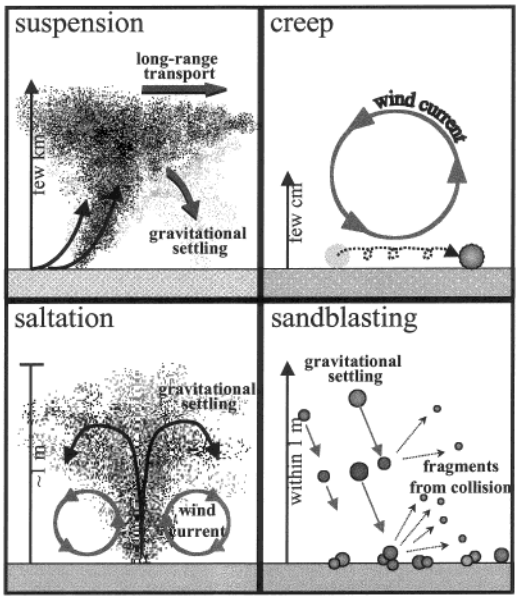

Figure 5. Schematic representation of the possible wind-induced entrainment processes to move, emit, and transport mineral dust particles from the source into the troposphere.

The flux of mineral dust into the troposphere varies greatly with location and season, and it is estimated that on average 1000−3000 Tg of mineral aerosol are emitted into the atmosphere annually,[13,23,79] with the Saharan Desert being the largest global contributor. Human activities, such as improper agricultural and grazing practices, can account for 20−50% of the atmospheric dust loading[80,81] and have resulted in expanding desertification of land.[82,83] The frequency and intensity of dust events, and ultimately the mineral aerosol loading in the atmosphere, are expected to continue to increase as long as the improper land-use practices are driven by economic, social, and political circumstances. By the year 2100, mineral aerosol production is anticipated to increase by 10% from its current level.[13]

Various factors determine whether soil particles can be aerosolized and include wind velocity, physical properties of the soil (e.g., particle size distribution, soil moisture, and particle cohesiveness), and surface conditions of the terrain (e.g., surface roughness and vegetation coverage). Combinations of these factors can cause soil particles to be moved by wind through one of three mechanisms:[16] (1) "suspension", or the upward transport of the particles through turbulent wind currents; (2) "saltation", or bouncing, whereby particles are vertically suspended up to a height of ~1 m and then settle to the surface due to the gravitational drag forces exceeding particle mass; or (3) "creep", which is the rolling or sliding of particles along the surface. These processes are represented schematically in Figure 5. The first two processes are the dominant processes in aerosolizing mineral dust and transporting the particles over considerable distances from the source. An additional aerosolization process that is important to consider is "sand-

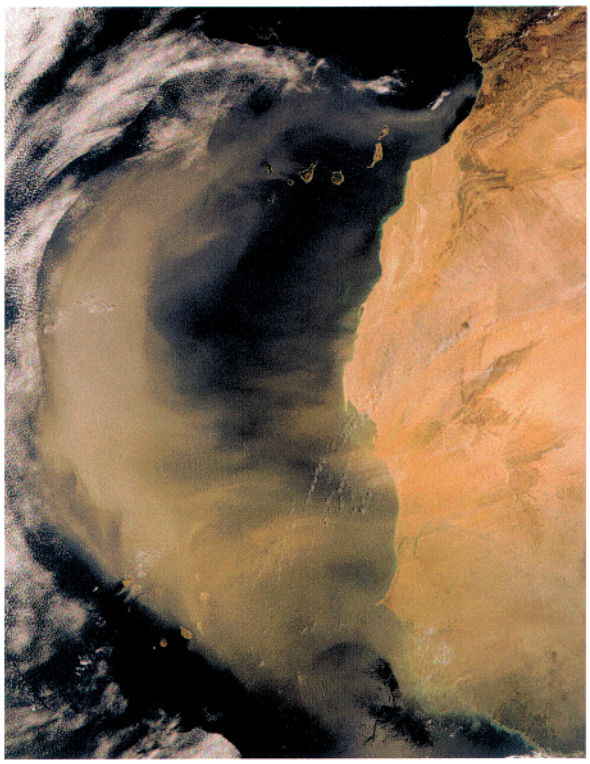

Figure 6. Massive dust storm, extending over 1600 km from the Canary Islands (top center) to the Cape Verde Islands (lower left), transported off the northwestern coast of Africa (right) on March 2, 2003, and detected with the Moderate Resolution Imaging Spectroradiometer (MODIS) on the Terra satellite. [Reprinted with permission from Visible Earth (http://visibleearth.nasa.gov). Copyright 2003 NASA/Goddard Spaceflight Center.[98]]

blasting",[84,85] which occurs when fine particles are released from an aggregate and/or the ground as a result of being impacted by larger aerosol particles settling out of the atmosphere (see Figure 5). The sandblasting process explains why submicrometer clay particles that exist only as aggregates in soil due to their strong cohesive forces are observed in a free state in the atmosphere. The specific transport process that a particle experiences is dependent on grain size, as creep typically occurs for particles >500 μm,[16] saltation for particles 70−500 μm,[16] suspension for particles <70 μm,[16,86] and sandblasting for particles 0.1−10 μm.[85] For further discussion about particle size and size distributions, the reader is referred to the next section (section 1.2.4).

Ground-based aerosol detectors have been used for years to observe and measure transoceanic mineral dust transport; however, these sites tend to be few in number and scattered throughout specific regions. The magnitude and global coverage of individual dust storms were not fully realized until satellite imaging provided a means to visualize these events. With remote sensing instruments and satellites, including AVHRR (Advanced Very High-Resolution Radiometer),[87−91] Meteosat,[91−94] and SeaWiFS (Sea-Viewing Wide Field-of-View Sensor),[67,95−97] researchers have been able to observe plumes of smoke, desert dust, and volcanic ash over oceans. For example, the MODIS (Moderate Resolution Imaging Spectroradiometer) image in Figure 6 demonstrates the immensity of one dust storm as it was being transported

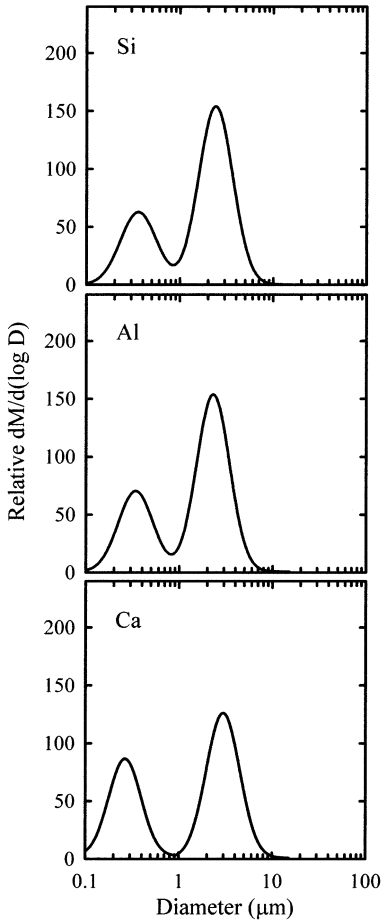

Figure 7. Observation of Si, Al, and Ca content in accumulation and coarse modes found in a typical mass size distribution of Saharan dust under high aerosol loading. The plotted lines represent log-normal fits to bimodal distributions. The raw data showing the particle mass loadings collected on the various stages of a cascade impactor were removed from the original figure for clarity. (Adapted with permission from *J. Geophys. Res. 95*, D9, pp 13927−13935; L. Gomes, G. Bergametti, G. Coudé-Gaussen, and P. Rognon, Submicron Desert Dusts: A Sandblasting Process. Copyright 1990 American Geophysical Union.)

from northwestern Africa.[98] In particular, the satellite Total Ozone Mapping Spectrometer (TOMS) has been extremely useful in providing images of dust over both oceanic and continental surfaces,[65,95,97,99−101] although currently only semiquantitative information is derived with this instrument.

1.2.4. Size Distribution

The total aerosol found in the atmosphere is typically described as having a trimodal size distribution and includes the nuclei mode, the accumulation mode, and the coarse mode. The nuclei and accumulation modes are composed of fine particles in the size ranges of 0.005−0.1 and 0.1−2.5 μm, respectively. Coarse particles are characterized as having diameters >2.5 μm. The total mass of anthropogenic and natural aerosol in the atmosphere is dominated by the coarse mode particles, whereas the accumulation mode contributes the most to the total particulate surface area in the atmosphere.[102] Figure 7 shows the presence of both the accumulation and

coarse modes in a Saharan dust sample collected on a cascade impactor during the dusty season.[84] By and large, mineral dust is typically considered as having a coarse mode type of distribution because it contributes considerably to the total mass of global aerosols; mineral dusts account for ~50% of the aerosol mass loading.[22,23] However, because a significant number of dust particles are found in the accumulation mode, they provide an important source of particulate surface area. It is these particles that may greatly affect the atmospheric processes by providing the means for heterogeneous reactions to occur.

The physical properties of minerals and the erosion conditions dictate the size of the particles that can be entrained into the atmosphere. This is important because as stated previously, the chemical composition and transport properties of mineral dust are dependent on the size distribution of the particles. Therefore, as dust is transported and larger particles settle, there is a relative shift in the size distribution toward the accumulation mode becoming increasingly important and an increase in the relative percentage of clay mineral content in the dust plume compared to the original soil particles and initial plume.

For all of the reasons just described, the size distributions of mineral aerosol are difficult to determine and characterize for large aerosol events. The size distribution of a given event is constantly changing as gravitational settling occurs with increased transport and lifetime. Additionally, the size distribution is dependent on the mineralogy of the source location and the extent of the particle erosion prior to entrainment into the atmosphere. In particular, the morphology of soil particles can change with increasing wind erosion.[32,103] Minerals, such as palygorskite, that are commonly found as fibrous structures in bulk soil may become rounded with repeated erosion processes,[32,103] whereas dolomite grains tend to show weathering voids and calcite grains tend to be fairly resistant to dry weathering processes.[32] Ultimately, erosion processes may change the particle size distribution from one dust event to another, both originating from the same source region, due to the amount of weathering prior to being emitted into the atmosphere.

With size distribution and chemical distribution being constantly evolving processes, wind-tunnel experiments[85,104] and computer modeling are often used to help estimate the particle size distribution within dust events.[86,105−107] Mass size distributions are best described as log-normal functions.[85,105] By inputting various aerosol properties and meteorological parameters and by comparing the computer model to remote sensing and ground-based measurements, it is hoped that a method will be established to predict the impact future dust events would have on humans, the environment, and climate.

1.3. Impacts on Global Processes

The combination of the large flux of mineral dust into the troposphere with a given dust event and the long-range global transport of these particles indicates that mineral dust will interact with many atmospheric, terrestrial, and oceanic systems. Figure 8 provides a pictorial schematic of the potential global impact that mineral dust may have on these systems, which are discussed in more detail in the following paragraphs.

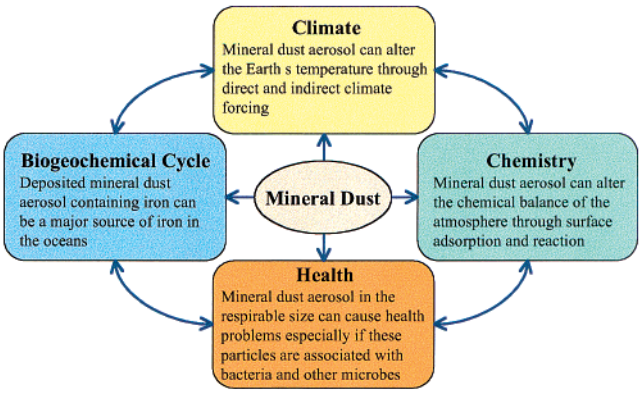

Figure 8. Impact of mineral dust on global atmospheric processes.

1.3.1. Chemistry

Later sections in this review will focus in depth on the various heterogeneous reactions on mineral dust or mineral dust proxies that have been studied by field measurements, in laboratory investigations, and with atmospheric models. The importance and relevance of each of these reactions in atmospheric chemistry will be stressed. In general, mineral dust aerosol may provide a surface with reactive sites on which reactions could occur in the troposphere. As a result, these particles may act as sinks for various atmospheric chemical species as well as sources of others.

Heterogeneous reactions that take place on mineral dust in the troposphere may provide the missing link for some reaction schemes that cannot be explained solely with gas-phase reactions.[108−111] Reactions on surfaces may provide additional pathways, which may explain the discrepancies between the field and laboratory measurements. The high loading of mineral aerosol into the troposphere during dust events may provide an important surface for these reactions.

Weathering or aging processes, such as exposure to reactive inorganic or organic chemical species or exposure to varying amounts of water vapor in the atmosphere, may influence the chemical nature of mineral dust. A mineral dust particle may have a coating of a chemical species due to the transport of that particle through an atmospheric region containing that species. For instance, Levin et al. observed sulfate coatings on desert dust believed to be a result of evaporating cloud droplets.[112] Consequently, the outermost layer of a dust surface may be different from the mineralogy of the original dust. The reactivity of these altered or coated mineral dust surfaces may enhance or prevent the reactivity of trace gases with dust particles.

1.3.2. Climate

Like atmospheric aerosols in general, mineral aerosol may affect local and global climate through the absorption and scattering of solar radia-

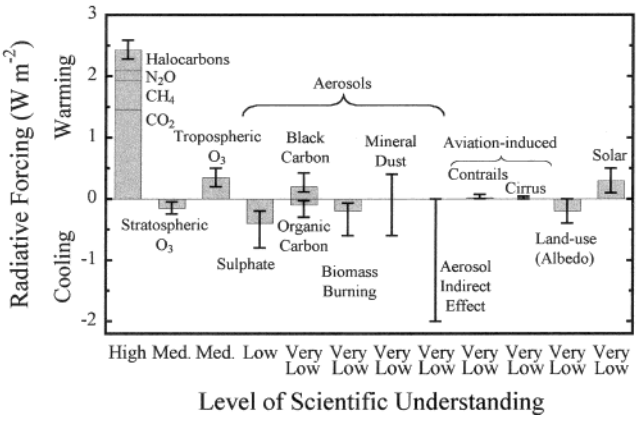

Figure 9. IPCC estimates of the global and annual mean radiative forcing of various chemical species in the atmosphere. (Reproduced with permission from IPCC. Copyright 2001 Intergovernmental Panel on Climate Change.)

tion.[14,81,113−117] When aerosol particles absorb and scatter radiation themselves, the resulting radiative forcing is deemed to be "direct", whereas if the particles influence the optical properties of clouds, then the radiative forcing is "indirect." Positive radiative forcing values, measured in W m^{-2}, result in a warming effect on Earth's surface, and conversely, negative forcing has a cooling effect.

Currently, researchers have a "very low level of scientific understanding" about the effect that mineral aerosol particles have on the radiative budget of the atmosphere, according to the latest report by the Intergovernmental Panel on Climate Change (IPCC), which estimates the net radiative forcing by mineral aerosol to range from −0.60 to +0.40 W m^{-2} (see Figure 9).[13] The radiative impact of mineral dust in the atmosphere is quite unclear due to the incomplete understanding concerning the diverse nature, the transport and removal processes, and the chemical and physical properties of the particles.[14] Specifically, a large part of this uncertainty is due to the fact that dust particles are capable of modifying both the incoming solar short-wave radiation and the outgoing long-range radiation. The submicrometer dust particles are efficient absorbers of solar radiation, thereby having a cooling effect. Moreover, variations in the mineralogy of the source soil can affect the absorption properties of airborne dust, as Asian soils and aerosols can be grayish in color, whereas soils and aerosols from African regions can range from light brown to bright red.[31] Mineral dust containing iron oxides, typically hematite, absorb visible radiation providing a red coloration of the particles; therefore, prediction of the radiative forcing due to mineral dust is highly dependent on the amount of iron oxide enrichment in the aerosol.[31,36,118] On the other hand, mineral dust particles, especially those containing silicates, can also absorb the infrared radiation emitted toward space, having a warming effect on the atmosphere, as well as scatter the incoming radiation, resulting in a cooling effect. It is the balance between all of these absorption and scattering processes that determines the overall effect that will occur. Ultimately, the optical properties of dust depend on the particle size distribution in a given event,[119] the chemical composition of the particles,[31,36,120,121] and the altitude and optical depth of nearby clouds.[122]

Additionally, weathering or aging processes, discussed under section 1.3.1, may alter the optical properties of original mineral dust particles. Dust plumes passing through clouds will change in their particle size distribution, as well as optical properties, due to water layers condensing on the individual particles. Water layers also change the chemical nature of the aerosol. Finally, various chemical species, which adsorb to mineral dust particles and form coatings, change the chemical character of the particles and, ultimately, may change the net radiative forcing. Specifically, mineral dust particles coated with sulfate species can promote their ability to act as cloud condensation[112,123,124] and ice nuclei,[125,126] which in itself will affect the optical properties, but additionally sulfate aerosols are known to effectively scatter radiation, producing a cooling effect.[127]

1.3.3. Health

Airborne mineral dust can have numerous repercussions on human health, the most notable and dangerous being the effects of inhaled particles on the human respiratory system.[128] Several reviews detailing lung diseases that can result from exposure to mineral dusts discuss the changes in the respiratory system that occur with exposure to bioreactive dusts and the importance of the particle size and morphology, the durability of the particles, and surface chemistry that takes place during exposure.[128−130] Small, thin, fibrous minerals such as palygorskite can become lodged in lung tissue due to their needle-like morphology,[131] and a study on the relationship of pulmonary health problems to mineral dusts done in Turkey showed that continuous exposure to doses of mineral fibers and silica particles may be the cause of a number of benign pulmonary disorders.[132] The collapse of the World Trade Center (WTC) towers in New York City on September 11, 2001, released aerosols containing a wide range of mineral components, and respiratory complaints were reported by not only the workers and volunteers at or near the WTC site but later by residents downwind of the site.[133] Additionally, long exposures to quartz particles could lead to silicosis. However, despite the respiratory conditions that can be induced, typical inhalation of mineral dust experienced by humans rarely leads directly to death.[131]

In 1997, the U.S. Environmental Protection Agency established the "PM (Particulate Matter) 2.5" standard,[134] which recognized the importance of aerosols that have diameters of ≤2.5 μm in causing health problems. Long exposures to or large doses of particles below this size can cause respiratory damage because they penetrate deep into the alveoli of the human lungs, produce scarring, and potentially lead to conditions such as emphysema. Because a significant fraction of the mineral dust size distribution contains particles below 2.5 μm in diameter, the welfare of humans who inhabit regions that have frequent incidences of dust storms should be considered.

In addition to the above, mineral aerosol can have other health effects. These aerosol particles may

provide surfaces whereby other hazardous chemical species can be produced through reaction. They may also act as carriers of organisms that can cause infectious diseases or pollens that can induce allergic responses. Negative responses can be provoked through the inhalation, ingestion, or contact with these other species or chemicals associated with airborne mineral dust.

1.3.4. Biogeochemical Cycles

In addition to the direct and indirect effects mineral dust has on atmospheric processes and climate, airborne soil particulates may have significant effects on biogeochemical cycles through the global transport, deposition, and accretion of these particles. Soils that entrain the deposited airborne particles may become enriched in nutrients that otherwise are not present in native soils. Investigations include extensive work by Prospero and colleagues on the transoceanic transport and deposition of African dust in the southeastern United States (for examples, see refs 20, 21, 44, and 135 and references therein) and the islands in the Atlantic Ocean.[136] Other examples include the deposition and accumulation of quartz-containing Asian dust in the Hawaiian Islands, which contain little quartz.[54]

The effects of mineral dust deposition into ocean waters have become a topic of interest in recent years (see reviews 18 and 19). It has been estimated that annually 360−500 Tg of mineral dust is deposited into the oceans,[18,22] with ∼50% of the total deposition occurring in the North Atlantic Ocean.[18] Specifically, wind-transported mineral dust may play a large role in supplying soluble iron to the oceans,[137−139] providing micronutrients to biological species,[140] such as phytoplankton,[141] and ultimately influencing the iron budget of the upper ocean.[142] Walsh and Steidinger correlated the formation of red tides in the eastern Gulf of Mexico, a phenomenon involving large-scale algal bloom events, to the transport of large amounts of dust from Saharan Africa.[141] The deposition of the aeolian dust is believed to release iron and trigger the growth of *Gymnodinium breve*, a toxic dinoflagellate that is responsible for fish kills, shellfish poisoning, discoloration of ocean waters, respiratory conditions in humans residing nearby onshore, and economic losses due to reduced tourism at affected beaches.

Chemical and photochemical processing of the mineral aerosols may reduce Fe(III) to a more soluble Fe(II) species. The solubility of iron in dust has been investigated in multiple studies.[137−139,143−146] In one investigation by Zhu et al., samples of airborne Saharan sand were collected on filters in Barbados followed by the quantification of the soluble Fe(II) content of the aerosol through a spectrophotometric method in which the Fe(II) was complexed with an absorbing dye molecule.[139] They concluded that the dust had a total iron content of 3.4%, with only 6.2% of the total iron being soluble and rapidly oxidized to the Fe(III) form. However, they also noted "the dispersed state of the oxidized product may make it more available for chemical and biological processing" and needs further consideration.

In addition to nutrient enrichment, aeolian dust may also be a successful carrier of pathogens, depositing them onto distant soils or oceans where they can affect the native species that inhabit these ecosystems. Shinn et al. hypothesize that the rapid decline in coral reef vitality in the Caribbean is due in large part to the increased transport of African dust to this region.[147] In support of this hypothesis, they report that spores were isolated from the collected aerosol and then used to inoculate healthy sea fans.[147]

1.4. Reactions on Mineral Dust in Atmospheric Chemistry Modeling Studies

The remainder of this review will focus on the chemistry of trace gases with mineral dust. In general, a very powerful way to evaluate the effects that heterogeneous reactions on aerosols may have on the atmosphere is through the development of computer models. Atmospheric chemistry models utilize data obtained from laboratory and field measurements. These models then can simultaneously take into account aerosol properties (e.g., particle composition and size distributions), gas-phase and heterogeneous chemistry, meteorology, and transport processes. Therefore, computer modeling is becoming increasingly important, as it can be used to predict and better explain the impact that a particular event or emission of a specific species may have on the balance of atmospheric processes and climate. Moreover, models can be useful tools in aiding the future direction of laboratory and/or field investigations.

The following subsections review two articles that address the use of models in determining the importance of heterogeneous reactions in the troposphere. The first is an article by Dentener et al.[148] This study was one of the first to fully consider the heterogeneous reactivity of mineral dust in a three-dimensional atmospheric model. Although many uncertainties were associated with the model itself due to the lack of supportive laboratory and field measurements, it predicted that mineral dust could greatly affect the nitrogen, sulfur, and photochemical oxidant cycles. The second article by Jacob addresses various gas-phase and heterogeneous reactions on aerosols and cloud droplets that could alter tropospheric ozone levels and how these pathways should be included in atmospheric models.[8] Jacob provides a thorough look at reactions on various types of atmospheric aerosol, particularly aqueous aerosols, and addresses mineral dust aerosol in a few specific cases.

1.4.1. Role of Mineral Aerosol as a Reactive Surface in the Global Troposphere—A Modeling Study

In this study by Dentener et al., the heterogeneous chemistry that can occur on mineral dust in the troposphere was considered.[148] In particular, the impact of heterogeneous chemistry on the nitrogen, sulfur, and photochemical oxidant cycles was investigated. The mineral dust reactions of interest included those with SO_2, HO_2, N_2O_5, HNO_3, and O_3. Because the gas-phase chemistry in the troposphere is very complex, a three-dimensional model was utilized to integrate heterogeneous reactions and to

simulate the sources, transport, and removal processes of mineral dust. Here we will summarize the main features of this modeling study including the major assumptions and uncertainties made in the model.

In Dentener et al., global sources of dust were simulated from reported monthly averaged data and resulted in dust storm frequencies of one to three "high dust days" per month during the dusty season. Particle size distributions for background and dusty conditions were derived from distributions reported in the literature, and particles ranging from 0.1 to 100 μm were included in the transport simulations. Aerosol properties such as number, surface, and mass concentrations were calculated. The model also included wet deposition and gravitational settling removal rates for the aerosols.

Of great interest to the focus of the current review, the heterogeneous reactions were treated as pseudo-first-order processes in which the rate coefficient (k_j) was calculated according to the equation

$$k_j = \int_{r_1}^{r_2} k_{d,j}(r) n(r)\, \mathrm{d}(r) \tag{1}$$

where $n(r)\, \mathrm{d}(r)$ is a size-dependent number density in cm^{-4} and $k_{d,j}$ is a size-dependent mass transfer coefficient in $cm^3\ s^{-1}$. The term $k_{d,j}$ is a function of the mass accommodation coefficient (α), where α is defined as the probability that a gas−surface collision will result in the adsorption of the gas molecule by the surface. Often α is used to describe gas collisions with aqueous surfaces because it accounts for the solvation of a gas molecule into an aqueous phase. However, for the uptake coefficient on a solid surface without consideration of solvation, the reaction probability or reactive sticking coefficient (γ), typically defined as the ratio of the number of gas molecules that are lost from the gas-phase per second to the total number of gas−surface collisions per second, is equivalent to α. The authors noted that in their model γ was used instead of α. Therefore, making the necessary substitution into the reported equation, $k_{d,j}$ was determined from

$$k_{d,j} = \frac{4\pi D_j V}{1 + K_n[1 + 4(1-\gamma)/3\gamma]} \tag{2}$$

where D_j is the gas-phase molecular diffusion coefficient in $cm^2\ s^{-1}$, K_n is the Knudsen number ($=\lambda/r$), λ is the effective mean free path of a gas molecule in air, and V is a ventilation coefficient. The variable γ is the important parameter under consideration in the current review because it is a measured value from laboratory measurements.

Another way to express the pseudo-first-order rate constant for the loss of a gas onto an aerosol surface through adsorption processes, as described by Preszler Prince et al., is

$$k = \frac{\gamma(\bar{c}/4)[C_{\mathrm{mass}}]S}{1 + \gamma/f(K_n)} \tag{3}$$

where $\bar{c}$ is the mean speed of the gas-phase species in $m\ s^{-1}$, C_{mass} is the concentration of the sample in $g\ m^{-3}$, and S is the specific surface area of the aerosol in $m^2\ g^{-1}$.[149] The λ and K_n terms are defined in the same way as in eq 2. Equation 3 takes into account the gas diffusion to the particle through the Fuchs−Sutugin correction term, $f(K_n)$, where

$$f(K_n) = \frac{K_n(K_n + 1)}{0.75 + 0.283K_n} \tag{4}$$

In the flow regime where the mean free path of the gas is much larger than the particle radius and in the limit where $\gamma \ll K_n$, eq 3 simplifies to

$$k = \gamma(\bar{c}/4)[C_{\mathrm{mass}}]S \tag{5}$$

and the rate constant is dependent only on the reactive uptake and the gas kinetic collision rate. Conversely, when K_n is relatively small compared to γ, then by following a method similar to one by Lovejoy and Hanson,[150]

$$k = \frac{D[C_{\mathrm{mass}}]S}{r} \tag{6}$$

where D is the diffusion coefficient in $m^2\ s^{-1}$, arriving from the relationship that $\lambda = 2D/\bar{c}$. Therefore, in this case, the rate constant is limited by the diffusion of the gas to the aerosol surface.

To gain an understanding of the overall effect that heterogeneous chemistry can have on the atmosphere, Dentener et al. included reaction probabilities for multiple species within the nitrogen, sulfur, and photochemical oxidant cycles. The γ values that they used in the model included those for HO_2, N_2O_5, HNO_3, O_3, and SO_2 and are listed in Table 3. Typically, the authors had to estimate the magnitude of γ on the basis of the uptake of the particular gas-phase species on other surfaces that may not be representative of mineral dust, which added a high level of uncertainty into the model. Specifically, ozone uptake on mineral dust was probably the most uncertain quantity due to the lack of direct measurements and was estimated from dry deposition experiments and uptake on soot and iron particles (see discussion by Dentener et al. and references therein). Numerical data also did not exist for the uptake of HO_2 on dry aerosol; instead, 0.1 was estimated from the results of experiments[151,152] involving the uptake of HO_2 on aqueous droplets. The authors hypothesized that the reaction on dry aerosol would occur just as quickly under humid conditions. The uptake of HNO_3 was derived in a similar fashion from literature on aqueous droplets[153] and assumed to be fast for both wet and dry dust particles. The value

Table 3. Reaction Probabilities (γ) of Various Chemical Species Considered for Heterogeneous Chemistry on Mineral Dust by Dentener et al.[148]

species	γ
HNO_3	0.1
N_2O_5	0.1
HO_2	0.1
O_3	5×10^{-5}
SO_2	3×10^{-4} at RH <50% 0.1 at RH >50%

for N_2O_5 was based on experiments involving sulfuric acid[153,154] and ammonium sulfate particles.[155] SO_2 was treated in a slightly different manner in which the uptake was dependent on the relative humidity of the environment surrounding the modeled aerosol. If the simulated dust event occurred with the relative humidity (RH) >50%, then the uptake was based on studies involving water droplets[156] and assumed to be 0.1. However, a value of 3×10^{-4}, calculated from dry deposition observations,[157] was used if the relative humidity was <50%.

There are several notable chemical species from the HO_x and NO_y chemical cycles that were not included in the model. Hydrogen-containing radicals (HO_x) typically include the hydroxyl radical (OH) and the hydroperoxy radical (HO_2). Reactive nitrogen (NO_y) is defined as the sum of the nitrogen oxides NO and NO_2, denoted NO_x, and all of the products of NO_x oxidation in the atmosphere, which commonly include nitric acid (HNO_3), nitrous acid (HONO), nitrate radical (NO_3), and dinitrogen pentoxide (N_2O_5), but additionally include peroxynitric acid (HNO_4), peroxyacetyl nitrate [PAN; $RC(O)OONO_2$], alkyl nitrates ($RONO_2$), and peroxyalkyl nitrates ($ROONO_2$).[102] Dentener et al. discussed reasons why important tropospheric species such as OH, hydrogen peroxide (H_2O_2), and NO_3 were disregarded. For example, heterogeneous reactions involving OH would not be nearly as fast or significant as the gas-phase loss. H_2O_2 reacts readily in water; however, they state mineral dust would have to adsorb very large amounts of water in order to make the heterogeneous reaction fast enough to consider. Finally, in the case of NO_3, there was a lack of experimental evidence to support including it in the model, and estimations showed that the heterogeneous reactions would not significantly remove NO_x, again defined as the reactive species NO and NO_2.

The results of the Dentener et al. study estimated that globally dust is emitted into the atmosphere at rates of 1800 Tg year^{-1} for particles with radii of <10 μm and 15500 Tg year^{-1} for particles with radii of <30 μm. The model showed that only 16 and 3% of those emitted particles with radii smaller than 10 and 30 μm, respectively, are transported long distances. Furthermore, when the model did not include days with high dust events, the global dust emissions were reduced by 50%. The model also calculated average dust concentrations, size distributions, column abundances, and removal rates, which were in good agreement with data from both field measurements and other computer models reported in the literature. More specific to the topic of this review, Dentener et al. found that the emission of mineral dust into the atmosphere and the subsequent heterogeneous reactions that occurred affected all of the chemical cycles—sulfur, nitrogen, and photochemical—but was highly dependent on the gas-phase lifetime of the various trace gases. A summary of the results is found in Table 4.

Table 4. Modeled Effects of Mineral Dust Emission on Several Atmospheric Species Based on Results of a Three-Dimensional Global Model by Dentener et al.[148]

species	effect on atmospheric concentrations in regions of high dust
NO_3^--containing[a]	>40% of total nitrate associated with dust (global average)
N_2O_5	"small" change
HO_2	10% decrease
O_3	10% decrease during dusty seasons (8% yearly average and 2−6% decrease due to direct decomposition)
SO_4^{2-}-containing[b]	50−70% of total sulfate associated with dust (at source) >10% of total sulfate associated with dust (global average)

[a] Nitrate may include, but is not limited to, solid and aqueous species such as HNO_3, NH_4NO_3, $NaNO_3$, and $Ca(NO_3)_2$ as well as dissolved ionic species. [b] Sulfate may include, but is not limited to, solid and aqueous species such as H_2SO_4, $(NH_4)_2SO_4$, NH_4HSO_4, $(NH_4)_3H(SO_4)_2$, Na_2SO_4, $CaSO_4$, and $MgSO_4$ as well as dissolved ionic species.

For the sulfate cycle, it was determined that near the source region 50−70% of the sulfate present in the atmosphere is associated with mineral dust, whereas most of the global mineral dust contains >10% of the total sulfate in the atmosphere. Importantly, the reaction of SO_2 on mineral dust is believed to be a faster removal process than dry deposition processes. This phenomenon could potentially affect the radiative forcing of these aerosols, as sulfate aerosols have a net cooling effect, and the authors note that by having more sulfate associated with larger mineral dust particles, rather than in the smaller accumulation mode particles, the actual cooling effect of the aerosol may be less than currently predicted. Conversely, sulfate associated with mineral dust would increase the likelihood that the dust could act as cloud condensation nuclei.

In the case of nitrate, it was found that in regions of high dust nearly all of the total nitrate in the atmosphere is nitrate on dust, and throughout most of the global atmosphere in both northern and southern hemispheres, >40% of the total nitrate concentration is coupled with mineral dust. It is believed that dust-associated nitrate is a large component of total atmospheric nitrate due to the presence of calcium in the mineral dust, which has a high buffering capacity to neutralize HNO_3. A significant aspect of their results concerning nitrate is that HNO_3 may adsorb onto mineral dust surfaces in the source region and be transported to remote locations, which otherwise do not have significant HNO_3 concentrations as gas-phase HNO_3 is unlikely to be transported long distances. The dust-transported HNO_3 could then participate in photochemistry in those remote locations. On the other hand, HNO_3 concentrations close to the source could be reduced when the species is associated with large dust particles because it may be removed from the atmosphere more quickly than by dry deposition.

Finally, the model showed that the photochemical oxidant cycle was also affected by the emission of mineral dust into the troposphere. A 10% decrease in ozone concentrations was estimated for regions experiencing high dust events during the dusty season, with an estimated 8% average yearly decrease in the same regions. The ozone concentrations in regions far from frequent dust storms showed very little decrease. Of the observed 10% decrease, the

authors note that 2−6% is predicted to be the result of direct decomposition on the mineral dust surfaces, albeit with great uncertainty due to the lack of relevant data reported in the literature. Additionally, HO_x concentrations were anticipated to decrease by 10% in regions of high dust; however, this reduction in HO_x would not subsequently affect the ozone concentrations because high dust regions typically have reduced NO_x concentrations.

Although this model demonstrated that mineral dust has a significant impact on tropospheric chemistry, Dentener et al. recognized that due to uncertainties in their model simulations, mainly from the lack of experimental data on the specific reactions or parameters, there would be some uncertainty in some of the conclusions. One uncertainty that Dentener et al. cites is the fact that the original sulfate content of the source soil where the mineral dust events occurred was not considered. It was discussed previously under section 1.2.1 that the mineralogy of the dust and parent soil is an important parameter and one that should be included in atmospheric models. Probably a more significant statement in the article is "In this work we assumed that uptake of HNO_3 on mineral aerosol did not hinder uptake of SO_2, other than depleting the $CaCO_3$ content of the aerosol. It would be valuable to verify this."[148] In fact, an important point arises from this statement in that the chemical history of the mineral dust needs to be taken into account. Chemical aging or weathering of the aerosol may functionalize the dust surfaces, resulting in hindered or enhanced reactivity toward additional species, and needs to be included in atmospheric models. Additionally, the heterogeneous reactivity used in this model assumed that all reactions followed a constant pseudo-first-order uptake and did not change with transport time, changing surface nature, or varying mechanisms for surface reaction. The validity of this approach taken in the model will be discussed in more detail under sections 2 and 3.

1.4.2. Heterogeneous Chemistry and Tropospheric Ozone

Jacob reviewed the various gas-phase and heterogeneous reactions that can affect the concentration of tropospheric ozone.[8] Specifically, Jacob primarily addressed the role of aqueous aerosol and cloud droplets and how their reactivity ultimately affected one particular chemical species, ozone. Mineral dust and its role in heterogeneous chemistry were also discussed.

The determination of tropospheric ozone concentrations is complicated in nature as the gas-phase reactions and processes that produce and destroy ozone in this region of the atmosphere are deeply intertwined. Figure 10 displays a schematic representation of these gas-phase reactions and demonstrates that the ozone concentration is intimately coupled to the HO_x and NO_x cycles. Although much of this gas-phase chemistry is known, Jacob cites multiple cases of discrepancies between the concentrations of particular species observed in field measurements and those calculated from models that considered only the gas-phase cycles. For several of these cases, the discrepancies were either nearly or completely rectified when known or proposed heterogeneous reactions were included in the models. Therefore, inclusion of heterogeneous chemistry into atmospheric models appears to be important and justified.

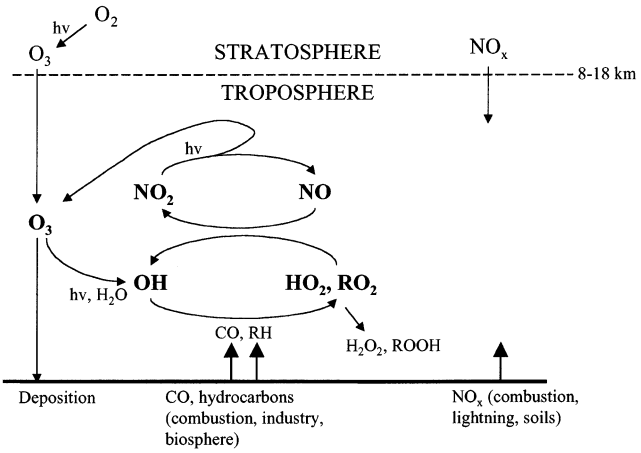

Figure 10. Schematic diagram illustrating the coupling of HO_x and NO_x cycles to tropospheric ozone levels. RO_2 represents organic peroxy radicals. (Reprinted from *Atmos. Environ., 34,* pp 2131−2159; D. J. Jacob, Heterogeneous chemistry and tropospheric ozone. Copyright 2000 Elsevier.)

An important part of the Jacob review was the discussion on mass transfer and reaction probability when one is dealing with heterogeneous reactions. Because aqueous aerosols were the main focus, the mass transfer of a reactant gas molecule onto the surface and into the bulk of a liquid layer was addressed as a significant consideration for cloud chemistry models. It is not sufficient to include only the kinetic aspects of adsorption and desorption processes; rather, consideration of the various lifetimes for chemical reaction, internal mixing, and vaporization will provide cloud models with more thorough results. By neglecting mass transfer limitations in aqueous aerosols, models may overestimate the concentration of various reactive species within the liquid.

Reaction probability (γ) is another important factor in the development of chemical models. Jacob concluded "...the most appropriate approach for parametrizing heterogeneous chemistry in 3-dimensional O_3 models is to use the reaction probability formulation with order-of-magnitude estimates for γ."[8] To accomplish this, it was noted that the reaction of a gas with an aerosol should be assumed to be a first-order process with the rate constant (k) determined by

$$k = \left(\frac{a}{D_g} + \frac{4}{v\gamma}\right)^{-1} A \qquad (7)$$

where a is the aerosol radius, D_g is the gas-phase molecular diffusion coefficient in air, v is the mean molecular speed of the gas-phase species, and A is the aerosol surface area per volume of air. By writing the equation in this format, it can easily be seen that the rate constant comprises a diffusion term (a/D_g) describing the gas-phase diffusion to the aerosol surface and a collision rate term ($4/v\gamma$) describing the

Table 5. Recommended Reaction Probabilities (γ) from Jacob[8] for Several Gas-Phase Species on Aqueous Aerosol and Clouds To Be Included in Atmospheric Chemistry Models

species	γ	reaction
HO_2	0.2	$HO_2 \rightarrow 0.5H_2O_2$
NO_2	10^{-4}	$NO_2 \rightarrow 0.5HONO + 0.5HNO_3$
NO_3	10^{-3}	$NO_3 \rightarrow HNO_3$
N_2O_5	0.1	$N_2O_5 \rightarrow 2HNO_3$

uptake of the gas on the surface. For obtaining size-dependent information of the heterogeneous loss of a gas to aerosols, eq 7 can be integrated over the aerosol size distribution, provided the distribution is known. It should be noted that despite the difference in appearance of eqs 2, 3, and 7, all three are equivalent. These equations were left in the form shown in each reference so that the reader could apply any one of them.

Jacob provided a thorough and comprehensive literature review of the knowledge, current at that time (2000), regarding heterogeneous reactions that alter the concentration of tropospheric ozone. Predominantly, the discussion stressed reactions of aqueous aerosols over those with solid aerosols, due to reaction probabilities on aqueous aerosol typically being an order of magnitude greater than those on dry aerosol. In fact, Jacob recommended, "In the absence of better information one may assume that the aerosol is aqueous,"[8] and supplied several values based on his evaluation of field and laboratory data (displayed in Table 5) to be included in ozone chemistry models. However, despite these recommendations, Jacob repeatedly acknowledges the fact that further research is needed, especially in the area of aerosol characterization, to include aerosol phase, size distribution, chemical composition of individual particles as well as in size-segregated distributions, surface area, and solid aerosol surface properties. Additionally, of interest to this review, it was noted that for the development of better ozone models, laboratory measurements were needed to determine the direct uptake of ozone on mineral dust.

2. Reactions of Mineral Dust with Trace Atmospheric Inorganic and Organic Compounds

This section attempts to cover the literature on mineral dust aerosol chemistry in the troposphere, summarizing aspects of laboratory, modeling, and field investigations. These reactions involve nitrogen oxides, sulfur oxides, ozone, and organics with mineral dust and mineral dust proxies.

2.1. Nitrogen Oxides

Heterogeneous processes involving nitrogen oxides have important implications for tropospheric chemistry because ozone is not directly emitted into the atmosphere but is instead produced through a series of nonlinear reactions of NO_x and volatile organic compounds.[158] Any process that affects the concentrations of nitrogen oxides will be important as understanding these processes is necessary to accurately describe tropospheric ozone formation.

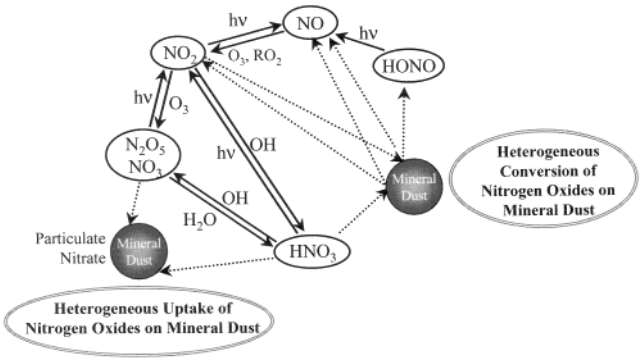

Figure 11. Schematic diagram illustrating possible reactions of nitrogen oxides on mineral dust including the heterogeneous conversion of nitrogen oxides and the heterogeneous uptake of nitrogen oxides to produce particulate nitrate.

Figure 11 shows a reaction scheme of the important gas-phase chemistry and photochemistry involving nitrogen oxides in the troposphere. Potential heterogeneous reactions on mineral dust are also shown in Figure 11 as dashed arrows. Specific heterogeneous reactions on mineral dust include the heterogeneous uptake of nitric acid and nitrogen pentoxide to yield particulate nitrate as well as the heterogeneous conversions of nitrogen dioxide to nitrous acid, nitric acid to nitrogen dioxide, and nitrogen dioxide to nitric oxide. These reactions, with the exception of a few for which there are currently no laboratory data, are discussed in more detail in the next several subsections.

2.1.1. Nitric Acid Uptake on Mineral Dust

Mineral dust particles collected in different regions of the world are often found associated with nitrate. For example, a field study conducted in 1994 by Wu and Okada[159] showed the presence of nitrate in both sea-salt and mineral dust particles in Japan during a high dust event (a so-called "Kosa" event, a sand storm with particles originating from East Asian deserts and loess regions). The particles collected in this study contained nitrate along with Si, Al, Fe, and Ca, elements present in abundance in the Earth's crust. It was concluded that heterogeneous reaction with dust particles could account for the accumulation of nitrate during high dust events. Nitrate ions associated with particles containing aluminosilicates were detected in single-particle mass spectra during the 1999 Atlanta, GA, SuperSite project.[160] The nitrate ion peak intensity was found to be at a maximum in the late afternoon when the gas-phase nitric acid peak was highest. In another study using single-particle analysis near Hong Kong, nitrate was associated with particles containing calcium when winds brought particles from the Chinese land mass, rather than from the sea.[161] The association between calcium ions and nitrate has been observed in several studies including one conducted in southern Finland, where it was proposed that the calcium carbonate component of the dust neutralized the ambient nitric acid.[162] A field study carried out in North Africa found that mineral material was involved in heterogeneous processes to partition compounds such as nitric acid between the gas and aerosol phases.[163] Finally, a

recent study measuring gas-phase HNO_3 and SO_2 at Monte Cimone, Italy, gives evidence for the efficient uptake of gas-phase HNO_3 by mineral dust particles in the atmosphere.[164] Thus, it is well established through field studies that throughout the world mineral dust is frequently associated with nitrate.

As discussed in the Introduction section, understanding what is observed and predictions based on what is already known are hampered by large uncertainties in heterogeneous reaction rates and mechanisms. To develop this understanding, laboratory measurements of HNO_3 reaction on authentic dust and simple model compounds under various conditions have been undertaken in several laboratories. By determining the kinetics, the relative importance of the heterogeneous loss pathways as compared to gas-phase routes can be assessed, whereas probing the mechanisms of the gas-to-surface reactions can give insight into the fate of both the gas-phase species and the particulate in the troposphere.

Although field studies show that mineral dust particles contain nitrate, the source of the nitrate is not well-known, although it is thought to occur through reactions of HNO_3 on the surface of particles. No evidence for this reaction was provided until 1992, when a study by Mamane and Gottlieb showed that reaction of nitric acid with natural mineral particles resulted in the formation of surface nitrate.[165] Samples of $CaCO_3$, sand, and two types of soil were reacted with gaseous nitric acid and analyzed by both bulk and individual particle techniques. Bulk analysis was done to determine the overall formation of nitrate. Using sub parts per million concentrations of nitric acid in dark conditions, nitrate formation in the range of 0.16−7.9 mg of NO_3^- g^{-1} was found for carbonate and mineral samples. Under UV radiation simulating sunlight, the amounts were higher, ranging from 1.4 to 28 mg of NO_3^- g^{-1} for carbonate and mineral samples.

Analysis of individual mineral dust particles was performed using scanning electron microscopy and energy-dispersive X-ray analysis (SEM/EDX). The compositions of the soil and sand were determined. Soil particles contained mostly carbonate or aluminosilicates, whereas sand particles contained mostly quartz. To detect particulate nitrate, the particles were treated with Nitron, a compound that reacts with nitrate ions and thus makes the presence of particulate nitrate easily visible in SEM micrographs. An example of Nitron-reacted particles is shown in Figure 12. Mineral samples exposed to 0.04 ppm of HNO_3 showed ~45% of the particles analyzed reacted to form nitrate. EDX analysis showed that the particles that did not react had the same composition as those that did; it was concluded that some poisoning of the surface of the unreacted particles must have taken place. Under UV radiation, the amount of particles that reacted to form nitrate increased somewhat to 55%. This study was the first to show that the reaction of HNO_3 with mineral dust does result in the formation of surface nitrate under atmospherically relevant conditions. More recently, there have been several laboratory studies directed toward understanding more of the fundamental aspects of the chemistry of nitric acid with mineral dust. Some of these studies are described in more detail below.

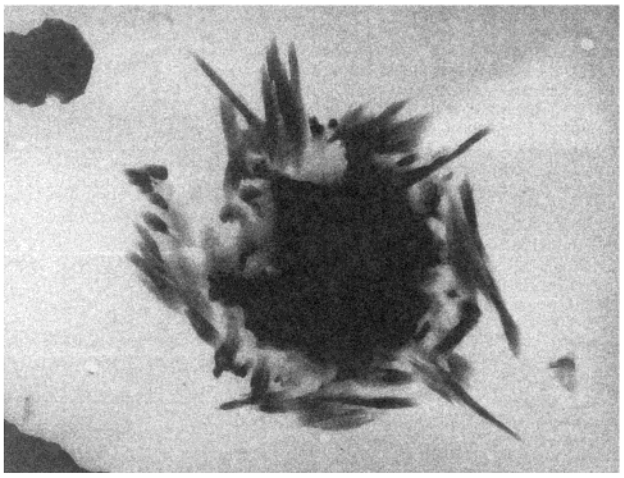

Figure 12. SEM image of soil particles after reaction with 0.04 ppm nitric acid vapor. The films were coated with a thin film of Nitron so that the presence of particulate nitrate could be easily visualized by the elongated fibers. See text for further details. (Reprinted with permission from *Atmos. Environ.*, *26A*, pp 1763−1769; Y. Mamane and J. Gottlieb, Nitrate formation on sea-salt and mineral particles—a single particle approach. Copyright 1992 Elsevier.)

Underwood et al.[166] investigated the reactivity of HNO_3 on oxide particles of some of the more abundant elements present in the Earth's crust, including SiO_2, α-Al_2O_3, α-Fe_2O_3, MgO, and CaO, using a Knudsen cell reactor. The Knudsen cell technique has been used and developed to measure the rates of heterogeneous reactions between gases and solid surfaces.[166−182] The heterogeneous uptake coefficient, γ, a measure of how likely it is that a molecule will be taken up by the surface through adsorption or reaction on a per-collision basis, is the quantity that is typically reported in these experiments. A Knudsen cell reactor operates at very low pressures, so the effect of water vapor on these reactions has been done in a very qualitative way. Other methods can yield more definitive and quantitative information concerning the role of water in heterogeneous reactions on mineral dust particles (vide infra).

In Underwood et al.,[180] the heterogeneous uptake coefficient, γ, was measured for the different oxides and determined to be in the range from 10^{-3} to 10^{-6} depending on the exact nature of the oxide. The more basic oxides, MgO and CaO, were found to be the most reactive, whereas SiO_2 was found to be the least reactive oxide. The values of the uptake coefficient were all calculated using the BET surface area of the samples as described in Underwood et al.[166,178] Besides measuring reaction rates, another important result from the laboratory experiments was that the rate of the reaction is time dependent, with the uptake coefficient decreasing as a function of time as the particle surface becomes saturated. After saturation, the dust particles can no longer take up any additional nitric acid.

In another study by Underwood et al.,[180] a box model was used to assess the importance of nitric acid

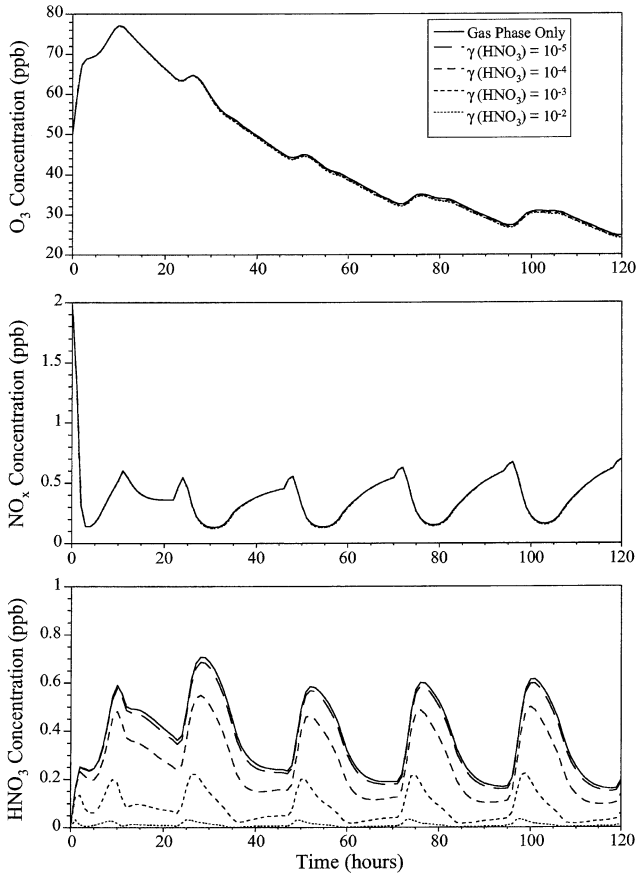

Figure 13. Box-model analysis of ozone, NO_x, and HNO_3 concentrations compares the concentration of these species when only gas-phase chemistry is considered to when heterogeneous chemistry is included in the model. The heterogeneous uptake of nitric acid is modeled at uptake coefficients of 1×10^{-5}, 1×10^{-4}, 1×10^{-3}, and 1×10^{-2}. (Reproduced with permission from *J. Geophys. Res. 106*, D16, G. M. Underwood, C. H. Song, M. Phadnis, G. R. Carmichael, and V. H. Grassian, Heterogeneous reactions of NO_2 and HNO_3 on oxides and mineral dust: a combined laboratory and modeling study. Copyright 2001 American Geophysical Union.)

uptake on mineral dust using the oxides as models for tropospheric dust. Importantly, the effect of surface saturation on the reaction was included in the atmospheric chemistry box model for the first time. The results of the box-model analysis are summarized in Figure 13. It can be seen that for uptake coefficients of $\geq 10^{-5}$, nitric acid uptake on mineral dust represents a significant loss mechanism for HNO_3. This loss results in a large decrease in the HNO_3 concentrations even when surface saturation effects are included. It is also seen from the model that for nitric acid uptake coefficients as high as 10^{-3}, O_3 and NO_x levels were not affected.

Börensen et al. used FT-IR spectroscopy to determine the mechanism and kinetics of the HNO_3 reaction on mineral dust by also using Al_2O_3 as a model for mineral dust.[183] The reaction of nitric acid on Al_2O_3 was monitored via diffuse reflectance infrared spectroscopy (DRIFTS) under dry conditions, similar to the conditions of the Knudsen cell experiments discussed above. The spectra are shown in Figure 14 as a function of nitric acid exposure. Intense absorption bands are seen in the spectra in

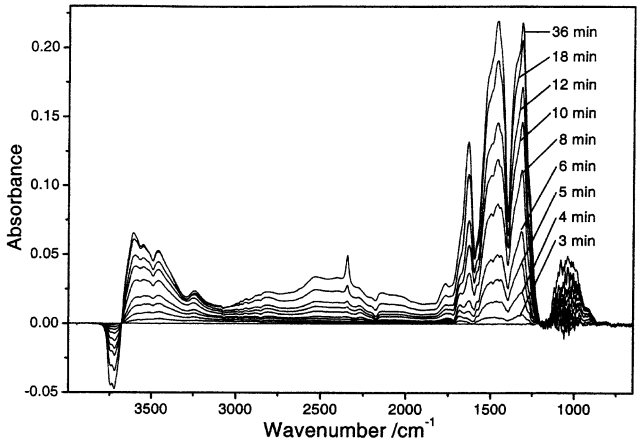

Figure 14. FT-IR absorption spectra recorded of alumina as a function of time as the reaction with nitric acid vapor proceeds ($[HNO_3] = 8.2 \times 10^{13}$ molecules cm^{-3}). (Reprinted with permission from ref 183. Copyright 2000 American Chemical Society.)

the spectral range extending from 1250 to 1570 cm^{-1} (ν_3 nitrate vibration) along with a nitrate $\nu_1 + \nu_3$ combination band at 2343 cm^{-1} and an increase in absorption from acidic OH groups. They determined that under the dry conditions present in their experiments, and that of the Knudsen cell experiments discussed above, HNO_3 reacts with surface hydroxyl groups to form adsorbed nitrate according to the reaction

$$AlOOH\cdots HNO_3 \rightarrow (AlO)^+(NO_3)^- + H_2O \quad (8)$$

They also determined that the reaction of HNO_3 with alumina is faster relative to alumina reaction with NO_2 (see section 3.1.2), but due to instrumental limitations, the reaction order and uptake coefficient could not be determined. An important conclusion drawn from the FT-IR experiments was that the nitrate ion will cover ~30% of the alumina surface and the reaction is limited to the surface only, in agreement with the Knudsen cell studies by Underwood et al.[179]

Although the Knudsen cell reactor operates under very low-pressure conditions,[167] the effect of adsorbed water was also investigated in the Knudsen cell reactor studies discussed above.[166] It was found that heating samples to drive off any water on the oxide surface could change the uptake coefficient by a factor of 10. Thus, it was proposed that adsorbed water plays a role in the uptake of nitric acid on oxide surfaces and that under the relatively dry conditions present in a Knudsen cell the rate should be enhanced for nitric acid uptake under atmospherically relevant conditions of higher relative humidity.

An FT-IR study was performed that further investigated the importance of adsorbed water in the nitric acid uptake onto oxide particles.[184] Oxide particles including SiO_2, α-Al_2O_3, TiO_2, γ-Fe_2O_3, and MgO were used as models for mineral dust aerosol. These particles were classified on the basis of the electronegativity of the cations as a measure of the acidity and pyridine adsorption to acid sites: neutral (SiO_2), amphoteric (α-Al_2O_3, TiO_2, and γ-Fe_2O_3), and basic (MgO and CaO). The water adsorption isotherms

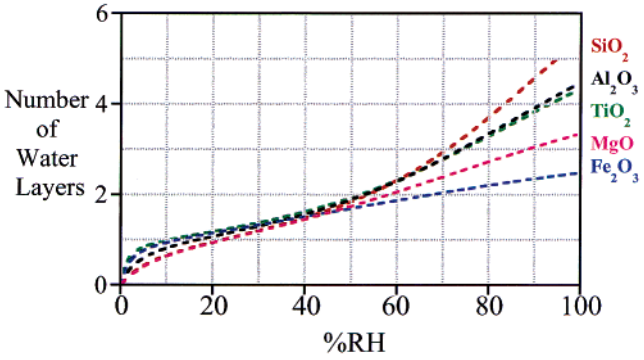

Figure 15. Water adsorption isotherms for several oxides at 296 K. The lines represent a fit to the FT-IR data reported in ref 184.

measured at 298 K were reported in Goodman et al. for these oxides. The water adsorption isotherm data were fit to a three-parameter BET equation, which limits the number of layers of gas adsorbing at high values of P/P_o by allowing n, the number of layers, to be an adjustable parameter. The three-parameter BET equation is then

$$V = \left(\frac{V_m c\left(\frac{P}{P_o}\right)}{1-\left(\frac{P}{P_o}\right)}\right)\left(\frac{1-(n+1)\left(\frac{P}{P_o}\right)^n + n\left(\frac{P}{P_o}\right)^{n+1}}{1+(c-1)\left(\frac{P}{P_o}\right) - c\left(\frac{P}{P_o}\right)^{n+1}}\right) \quad (9)$$

where V is the volume of gas adsorbed at equilibrium pressure P, V_m is the volume of gas necessary to cover the surface of the particles with a complete monolayer, P is the equilibrium pressure of the adsorbing gas, P_o is the saturation vapor pressure of the adsorbing gas at that temperature, and n is the maximum number of layers of the adsorbing gas and is related to the pore size and properties of the oxide powders. The parameter c is a temperature-dependent constant related to the enthalpies of adsorption through

$$c = \exp -\left[\frac{\Delta H_1^\circ - \Delta H_2^\circ}{RT}\right] \quad (10)$$

where ΔH_1° is the standard enthalpy of adsorption of the first layer, ΔH_2° is the standard enthalpy of adsorption of subsequent layers and is taken as the standard enthalpy of condensation, R is the gas constant, and T is the temperature.

The fitted-isotherm curves for several of these oxides (SiO_2, α-Al_2O_3, TiO_2, γ-Fe_2O_3, and MgO) are reproduced in Figure 15. The curves show that for all of the oxides investigated, there is approximately one monolayer of water on the oxide surfaces at 20% RH. At higher relative humidity between 50 and 60%, there are approximately two layers of water on the oxide surface, and at even higher relative humidity, near 90%, there are between two and five layers of water on the oxide surface.

In the Goodman et al. study, it was found that under dry conditions (~0% RH), HNO_3 molecularly adsorbs on the surface of SiO_2 and the adsorption is reversible according to reaction 11.

$$HNO_3(g) + \text{site} \leftrightarrows HNO_3(a) \quad (11)$$

Changes in the OH region indicated that the site of adsorption involves OH groups, specifically hydrogen bonding between surface OH groups and adsorbed nitric acid. There was no evidence for dissociative adsorption on SiO_2, and the reaction was nearly quantitatively reversible. However, the reaction of HNO_3 on α-Al_2O_3, TiO_2, and γ-Fe_2O_3 was found to be irreversible and nitric acid dissociated to form an adsorbed, oxide-coordinated nitrate surface species. The adsorbed nitrate remained even after evacuation of the gas phase. Somewhat different results were observed when MgO and CaO were exposed to HNO_3 as a function of increasing pressure. Absorption bands developed corresponding to what they described as ion-coordinated nitrate. These bands compared well with the absorption frequencies found for solid nitrate salts such as $Mg(NO_3)_2$ and $Ca(NO_3)_2$. In the case of MgO, the following reaction was written as

$$MgO + 2HNO_3 \rightarrow Mg(NO_3)_2 + H_2O \quad (12)$$

However, if there are OH groups on the surface, then the reaction could proceed via eqs 13 and 14:

$$Mg(OH)_2 + HNO_3 \rightarrow Mg(OH)(NO_3) + H_2O \quad (13)$$

$$Mg(OH)(NO_3) + HNO_3 \rightarrow Mg(NO_3)_2 + H_2O \quad (14)$$

A band corresponding to adsorbed water at 1645 cm^{-1} was seen in the infrared spectrum following reaction of MgO with nitric acid.

The effect of relative humidity for nitric acid uptake onto α-Al_2O_3 and CaO was investigated in further detail. In particular, the kinetics of nitric acid uptake was monitored from 0 to ~20% RH. Adsorbed water was found to significantly enhance nitric acid uptake kinetics, in agreement with the Knudsen cell data. The relative uptake kinetics of $\gamma(H_2O)/\gamma(dry)$ was determined to increase >10-fold near 20% RH.

The different oxides were further classified according to their reactivity with HNO_3 in the presence of water: nonreactive neutral insoluble (SiO_2), reactive insoluble (α-Al_2O_3, TiO_2, and γ-Fe_2O_3), and reactive basic soluble (MgO and CaO). These classifications describe whether HNO_3 reacts and dissociates on the surface or simply weakly adsorbs, as well as the ability of the oxide to dissolve in and/or immerse in nitric acid aqueous solutions. CaO and MgO instantly dissolved in the nitric acid solution, whereas the others did not. This indicates reactivity into the bulk of the particle is possible with these two oxides, where it will be limited to the surface of the other insoluble oxides. This discussion of bulk reactivity will be elaborated in the next few paragraphs for the reaction of nitric acid on calcium carbonate.

Reaction of HNO_3 with $CaCO_3$ appears to be even more strongly dependent on the water content of the samples. The reaction of nitric acid with $CaCO_3$ was examined by Goodman et al. in another study.[170] The aim of the study was to address questions related to the mechanism of the reaction. In particular, experiments were designed to determine whether HNO_3

reacts only with the surface of the particles or into the bulk of the particles and to determine if adsorbed water played a role in the reaction

$$2HNO_3 + CaCO_3 \rightarrow Ca(NO_3)_2 + CO_2 + H_2O \quad (15)$$

In this study, Knudsen cell measurements were done at higher pressures to yield quantitative information about the products formed in the gas phase and at lower pressures to measure the uptake coefficient. The higher pressure experiments were done using both wet and dry nitric acid vapor. Both sets of experiments yielded similar results. Wet HNO_3 (i.e., a gaseous nitric acid sample that contained water vapor) exhibited a decrease in the H_2O flow, showing H_2O adsorbed to the surface. The CO_2/HNO_3 ratios were 0.44 for dry HNO_3 and 0.33 for wet; the H_2O/HNO_3 ratios were 0.22 and 0.16 for dry and wet HNO_3, respectively. The ratios are less than stoichiometrically predicted by eq 3, as observed by Hanisch and Crowley,[171] possibly indicating that CO_2 dissolves into bicarbonate in the water layer rather than being released into the gas phase and that water remains adsorbed rather than going into the gas phase, due to the solubility and hygroscopicity of the $Ca(NO_3)_2$ formed.

The low-pressure experiments ensured that the flux of HNO_3 to the surface was not great enough such that the sample saturated in the first few seconds. An uptake coefficient was determined using the BET surface area of the samples to be $(2.5 \pm 0.1) \times 10^{-4}$. Importantly, as this was measured under dry conditions (~0% RH), and accounting for the entire BET surface area, this value should be considered a lower limit. By qualitatively changing the water content in the experiment through heating a sample to 40 °C overnight during evacuation, a 10-fold decrease in the rate of adsorption was observed, whereas the rate increased by a factor of 2 when a wetter nitric acid source was used to measure samples. Similarly, Fenter et al. found that the presence of water in $CaCO_3$ pellets that had not been dried enhanced the uptake of nitric acid by a factor of 2.[185]

To probe the nitric acid/calcium carbonate reaction in greater detail, Goodman et al. employed transmission FT-IR spectroscopy to monitor spectral changes upon exposure of $CaCO_3$ to nitric acid vapor.[170] FT-IR measurements were carried out under dry conditions and in the presence of water vapor. It was determined that when dry $CaCO_3$ was exposed to HNO_3, there was a loss of an absorption at 874 cm^{-1} associated with a loss of carbonate, while weak nitrate bands became apparent in the spectrum. Upon increasing exposure and pressures of nitric acid these bands did not grow very much in intensity. However, when the reaction was performed under wetter conditions at 20% RH, there was a large increase in the infrared absorption bands associated with calcium nitrate as the calcium carbonate bands decreased in intensity. These spectra are shown in Figure 16, where bands corresponding to surface nitrate appeared at 813 and 1045 cm^{-1} with a concomitant negative band at 874 cm^{-1}, demonstrating the loss of surface carbonate. It was found that this reaction continued in the presence of water vapor

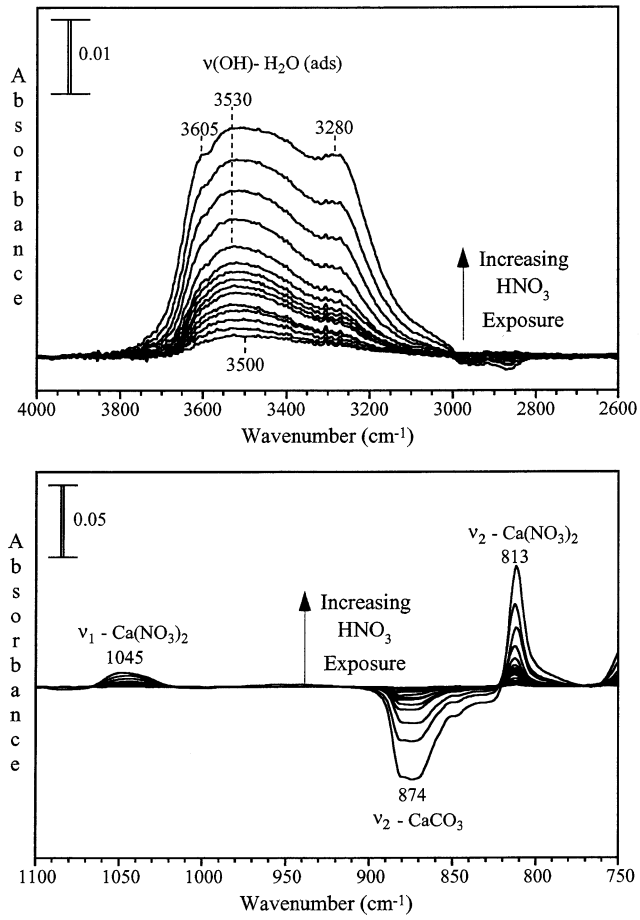

Figure 16. Difference FT-IR absorption spectra recorded of calcium carbonate as a function of time nitric acid exposure. The spectral region between 750 and 1100 cm^{-1} shows that as absorption bands associated with calcium nitrate increase in intensity as the reaction proceeds, absorption bands associated with calcium carbonate decrease in intensity. The spectral region between 2600 and 4000 cm^{-1} shows that water adsorption on the particle increases as the reaction proceeds. This is seen by the increase in intensity in the water O−H stretching region (3100−3700 cm^{-1}). (Reproduced with permission from *J. Geophys. Res. 105*, 23, pp 29053−29064; A. L. Goodman, G. M. Underwood, and V. H. Grassian, A laboratory study of the heterogeneous reaction of nitric acid on calcium carbonate particles. Copyright 2000 American Geophysical Union.)

at 20% RH without any evidence for surface saturation, indicating that more than surface $CaCO_3$ was reacted with gas-phase nitric acid. A similar conclusion was reached by Hanisch and Crowley[171] when they reacted a sample of $CaCO_3$ that had been previously reacted with HNO_3 and found the reactivity of the sample to be partly or almost fully restored. They observed uptake coefficients similar to that of unreacted samples but that the time to reach saturation was greatly reduced. They explained this observation as due to calcium nitrate recrystallizing on the $CaCO_3$ surface, forming islands and leaving bare $CaCO_3$ sites for further reaction.

Changes in the spectral region associated with the OH stretching mode are also shown in Figure 16. There is a large increase in the absorption band associated with an increase in the amount of water adsorbed on the particle surface as nitric acid reacts

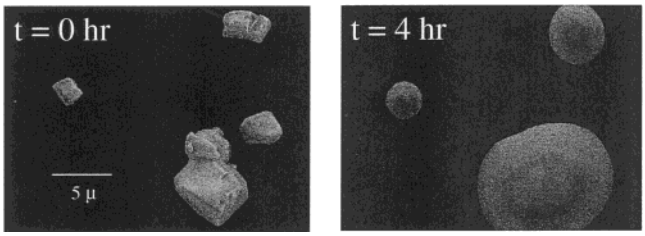

Figure 17. SEM images of calcium carbonate particles before ($t = 0$ h) and after ($t = 4$ h) reaction with nitric acid vapor at 40% RH. The images show that the solid calcium carbonate particles transform into aqueous droplets as the particle converts to calcium nitrate. The SEM image at $t = 4$ h shows that the calcium nitrate product deliquesces to form an aqueous-like droplet. (Adapted from *Geophys. Res. Lett. 30*, 3, DOI 10.1029/2002GL016563; B. J. Krueger, V. H. Grassian, A. Laskin, and J. P. Cowin, The transformation of solid atmospheric particles into liquid droplets through heterogeneous chemistry: laboratory insights into the processing of calcium containing mineral dust aerosol in the troposphere. Copyright 2003 American Geophysical Union.)

with the calcium carbonate particles. It was also reported by Goodman et al. that the structure seen in the water absorption band was characteristic of a concentrated calcium nitrate solution.[170] A more recent study by Krueger et al. using SEM/EDX analysis shows that the calcium carbonate particles convert from solid, dry particles to liquid, aqueous droplets.[186] This transformation from solid to droplet is clearly seen in Figure 17 for particles reacted at 40% RH. The transformation is proposed to occur via a two-step mechanism. In the first step, nitric acid reacts with calcium carbonate to form calcium nitrate followed by the deliquescence of calcium nitrate. The deliquescence of calcium nitrate occurs below 20% RH.

The implications of these studies are summarized as follows. First, because the reaction is not limited to the surface, as demonstrated by gravimetric analysis,[170] the total calcium content of the particle may be available for reaction; thus, surface saturation effects will not play a significant role in the reactivity as found with the insoluble oxides, for example, α-Al_2O_3. Second, changes in morphology and phase of the particle will change the optical properties of these particles as they react in the atmosphere. Third, the increase in water adsorption indicates that the reacted particles can act as cloud condensation nuclei.

The role of alkaline mineral aerosol (such as particles that contain $CaCO_3$) in the partitioning of HNO_3 was assessed in a modeling study by Song and Carmichael.[187] The modeling analysis was carried out using the STEM-II model, which takes into account transport, chemical information, and emission and deposition of atmospheric gases and particulates, including 90 reactive species, 4 constant species (CO_2, O_2, H_2O, and H_2), and 7 particulate ion species (including Ca^{2+}) among other particulate material. The gas-phase chemistry component of the model accounts for 185 known reactions, whereas heterogeneous interactions between gas and particulates are also incorporated. The important result determined by this model was that in large parts of the modeling domain which contain the boundary layer and free troposphere, HNO_3 levels were reduced by >30% due to interactions with dust particles. High nitrate regions were found to coincide with regions of raised dust levels. It was concluded that nitric acid has a strong tendency to react with alkaline aerosol and that the partitioning of HNO_3 to dust surfaces containing Ca^{2+} was significant, forming surface nitrate. These results were obtained from data acquired over East Asia and the western North Pacific,[187] but data acquired by Talbot et al.[188] reveal that measurements made over the south-central United States show levels of calcium similar to those regions used in this modeling analysis, suggesting then that results obtained for Asia could be extrapolated to other parts of the world.

The impact of HNO_3 partitioning to alkaline aerosol on the HNO_3 to NO_x ratio was evaluated. When the partitioning was considered in the calculations, the ratio was reduced by a factor of 2. Although it is still higher than what is observed, the impact of HNO_3 loss to alkaline particles is significant. It is postulated that the inclusion of other partitioning processes, such as HNO_3 loss to mineral dust surfaces, may contribute especially when the dust contains calcium carbonate. Thus, models should include the chemical composition of the dust along with size distributions in order to fully understand the impact that heterogeneous reactions involving mineral dust have on the atmosphere.

In an attempt to better approximate mineral dust composition, Hanisch and Crowley reacted nitric acid with a variety of clay mineral compounds in a Knudsen cell and compared the reactivity of the clays with authentic dust samples from African and Asian desert regions.[172] The clays used included dolomite, orthoclase, kaolinite, chlorite, montmorillonite, illite, smectite, and palygorskite; these clay minerals contain different elements (Ca, Mg, K, Al, Si, and Fe) in different ratios and combinations. In another study, Hanisch and Crowley also investigated the heterogeneous reactivity of HNO_3 with Al_2O_3, $CaCO_3$, and authentic mineral dust samples from Arizona and the Saharan desert.[171] The main conclusion from these studies, which differs from those of the studies described above by Underwood et al. and Goodman et al., is that the "best" surface area used to calculate uptake coefficients measured with a Knudsen cell reactor is the geometric uptake coefficient. Uptake coefficients were calculated from different experiments on different clays in which parameters such as geometric surface area, sample mass, grain size, HNO_3 flow, and temperature were varied. It was found that the mean γ values for Saharan dust, dolomite, and orthoclase were $(13.6 \pm 1) \times 10^{-2}$, $(14.0 \pm 1.5) \times 10^{-2}$, and $(8.4 \pm 1.6) \times 10^{-2}$, respectively, and were independent of HNO_3 flow, showing little variation for different flows. By varying the surface area of illite and mixed illite/smectite samples, no dependence of γ on geometric surface area was found. The mean γ for illite was calculated as 10.8×10^{-2}, and for the 70:30 mixture of illite/smectite sample, the mean γ was calculated as 8.9×10^{-2}. The Chinese dust sample was examined by changing sample mass

and particle size. No variation in uptake was observed for changing particle size either, and the mean γ was determined to be $(17.1 \pm 3.0) \times 10^{-2}$.

Kaolinite samples of varying mass were dispersed on either an optical glass flat or an alumina single crystal, which is considered to be an unreactive substrate for this experiment. Blank experiments on the support substrates showed measurable HNO_3 uptake by the glass. This effect had to be accounted for in the determination of γ for the dust on that support. No uptake was observed on the uncoated Al_2O_3 crystal; therefore, no correction was necessary for experiments on that support. It was observed that γ differed by a factor of >2, with dust on the Al_2O_3 single crystal having the greater value. It was determined that a simple correction for uptake into an "empty" sample compartment is not at all times appropriate and suggested that for HNO_3 a number of factors can influence the measurement of γ and correction for blank uptake. These factors include the influence of HNO_3 desorption rates from the walls of the reactor if a sink such as a very reactive sample is present, a difference in gas concentration gradients between weak and strong sinks (i.e., sample support and sample), and a time difference between uptake to the support and uptake to the sample. It was concluded that the influence of unwanted reactive surface should be minimized. The mean γ for kaolinite on the alumina single crystal is reported to be $(11.4 \pm 1.6) \times 10^{-2}$. Similar experiments were done for palygorskite distributed on both glass flats and single crystals, but no detectable difference in γ was observed between the supports. No variation with sample mass was observed in this case either, and an uptake coefficient of $(19.6 \pm 3.0) \times 10^{-2}$ was reported. The main conclusion drawn from this study is that no significant role for internal surfaces is evident, which is in direct contrast to the measurements and conclusions made by Underwood et al.[166,178,180] The other major conclusion culled from these experiments showed that HNO_3 uptake onto individual clay compounds is approximately similar to that observed for authentic dust samples. It was concluded that the uptake of nitric acid onto mineral dust and clay components is efficient, with large uptake values near 0.1. It was also suggested that discrepancies between values in the literature arise in part from correction factors to account for diffusion into the bulk of the samples, errors from calculating uptake coefficients due to competitive uptake on surfaces other than the sample, and determining uptake coefficients at different nitric acid pressures.

Further discussion of this apparent discrepancy of the uptake coefficient for nitric acid on dust is warranted, as it seems that there are difficulties in measuring and interpreting nitric acid uptake on powdered samples that contain many layers of particles. One of the most important differences in the calculated uptake coefficients is related to surface area used in the calculation. The SEM photos of the samples used by Hanisch and Crowley (see Figure 18) clearly show that the geometric area is, at best, a lower limit to the available surface area as it is quite apparent that the surfaces of these particles

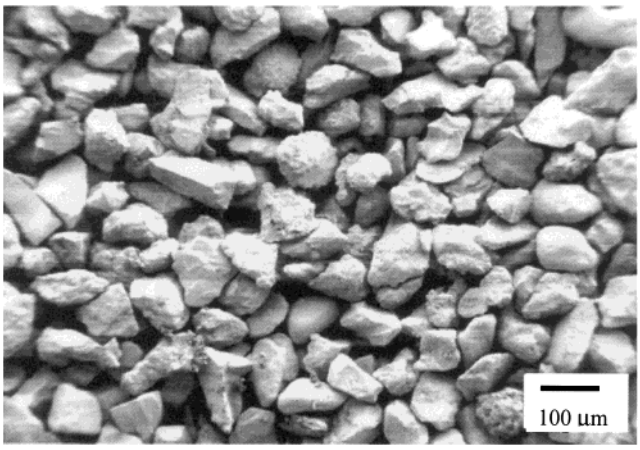

Figure 18. SEM image of a Chinese dust sample with grain size, d, of 54 μm < d < 85 μm. The image is of a sample used for Knudsen cell reactor experiments. (Reproduced with permission from *Phys. Chem. Chem. Phys.* *3*, pp 2474−2482; F. Hanisch and J. N. Crowley. Copyright 2001 PCCP Owner Societies.)

are not perfectly flat or perfectly smooth and that there are many void areas that nitric acid molecules can easily diffuse through. In recent work by Finlayson-Pitts and co-workers, it has been reaffirmed that the geometric surface area underpredicts the available surface area of reaction, and in order to avoid issues of diffusion into underlying layers, less than one layer of particles should be deposited onto an inert substrate.[189] An idealized diagram of isolated particles deposited on an inert substrate is shown in Figure 19.[189] This approach seems to be quite reasonable, and the calculation of the number of collisions is done such that the uptake coefficient can be more accurately determined. Further studies of available surface area are warranted so that that these kinetic data can be included in atmospheric chemistry models with greater certainty, a major goal of the laboratory studies.

2.1.2. Nitric Acid and Ammonia To Form Ammonium Nitrate Coatings on Mineral Dust

A significant fraction of tropospheric ammonium nitrate aerosol, a volatile species formed from the reaction of NH_3 and HNO_3 gas, is found to be associated with particles 100−300 nm in diameter.[190] The NH_4NO_3 aerosol exists in equilibrium with gas-phase NH_3 and HNO_3, with the direction of the equilibrium depending on relative humidity and ambient temperature.[191] Whether or not the pure ammonium nitrate particles exist as liquid or solid is also determined by these factors. It has been found that NH_4NO_3 particles do not typically crystallize until the relative humidity is very low, and at higher relative humidity, the particles are likely to be liquid, because NH_4NO_3 will deliquesce at ~60% RH at ambient temperatures.[102] Although particles of pure NH_4NO_3 exist in the troposphere, particles of mixed mineral and ammonium nitrate material have been observed. Using ATOFMS, single particles collected near Riverside, CA, were analyzed for their composition.[192] Many particles contained NH_4NO_3 mixed with organic material, other inorganic material, and inorganic oxide material.

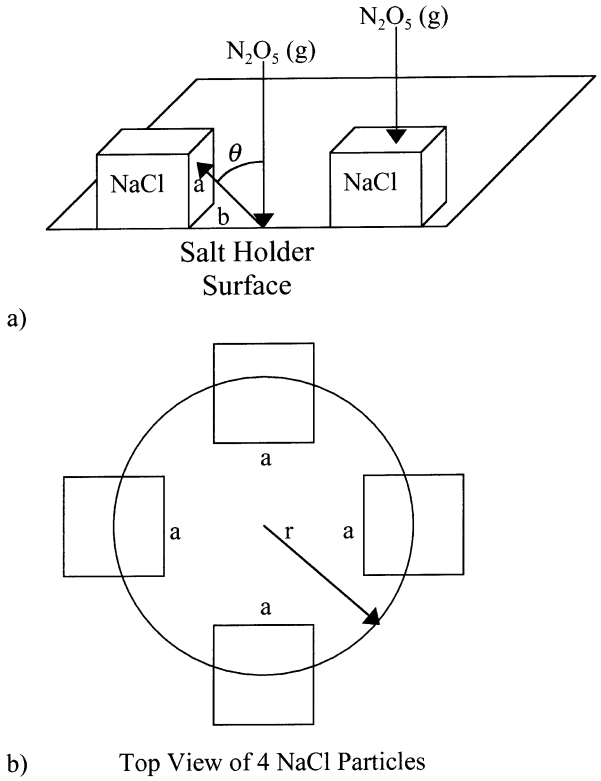

Figure 19. (a) Diagram of a sample holder dispersed with submonolayer particles of NaCl crystals for Knudsen cell experiments. (b) Schematic of a method used to correct for the spaces between evenly spaced NaCl particles for best determining the available reactive surface area. (Reproduced with permission from *Phys. Chem. Chem. Phys. 5*, pp 1780−1789; R. C. Hoffman, M. E. Gebel, B. S. Fox, and B. J. Finlayson-Pitts. Copyright 2003 PCCP Owner Societies.)

An extensive review detailing studies of phase transitions of atmospherically relevant particles has been done by Martin.[193] Han et al.[194] have examined the effect of such inorganic oxide material inclusions on the efflorescence of NH_4NO_3 under tropospheric conditions. NH_4NO_3-coated particles were produced by first reacting hematite (α-Fe_2O_3) and corundum (α-Al_2O_3) with nitric acid vapor and then neutralizing the particles through reaction with NH_3 gas. NH_4NO_3 is confirmed on the surface through infrared spectroscopy, which showed absorptions for both NH_4^+ and NO_3^-. Deliquescence and efflorescence experiments were performed using these particles and compared to the same experiments done on NH_4NO_3 particles without mineral inclusions. The expected changes in relative volume as a function of increasing and decreasing relative humidity are shown in Figure 20. The red curve shows the path taken as crystalline particles are exposed to increasing water vapor until at the deliquescence point the particle changes volume due to conversion from a solid particle to an aqueous droplet. The droplet continues to grow in size as a function of relative humidity. The blue curve shows what happens to this aqueous droplet as the relative humidity decreases. Because of the kinetic barrier associated with crystal nucleation, the particle does not convert back to the solid form until much lower relative humidity. This is marked as homogeneous nucleation. In the case

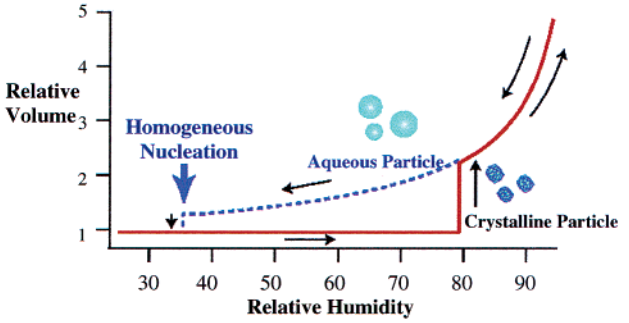

Figure 20. Pictorial representation of the changes in relative volume of an atmospheric particle undergoing a crystalline to aqueous phase transition as a function of increasing relative humidity and the reverse transition, efflorescence, as a function of decreasing relative humidity. Because of the barrier to nucleation kinetics, efflorescence occurs at a much lower relative humidity as compared to deliquescence. (Reprinted with permission from ref 193. Copyright 2000 American Chemical Society.)

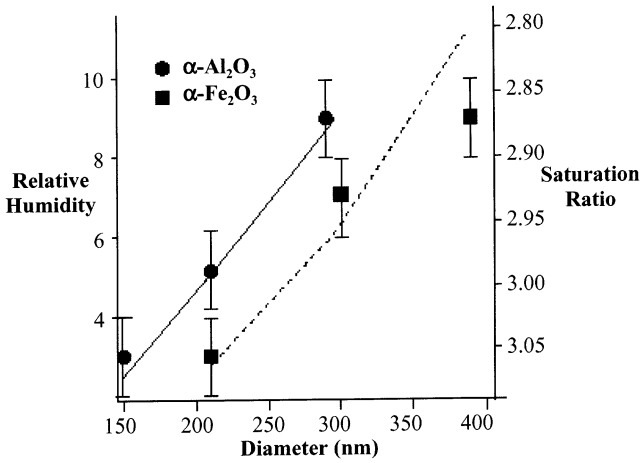

Figure 21. Relative humidity values observed for the efflorescence of ammonium nitrate by heterogeneous nucleation as a function of the mode diameter of the inclusions α-Al_2O_3 (solid circles) and α-Fe_2O_3 (solid squares). The line drawn through the data is the optimized fit to the active site model. Also shown, on the right axis, is the saturation ratio, *S*, and the salt mole fraction of the aqueous phase. (Reproduced with permission from *J. Geophys. Res. 107*, D10, DOI 10.1029/2001JD001054; J.-H. Han, H.-M. Hung, and S. T. Martin, Size effect of hematite and corundum inclusions on the efflorescence relative humidities of aqueous ammonium nitrate particles. Copyright 2002 American Geophysical Union.)

of ammonium nitrate, Han et al. showed that pure NH_4NO_3 particles do not exhibit evidence of recrystallization or efflorescence, whereas particles internally mixed with a mineral oxide did. The efflorescence of ammonium nitrate was found to occur between 8 and 10% RH when an oxide inclusion was present. It was also determined that the relative humidity at which efflorescence of the ammonium nitrate coating occurs decreased as the size of the mineral oxide inclusion decreased. The size dependence of the mineral oxide inclusion is shown in Figure 21. These data have been fit to an active-site model. The details of the model are discussed under section 2.2.2 for ammonium sulfate coatings.

Thus, mineral oxides provide a surface with active sites toward crystallization of the coating. Because

the phase of the particles in the troposphere will dictate the effects they will have on the chemical and radiative properties of the troposphere, it is important to take into account the presence of mineral dust in air parcels containing ammonia and nitric acid.

2.1.3. Nitrogen Dioxide and Nitric Oxide Adsorption and Reaction on Mineral Dust

As previously discussed, NO_2 in the troposphere is intimately linked to tropospheric ozone formation. It is thus essential to adequately understand all of the possible mechanisms of NO_2 reactions in the troposphere, both homogeneous and heterogeneous. This is important in order to accurately describe the chemistry of the troposphere and to assess the importance of these mechanisms not only with respect to the impact they may have on tropospheric ozone but for the potential to act as sources of other important gas-phase nitrogen oxide containing species, such as HONO, a precursor to the OH radical.

Even before Dentener et al.[148] proposed that mineral dust in the troposphere could serve as a significant participant in the chemistry of the atmosphere, heterogeneous reactions of nitrogen dioxide and nitric oxide were considered by Judeikis and Wren.[195] They investigated the viability of the deposition of NO_2 onto the surfaces of soil and cement particles in an attempt to gain insight into the lifetimes and transport properties of NO_2 in regard to deposition onto ground-level surfaces. Using a cylindrical flow reactor, particles representative of the area (sandy loam and adobe clay soils) as well as commercial bagged cement were reacted with gas mixtures containing NO_2. Similar experiments were performed with model compounds such as wood charcoal, MnO_2, PbO, and Al_2O_3. Analysis of the reaction of NO_2 with such particles was carried out by mass spectrometry and wet chemical techniques to determine amounts of surface nitrate formed.

Initial deposition rates were reported as follows: 0.60, 0.77, and 0.32 cm s^{-1} for loam, clay soil, and cement, respectively. They were found to be invariable between dry or humidified conditions or between anoxic and oxygenated gas mixtures. The deposition velocities were observed to decrease with continued exposure, demonstrating the finite capacity of such surfaces for NO_2 removal. Although initial rates were not affected by humidity, the decrease toward zero deposition was much more gradual under humid conditions, suggesting a higher capacity in humid environments. The deposition was found to be largely irreversible.

Saturation of particle surfaces is an important issue in assessing the importance of the heterogeneous processes in the troposphere. If the surface is deactivated with exposure to pollutants, the heterogeneous pathway may not represent an effective sink compared to other processes having rates that do not gradually diminish. Therefore, the reactivation of the surfaces was given consideration here. To evaluate possible reactivation, samples were saturated with NO_2 and then subjected to treatments including overnight evacuation, exposure to gas streams void of NO_2, reaction with ammonia, and the physical washing of the surfaces with water. Regeneration of surface reactivity occurs when a saturated surface is reacted with ammonia. It was found that exposure to NH_3 amounts equivalent to 170% of the NO_2 saturation exposure (per molar basis) completely restored the surface to its initial deposition level. Rinsing the reacted surfaces with water also partially restored the surfaces to NO_2 reaction to ~60% of its initial value. However, overnight evacuation or exposure to nonreactive gas streams had no appreciable effect on restoring the surface reactivity. Exposure to ammonia and water represent two feasible tropospheric processes for surface reactivity regeneration.

The mechanism of NO_2 reaction with the mineral surfaces was not explicitly stated; however, it was found that the conversion of NO_2 to adsorbed species was less than quantitative as the formation of NO in the gas phase began. Initially only NO_2 loss was seen; with exposure time, NO began to form. It was observed that the amount of NO produced relative to the amount of NO_2 gradually increased until saturation levels, when both gas-phase NO and adsorbed NO_2 products began to decrease. The mechanism for this reaction was addressed in later studies (vide infra). In the study by Judeikis and Wren, it was also determined that NO−surface interactions were of much less importance than NO_2−surface interactions on the basis of lower deposition rates and lower capacities for NO. In addition, there was the observation that a surface saturated with NO will still exhibit reactivity toward NO_2.[195] A very recent study has shown that NO can be oxidized to NO_2 on mineral dust surfaces by adsorbed ozone.[174] In summary, the implications for the results determined in the earlier study of Judeikis and Wren show that removal of NO_2 by surfaces will depend on the saturation levels of the surface with regard to NO_2 or the degree of reactivation by reaction with NH_3 or exposure to water.

Studies by Mamane and Gottlieb[165,196] examined NO_2 reaction with mineral particles based on the acknowledgment that mineral particles constitute part of the coarse fraction of atmospheric aerosols and are often associated with NO_3^-. The purpose of the study was to supply direct evidence for the reaction of nitrogen oxides on the surface of mineral particles. "Local soil" and cement particles were exposed to known concentrations of NO_2 under constant relative humidity in a static reaction chamber with bulk and individual particle analysis techniques. Bulk analysis presented quantitative information, whereas individual particle analysis yielded direct evidence of nitrate formation on the surface.

It was determined that after 1−3 days, nitrate formation plateaued but then increased again with a final nitrate capacity of 3−4 mg of NO_3^- g^{-1} of mineral. The conclusions drawn from the bulk analysis in this experiment in regard to NO_2 were as follows: nitrate formation was linearly dependent on the mass of the mineral sample, and changing the relative humidity from 40 to 85% did not increase nitrate formation. Further analysis using TEM to analyze individual particles that had been reacted with NO_2 showed no changes in particle morphology,

and after 3 days of exposure, 60−70% of the particles in the sample had formed mixed-nitrate mineral particles with the nitrate limited to the surface. An interesting observation was that not all of the particles in the sample had reacted, but it was unknown which minerals in the particles did or did not react.

The study by Mamane and Gottlieb[165,196] was performed with SO_2 as well (see section 3.1), and the results from both gases were compared. Whereas the capacities for NO_2 were considerably lower than for SO_2, a larger percentage of the particles reacted with NO_2 than with SO_2. It was determined that SO_2 interaction with mineral surfaces may be an important process for sulfate formation as calculations for NO_2 are reported to be an order of magnitude lower than those for SO_2 (0.15−0.45 mg m^{-3} sulfate formed on particle surfaces).

Further studies by Mamane and Gottlieb in 1992[165] compared NO_2 reaction on mineral surfaces to HNO_3 reaction on the same particles that included $CaCO_3$, a soil sample composed mainly of carbonates, a soil sample dominated by aluminosilicates, and sand. It was found that nitrate formation increased linearly with the mass of the sample. Measured capacities ranged from 0.5 to 4.7 mg of nitrate g^{-1} of mineral for carbonates and from 0.16 to 7.9 mg of nitrate g^{-1} of mineral for different minerals, and it was found that these capacities depended on NO_2 concentrations. It was also found that capacities increased when the samples were exposed to UV radiation simulating sunlight. When samples were exposed to NO_2 or HNO_3, capacities for nitrate formation were appreciably lower for high molar concentrations of NO_2 than for low molar concentrations of HNO_3, perhaps indicating that the mechanism of nitrate formation is different for each system.

The reaction of NO_2 on Al_2O_3 was followed under dry conditions, and infrared absorption bands due to species formed on the surface were monitored as a function of NO_2 pressure.[197] The spectra are shown in Figure 22. Initially bands are observed that correspond to bridging nitrito groups (NO_2^-). These increase as NO_2 pressure increases, while other bands begin to become apparent, corresponding to adsorbed NO_3^-. Also observed is the formation of gas-phase products, in particular NO as shown in the inset of Figure 22, in agreement with the studies by Judeikis and Wren.[195]

The formation of both the two surface species, nitrite and nitrate, on the aluminum oxide surface was confirmed by diffuse-reflectance UV−vis spectroscopy, observing transitions of $\pi\rightarrow\pi^*$ and $n\rightarrow\pi^*$ for both species as a function of NO_2 pressure. Initially, features at 370 and 208 nm were observed and assigned to the $n\rightarrow\pi^*$ and $\pi\rightarrow\pi^*$ transitions for adsorbed nitrite. These maxima shifted to 270 and 201 nm as NO_2 pressure increased, corresponding to adsorbed nitrate transitions. Thus, on the basis of both FT-IR and the UV−vis results, it was concluded that at low NO_2 pressures, NO_2^- is formed with NO_3^- appearing at higher NO_2 pressures.

In a series of studies, additional spectroscopic and kinetic measurements were made on the heterogeneous reaction of NO_2 on oxide surfaces and authentic dust samples.[178−180,198] In one of these studies, Underwood et al. investigated the heterogeneous uptake of NO_2 with mineral oxide and authentic dust powders and considered the results in an atmospheric computer model.[180] In addition to oxide powders including Al_2O_3, Fe_2O_3, TiO_2, SiO_2, CaO, and MgO, the reactivity of samples of dust from the Gobi and Saharan desert regions were also investigated. Mass- and surface area-independent initial uptake coefficients were determined according to methods described in Underwood et al.[178] from experiments using a Knudsen cell reactor. Measured uptake coefficients ranged from 2.0×10^{-8} (γ-Al_2O_3) to 2.2×10^{-5} (CaO). Most of the oxides and authentic dusts had values of the initial uptake coefficient in the 10^{-6} or 10^{-7} range with the exception of SiO_2, which did not exhibit any appreciable uptake under the dry conditions of this study.

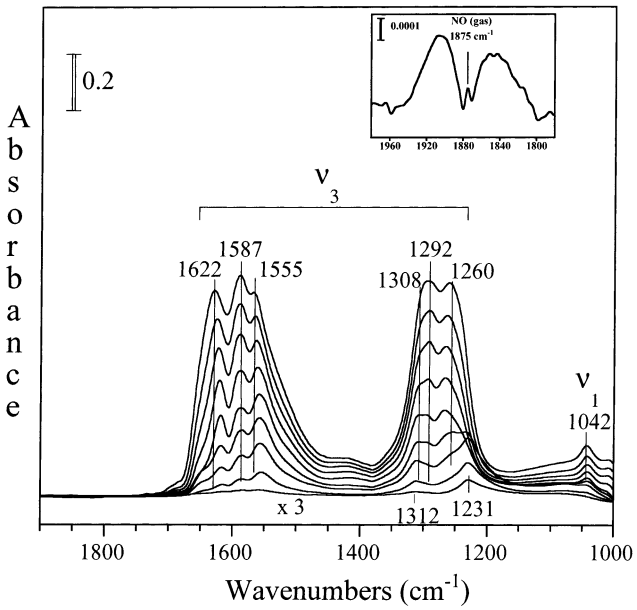

Figure 22. FT-IR spectra of Al_2O_3 as a function of increasing NO_2 exposure. The inset shows the spectrum of the gas-phase product NO that forms during NO_2 uptake. (Reprinted with permission from ref 197. Copyright 1998 AVS.)

The mechanism for NO_2 uptake is described, on the basis of earlier FT-IR and Knudsen cell studies published by Underwood et al.[179,180] Initially, NO_2 reacts with the surface to form nitrite, and then as the reaction proceeds nitrate is formed on the surface. In addition, gas-phase NO is produced. NO does not form immediately but only after an induction period, determined to be at an adsorbed NO_2 surface coverage of ~30%. The reaction of NO_2 with oxide and authentic dust surfaces is found to be stoichiometric and not catalytic in nature, indicating that surface saturation must be taken into account in the modeling analysis.

The modeling investigation used a box-model analysis to determine the importance of the heterogeneous reaction of NO_2 on oxides and dust, using conditions representative of a region in China affected by anthropogenic pollution and mineral aerosol in the spring. Simulations examined a range of chemical and physical conditions and took into account some

of the findings based on the Knudsen cell study. The following reaction series was employed:

$$NO_2(g) \rightarrow NO_2(a) \quad \text{until 30\% coverage} \qquad (16)$$

$$2NO_2(g) \rightarrow NO_3(a) + NO(g) \quad \text{after 30\% to full coverage} \qquad (17)$$

$$\text{no reaction} \quad \text{after full coverage} \qquad (18)$$

The results of the simulation showed a quick increase in ozone, but as NO_x is quickly converted, the ozone production decreases rapidly. The system becomes destructive to ozone after ~15 h. In summary, the NO_2 heterogeneous reaction serves to accelerate NO_x loss and to reduce net O_3 production and nitric acid concentrations; however, for the heterogeneous uptake of NO_2 to be important, the uptake coefficient must be $\geq 10^{-4}$ to have any effect. Because the experimental values determined in the study were all at least an order of magnitude lower, the NO_2 reaction on mineral particles is not expected to greatly affect the concentrations of NO_x or O_3 in the troposphere. Importantly, though, these values were determined under very dry conditions and must be considered lower limits as adsorbed H_2O may play a significant role.

A separate study by Börensen et al. used DRIFTS to examine the mechanism and kinetics of NO_2 reaction on alumina.[183] The reaction order and uptake coefficient were determined, and the number of nitrite and nitrate ions formed was measured by ion chromatography. NO_2 was added to an IR cell with heat-treated alumina, and the clearest bands observed were assigned to nitrate, in concurrence with other studies (vide supra). It was noted that heating the reacted sample to 773 K did not result in desorption of any products, indicating a strongly bound adsorbed species. Absorption bands due to nitrite also appeared to grow in fast initially to a maximum, after which they decreased. On the basis of observations of changes in the OH region, the following mechanism for NO_2 adsorption onto Al_2O_3 surfaces was proposed:

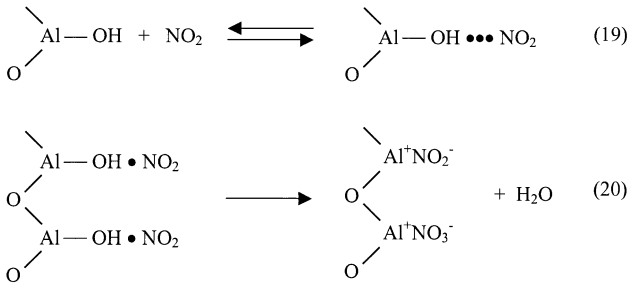

involving a cooperative effect for NO_2 adsorption via a disproportionation reaction for the two NO_2 molecules in close proximity, resulting in both nitrite and nitrate on the surface.

Determination of the reaction order was accomplished by plotting the log of the rate of nitrate formation as a function of the log of the NO_2 concentration. It was found that the reaction order is nearly 2 in NO_2 (1.86 ± 0.1), which supports the mechanism above. The surface coverage was determined by ion chromatography, which yielded the value of 2.3×10^{18} ions m^{-2} for a saturated sample, in good agreement with Underwood et al.[179] and Judeikis et al.,[195] and amounts to ~30% of the total surface covered in nitrate. Uptake calculations yielded an uptake coefficient of 1.3×10^{-9} to 2.3×10^{-8}, values which were also in good agreement with that calculated by Underwood et al.[178,179] The importance of the NO_2 reaction with alumina was estimated to be negligible on the basis of assumptions of dust concentrations and aerosol size with calculated uptake coefficients. This serves to corroborate the conclusions of previously discussed studies.

Although the studies described above were all performed under conditions of 0% RH, the presence of water on the surface of mineral dust in the atmosphere may change the surface chemistry. To address this, Goodman et al. probed the reaction of NO_2 with water molecules adsorbed to the surface of silica particles to examine the importance of the reaction

$$2NO_2(g) + H_2O(a) \rightarrow HONO(g) + HNO_3{-}SiO_2 \qquad (21)$$

as a source of HONO in the troposphere.[169] HONO is an important compound in the troposphere, serving as a major source of OH radicals, through its photolysis in the gas phase.[199,200] The importance of this compound is recognized, but its sources are not well understood. Gas-phase mechanisms, such as the reverse of the photolysis reaction to form HONO through homogeneous pathways, have been proposed. However, HONO concentrations remain high at night, when OH species are low, so this mechanism cannot be responsible for the persistence of HONO in the dark. The reaction of NO_2 with H_2O in the gas phase is shown to be too slow to be relevant under atmospheric conditions, but evidence suggests it may be accelerated via heterogeneous pathways, and mechanisms suggesting reaction of nitrogen oxides and water on surfaces have been proposed.[201−213] A field study done in New Zealand over the city of Christchurch reported close correlations between the ratio of HONO concentrations to NO_2 concentrations and aerosol densities, suggesting significant HONO formation potentially occurred on aerosol surfaces.[214] Finally, during two dust storm events in Phoenix, AZ, in the summer of 2001, Shuhui et al. measured a significant increase in the ratio of HONO to NO_2.[215] The authors suggest this was due to a highly efficient NO_2 to HONO conversion process on the surface of mineral dust particles.

In the study by Goodman et al.,[169] the reaction of NO_2 on hydrated silica particles was examined by FT-IR and UV−vis spectroscopy to characterize gas-phase and surface-bound species and with a flow reactor (Knudsen cell) to quantify the HONO production. When NO_2 was added to an IR cell containing silica particles having a surface water coverage of ~0.08 monolayer, bands appeared in the IR spectrum that were assigned to the vibrational modes of adsorbed HNO_3. The reaction was followed as a function of NO_2 pressure, and at low pressures the bands assigned to adsorbed HNO_3 increased until at

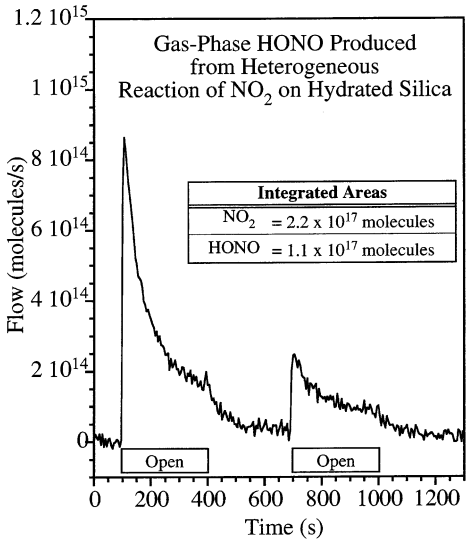

Figure 23. HONO production monitored by mass spectrometry as a function of NO_2 exposure on a hydrated SiO_2 sample in a flow reactor cell. HONO is produced from the reaction of nitrogen dioxide with water adsorbed on the silica surface according to the reaction $2\ NO_2(g) + H_2O(g) \rightarrow HONO(g) + HNO_2(a)$. The integrated areas of the calibrated amount of NO_2 taken up by the surface compared to HONO produced agree very well with the stoichiometric reaction (21). (Reprinted with permission from ref 169. Copyright 1999 American Chemical Society.)

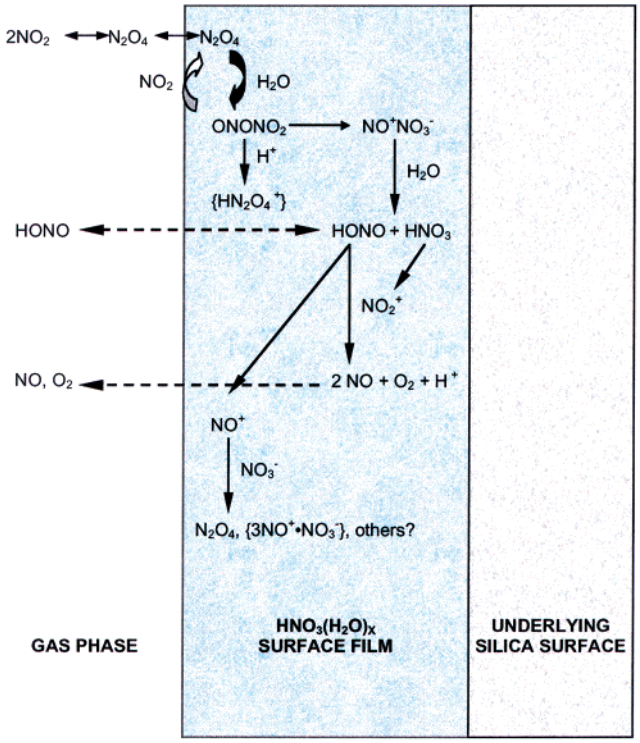

Figure 24. Schematic diagram of proposed mechanism of heterogeneous hydrolysis of NO_2. (Reproduced with permission from *Phys. Chem. Chem. Phys.* 5, pp 223−242; B. J. Finlayson-Pitts, L. M. Wingen, A. L. Sumner, D. Syomin, and K. A. Ramazan. Copyright 2003 PCCP Owner Societies.)

even higher pressures peaks for N_2O_4 also appeared. When the gas phase was evacuated, weak bands for oxide-coordinated nitrate remained. HONO production was also observed in the gas phase in the flow reactor (see Figure 23). The formation of HONO was confirmed by transmission UV−vis spectroscopy, apparent from the absorption between 310 and 390 nm.

Flow cell measurements showed that NO_2 was not significantly lost to the surface of SiO_2 that had been dehydrated through overnight evacuation, but NO_2 uptake was observed when the sample had been pumped for a considerably shorter time period. HONO was also shown to be produced immediately when the sample of silica was exposed to NO_2, and the production decreased as NO_2 uptake decreased. The ratio of HONO formation to NO_2 taken up by the surface was determined to be 2, consistent with the stoichiometry expected from the reaction. The study demonstrated that adsorbed water participates in surface reactions and does not only serve as a medium for adsorption and reaction of ionic species. Mineral dust surfaces in the troposphere will surely have adsorbed water and can provide a surface on which nitrous acid can form.

Finlayson-Pitts and co-workers[216] have recently summarized their extensive work, along with that of several others, concerning the heterogeneous hydrolysis of NO_2 on surfaces such as glasses (containing silicates). It was found that this reaction produces HONO and NO as the two major gas-phase products. The proposed mechanism of the reaction was explored in detail and is pictorially represented in Figure 24. The salient features of the mechanism are summarized as follows. First, gas-phase NO_2 forms N_2O_4 on the surface, and it is the N_2O_4 that is the important precursor species in the reaction. Second, adsorbed N_2O_4 may interact with water molecules, undissociated HNO_3 molecules (formed in the reaction of NO_2 with hydrated silica surfaces), or HNO_3-H_2O complexes or hydrates. Third, N_2O_4 isomerizes to form surface asymmetric $ONONO_2$, which subsequently autoionizes to form $NO^+NO_3^-$. Fourth, $NO^+NO_3^-$ reacts with water to generate HONO and HNO_3. Finally, secondary reactions of HONO are the likely source of the observed gas-phase NO.

The reaction order in NO_2 was determined through two different analyses. First, the data were evaluated by comparing the linearity of first-order reaction plots (i.e., ln $[NO_2]$ vs time) to the linearity of second-order reaction plots (i.e., $1/[NO_2]$ vs time). However, data plotted in both ways were found within statistical error to be more or less linear. Thus, this method was determined to be inconclusive in determining the NO_2 reaction order. The second method utilized the rate law, $R = k[NO_2]^a[H_2O]^b$, whereby the log of the initial rate loss of NO_2 was plotted versus the log of the initial NO_2 concentration, in the form $\log(R) = \log k + a \log [NO_2] + b \log [H_2O]$, where a is the order of the reaction with respect to NO_2 concentration. Ultimately, the order of the NO_2 hydrolysis reaction with respect to NO_2 was reported as 1.6 ± 0.2, which is somewhat higher than the 1.0−1.2 range determined in other studies.[202−205] These new results suggest in contrast to the other studies that the reaction is not first-order in NO_2 concentration.

The hydrolysis of NO_2 to form HONO was seen to occur regardless of the surface on which the reactions took place, indicating that the underlying surface did

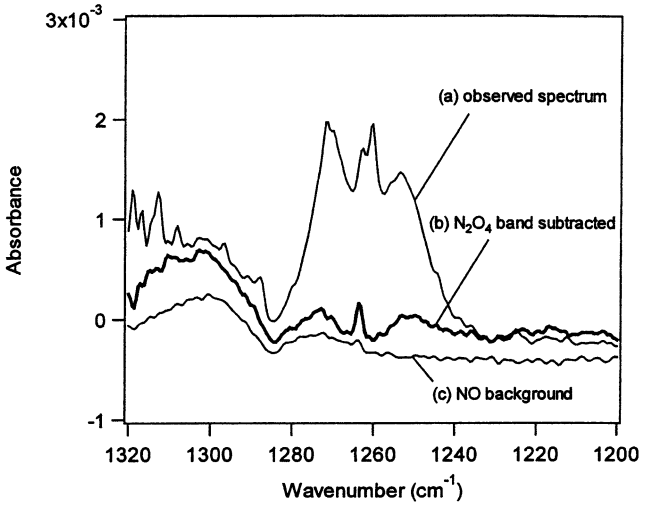

Figure 25. Gas-phase infrared spectra recorded after 120 min during the reaction of adsorbed nitric acid with nitric oxide. The observed spectrum clearly shows the ν_3 band of gas-phase *trans*-HONO at a concentration of $\sim 2 \times 10^{14}$ molecules cm^{-3}. Also shown in the figure is the spectrum of background NO. (Reprinted with permission from ref 218. Copyright 2000 American Chemical Society.)

not significantly affect the chemistry; rather, reaction takes place in a film on the surface that contains water, nitric acid, and species that are formed from these components. Thus, the authors anticipated that such reactions may take place not only on glass but also on other surfaces that take up water and provide the thin film necessary for the reaction. Stone, soil, and vegetation surfaces all are capable of water uptake and are expected to participate in HONO production in areas with high NO_2 levels.[217] Additionally, the wide variety of airborne particles, including mineral dust, will provide surfaces for this hydrolysis reaction. Using the results of the laboratory studies described in that report and assuming a NO_2 concentration of 0.1 ppm at 50% RH, it was determined that over 10 h the total HONO concentration formed on the estimated available surface area of sand and soil would be in the range of 40−600 ppt, easily accounting for the typical range of HONO concentrations measured in the atmosphere.

2.1.4. Nitric Acid Reaction with Nitric Oxide on Mineral Dust: Another Source of HONO?

Finlayson-Pitts and co-workers have also investigated another heterogeneous HONO-producing reaction.[218−220] The surface reaction of gas-phase NO with adsorbed HNO_3 in the presence of water vapor was found to produce HONO.[218−220] Glass was used as the surface on the basis of the prevalence of silica surfaces found in the troposphere. Using transmission FT-IR, Mochida and Finlayson-Pitts showed that porous glass could act as a surface to hold adsorbed HNO_3 and H_2O.[218] NO was then introduced to the reaction chamber, and after 60 min, the surface HNO_3 coverage was seen to decrease while NO_2 and its dimer, N_2O_4, increased. Almost all of the NO_2 and small amounts of HONO were observed in the gas phase (see Figure 25). Because the product yield was small (but considerably greater than background impurities in the NO), removal of HONO by rapid, simultaneous secondary reactions must be occurring, perhaps with adsorbed nitric acid.

The proposed mechanism for the heterogeneous reaction involves the following steps

$$NO(g) + HNO_3(a) \rightarrow NO_2 + HONO \quad (22)$$

$$HONO(g) + HNO_3(a) \rightarrow 2NO_2 + H_2O \quad (23)$$

$$2HONO(g) \rightarrow NO + NO_2 + H_2O \quad (24)$$

with a net reaction from combinations of the above reactions as

$$NO + 2HNO_3(a) \rightarrow 3NO_2 + H_2O \quad (25)$$

and was found to be consistent with measured stoichiometry.

The small amounts of HONO in the system suggest that there are comparable formation and removal rates, possibly through reactions 23 and 24. Experiments in excess HNO_3 compared to NO showed that HNO_3 formation levels off above zero at longer reaction times and that 25% of NO remains unreacted, suggesting that NO and HNO_3 are renewed in secondary reactions. The reaction kinetics were studied by following the decay of nitric acid and the production of NO_2 gas as a function of time. The reaction was found to be first-order in NO.

A discussion of this reaction in regard to its atmospheric relevance revealed that the reaction of HNO_3 with NO is significantly enhanced in the presence of SiO_2 relative to reaction between only gas-phase species. The importance of the net loss of HNO_3 will depend on the amount of HNO_3 that is adsorbed to surfaces relative to the total HNO_3 in the troposphere and also on the ability of the heterogeneous mechanism to compete with homogeneous loss mechanisms. The reaction is shown to regenerate photochemically active forms of NO_x and possibly act as a source of HONO and, as such, is of potential importance in the chemical processes of the troposphere.

Further examination of the HONO-producing capabilities of the reaction of NO with adsorbed nitric acid was performed by Saliba et al.[219] Extending the studies described previously allowed for extrapolation of results to ambient conditions to determine the importance of the reaction as a source of HONO. Using FT-IR spectroscopy to analyze for both adsorbed and gas-phase species, NO_2 was the major product of the reaction between adsorbed nitric acid and nitric oxide, consistent with the described reaction 22. Small amounts of HONO were generated but thought to be removed under the laboratory conditions. Kinetics showed first-order behavior in NO for all ranges of NO concentrations, suggesting it is realistic to extrapolate to atmospheric levels. The relative importance of several reaction mechanisms was assessed under a set of assumptions concerning NO and NO_2 concentrations, density, size and surface area of particles, and relative humidity. With rates measured for reaction 22 under the assumed conditions, $\sim$1 ppb of HONO would be generated in 8 h, which is an estimate that is of the same order of

magnitude as measured for tropospheric HONO levels. Therefore, the authors suggested that the reaction cannot be ignored as a potential HONO source. However, reaction of NO + NO_2 + H_2O on surfaces would form only 10^{-6} ppb of HONO in 8 h, on the basis of measured rates, which is far too low to be significant. In contrast, the reaction $2NO_2$ + H_2O on surfaces was calculated to yield ~0.9 ppb of HONO, similar to yields formed by reaction 22. It is concluded that heterogeneous reaction of NO with adsorbed nitric acid could be a significant source of HONO in polluted areas, and because the reaction converts nitric acid to NO_x, it could serve to reconcile discrepancies between measured and modeled ratios of HNO_3 to NO_x.

Finally, the dependence of reaction 22 on surface adsorbed water was investigated by Saliba et al.[220] The net reaction described earlier (reaction 5) shows that water as a product may affect the process. Reaction 22 was studied as a function of surface water to probe the reactive forms of nitric acid on the surface. In a cell void of water, there was no detectable loss of NO by reaction with adsorbed HNO_3 and only slow formation of NO_2 was seen. When the surface was covered in ~1 monolayer of water, NO_2 was formed at a slightly higher rate. With 3 monolayers, the reaction was observed to be much faster, noting measurable losses of NO and rapid formation of NO_2. However as the water coverage increased to five monolayers, the rate of the reaction decreased. The results demonstrate a complex dependence of the reaction rate on the presence of water on the surface.

The adsorbed water is capable of solvating reaction products. HONO is shown by Henry's law constants to be far more soluble than NO_2, so the solvation of product HONO would be important. HONO can remain on the surface and be subjected to further reaction with the adsorbed HNO_3, a reaction that seems more likely than a bimolecular reaction of two HONO molecules, although the latter cannot be ruled out. The reaction of HONO with HNO_3 is thought to form N_2O_4 initially, rather than two NO_2 molecules, so the mechanism of that reaction is reported to be

$$HNO_3(a) + HONO(a) \rightarrow N_2O_4(a/g) + H_2O(l) \quad (26)$$

with N_2O_4 eventually dissociating into two NO_2 gas molecules. On the basis of the important role of water as observed in the experiments, the reaction

$$2HNO_3(a) + 3H_2O(a) + NO(g) \rightarrow NO_2(g) + N_2O_4(a) + 4H_2O(l) \quad (27)$$

may be thought to be a more accurate representation of the overall reaction.

A recent report by Rivera-Figueroa et al. describes potential mechanisms involving nitric acid for the "renoxification" of the troposphere.[221] The heterogeneous reactions of nitric acid in thin water films on the surface of silica with NO, CO, CH_4, and SO_2 were studied with FT-IR. Although no reaction was observed between the nitric acid−water thin films and CO, CH_4, and SO_2, NO was found to react with HNO_3 on the surface, as described in earlier studies. The reaction probability, γ^{NO}, was determined to be $(6 \pm 2) \times 10^{-9}$ and is considered to be a lower limit. Although the value is small, the reaction can occur over hours to days in a polluted atmosphere.

Because silica surfaces will be ever-present in the troposphere, as well as water vapor, these studies by Finlayson-Pitts and co-workers show that with appropriate amounts of water in which HNO_3 remains undissociated, the heterogeneous conversion of HNO_3 to NO_2 on some kind of silica surface could have significant implications for the chemistry of the troposphere. Therefore, it was concluded that these reactions need further consideration.

2.1.5. Summary of Nitrogen Oxide Studies

The studies described in section 2.1 on nitrogen oxides are compiled in Table 6. The reactive gas, surface, and techniques used to investigate gas−surface interactions are listed along with the reference citations. The results of the HNO_3 studies show that uptake of nitric acid is an important process, especially for carbonate-containing minerals, and that adsorbed water plays a significant role in this chemistry. HONO production involving the reactions of NO_2 (reaction 21) and nitric acid (reactions 22−24) may be important as sources of HONO in the troposphere. Reactions of molecular nitric acid with NO can also serve as a source of HONO; however, it is important to note that under realistic tropospheric conditions with a lot more basic minerals than pure SiO_2, surface-adsorbed nondissociated HNO_3 may or may not be a prevalent surface species. Further studies using authentic mineral dust samples are needed. Finally, there exists a discrepancy between laboratories with regard to uptake coefficients of nitric acid measured on powdered samples with many layers, indicating that studies on single and isolated particles are warranted.

2.2. Sulfur Dioxide

The major source of tropospheric sulfur dioxide is coal-fired power plants, with some small amounts emitted by volcanoes. About 75% of the total sulfur emissions are anthropogenic, with 90% of those occurring in the northern hemisphere.[102] SO_2 is the principal sulfur-containing anthropogenic pollutant, with urban concentrations reaching into hundreds of parts per billion.[102] SO_2 acts as a precursor to sulfuric acid, which contributes to acid rain and particulate formation. Atmospheric SO_2 can be oxidized to sulfuric acid through several pathways in the troposphere, including in clouds and liquid droplets; however, not all of these pathways are completely understood.[222]

Sulfuric acid may perhaps be the most important precursor compound involved in the formation of secondary inorganic aerosol in the atmosphere.[223] Nearly half of the global emissions of SO_2 are converted to particulate sulfate, and this sulfate is often associated with particles, either sea-salt in marine regions or mineral dust.[112] Conversion of SO_2 to SO_4^{2-} on sea-salt aerosols may account for up to 60% of the oxidation in the marine troposphere,[222] whereas mineral aerosol has also been shown to participate in the accumulation of particulate sulfate

Table 6. Summary of Laboratory Studies Reviewed under Section 2.1

reactive species	sample(s)	technique	measurements	reference
NO, NO_2	sandy loam, adobe clay soil, commercial bagged cement, wood charcoal, MnO_2, PbO, Al_2O_3	cylindrical flow reactor	deposition velocity	Judeikis and Wren, 1978 (ref 195)
HNO_3, NO_2	NaCl, $CaCO_3$, "soil I" (mostly carbonates), "soil II" (mostly aluminosilicates), sand, seawater	SEM/EDX, TEM, wet chemistry for nitrate analysis	quantification of surface product, observation of surface product	Mamane and Gottlieb, 1992 (ref 165)
HNO_3	$CaCO_3$, Na_2CO_3, "marble powder" ($CaCO_3$), oolithique calcaire (contains $CaCO_3$, SiO_2, Al_2O_3, Fe_2O_3, MgO)	Knudsen cell	uptake coefficient	Fenter et al., 1995 (ref 185)
NO_2	NaCl, Al_2O_3	FT-IR, diffuse reflectance UV−vis	surface adsorption, reaction mechanism	Goodman et al., 1998 (ref 197)
NO_2	Al_2O_3, TiO_2	FT-IR, diffuse reflectance UV−vis	surface adsorption	Miller and Grassian, 1998 (ref 198)
NO_2	SiO_2	FT-IR, diffuse reflectance UV−vis, Knudsen cell	surface adsorption, reaction product identification	Goodman et al., 1999 (ref 169)
NO_2	Al_2O_3, Fe_2O_3, TiO_2	Knudsen cell, FT-IR	surface adsorption, reaction mechanism, uptake coefficients	Underwood et al., 1999 (ref 179)
HNO_3 + NO	borosilicate glass	FT-IR	surface adsorption, reaction product identification, reaction mechanism	Mochida and Finlayson-Pitts, 2000 (ref 218)
HNO_3, NO_2	Al_2O_3	DRIFTS	surface adsorption, uptake coefficients	Börensen et al., 2000 (ref 183)
HNO_3	$CaCO_3$	FT-IR, Knudsen cell	surface adsorption, uptake coefficients, reaction mechanism	Goodman et al., 2000 (ref 170)
NO_2, HNO_3	γ-Al_2O_3, α-Al_2O_3, α-Fe_2O_3, carbon black, TiO_2, $CaCO_3$	Knudsen cell	uptake coefficients	Underwood et al., 2000 (ref 178)
HNO_3 + NO	borosilicate glass	FT-IR	reaction product identification, reaction mechanism	Saliba et al., 2000 (ref 219)
HNO_3 + NO, H_2O	borosilicate glass	FT-IR	surface adsorption, reaction product identification, reaction mechanism	Saliba et al., 2001 (ref 220)
HNO_3	Al_2O_3, $CaCO_3$, Saharan sand, Arizona test dust	Knudsen cell	uptake coefficients	Hanisch and Crowley, 2001 (ref 171)
HNO_3	dolomite, orthoclase, kaolinite, chlorite, montmorillonite, illite, smectite, paly-gorskite, Chinese dust	Knudsen cell	uptake coefficients	Hanisch and Crowley, 2001 (ref 172)
HNO_3, H_2O	SiO_2, α-Al_2O_3, TiO_2, γ-Fe_2O_3, CaO, MgO	FT-IR	surface adsorption, uptake coefficients	Goodman et al., 2001 (ref 184)
HNO_3	α-Al_2O_3, α-Fe_2O_3, SiO_2, MgO, CaO, China loess, Saharan sand	Knudsen cell	uptake coefficients	Underwood et al., 2001 (ref 166)
HNO_3, NO_2	α-Al_2O_3, γ-Al_2O_3, α-Fe_2O_3, γ-Fe_2O_3, TiO_2, SiO_2, MgO, CaO, China loess, Saharan sand	Knudsen cell	uptake coefficients	Underwood et al., 2001 (ref 180)
NO_2	borosilicate glass	FT-IR	reaction product identification, reaction mechanism	Finlayson-Pitts et al., 2003 (ref 216)
HNO_3 + NO, CO, CH_4, or SO_2	borosilicate glass	FT-IR	surface adsorption, uptake coefficients	Rivera-Figueroa et al., 2003 (ref 221)

in the troposphere. It is well-known that SO_2 can be oxidized to sulfate in aqueous aerosol by ozone and hydrogen peroxide;[156,222,224−235] however, the mechanisms of sulfate formation on mineral aerosol are not completely understood.[148,222] It has been proposed that ozone can oxidize adsorbed sulfite to adsorbed sulfate on particle surfaces.[236,237] In addition, S(IV) oxidation by molecular oxygen can be catalyzed by iron-containing species.[227,238,239] Sulfate particles are known to affect climate by scattering solar radiation, resulting in a net cooling effect, as well as acting as cloud condensation nuclei and thereby indirectly affecting climate.[102,148,240−242] On the basis of these known important properties, a better understanding of the origin of sulfate on mineral dust particles is desirable. In the next few subsections, laboratory experiments on the heterogeneous uptake and oxidation of SO_2 are described as well as phase changes associated with sulfate coatings on mineral dusts.

2.2.1. Sulfur Dioxide Uptake and Oxidation on Mineral Dust

Laboratory studies have been initiated to better understand the interaction of sulfur dioxide with dust and the role that dust may play in the oxidation of tropospheric sulfur dioxide to sulfate. The motivation of these studies was based on the assessment of the impact of heterogeneous conversion on dust surfaces in partitioning sulfur dioxide from the gas phase to particulate sulfate, as well as to glean information about the mechanisms by which these reactions occur.

In the late 1960s and 1970s, laboratory studies of the heterogeneous reactions of SO_2 were undertaken with the recognition that gas−aerosol reactions could be important in the atmosphere.[243,244] It had been noted that SO_2 removal from gas mixtures was more efficient by the presence of certain solid materials. Metal oxides have been studied as adsorbents to clean industrial emissions of SO_2.[245−257] However, these studies cannot be directly used to understand the heterogeneous atmospheric chemistry of SO_2 due to the atmospherically irrelevant conditions used.

Early studies noted that solid particulates were not able to continuously scrub SO_2 from gas mixtures, and SO_2 uptake had a "capacity limited" nature.[258−262] For example, Urone et al. determined that the reaction of SO_2 with hydrous ferric oxide went to completion within seconds to minutes, whereas the reaction with Fe_3O_4 was only 17% in 4 min and was thought to be slower due to the smaller BET surface area.[263] Rates for other mineral compounds such as $CaCO_3$, CaO, Al_2O_3, and other metal oxides were much smaller than for the iron compounds, indicating that particles containing iron may be important for the removal of SO_2 from gas mixtures. Smith et al. also found that SO_2 will adsorb to metal oxide surfaces in the parts per million concentration range.[264] The capacity of iron-containing particles to adsorb SO_2 was examined by Chun and Quon.[244] Iron oxide particles that were produced through combustion of iron pentacarbonyl were exposed to SO_2 concentrations of 5−19 ppm in air, and the sulfate formed on the surface was determined through analysis of the filtrate after the particles were boiled and washed in water. Average quantities of sulfate formed were between 7 and 18 mg of SO_4^{2-} per 5 g of iron oxide. Importantly, it was determined that the surface of the iron oxide was not catalytic toward oxidation of SO_2 and that reactive sites on the surface were blocked toward further reaction.

The capacity-limited nature of SO_2 removal was also studied by Judeikis et al., who investigated the heterogeneous uptake of SO_2 onto various solids.[243] The heterogeneous uptake of SO_2 with a variety of fly ash samples from different coal-fired power plants in the United States and certain selected metal oxides was performed in a cylindrical flow reactor. Solid samples were exposed to gas mixtures of SO_2 in nitrogen, containing 0−10% oxygen, with SO_2 concentrations in the range of 3−100 ppm. Analysis of SO_2 loss was measured by mass spectrometry, whereas sulfate formation was determined by wet chemical methods and X-ray photoelectron spectroscopy (XPS).

The reactivity of each sample with SO_2 was expressed in terms of an initial collision efficiency. The initial collision efficiency is defined as the ratio of the number of gas molecules that are lost from the gas phase per second to the total number of gas−surface collisions per second, which is the same definition of the uptake coefficient described previously. These values ranged from 1×10^{-3} for MgO down to 1×10^{-6} for a sample of fly ash from River Bend in Charlotte, NC. The values of the initial collision efficiency were found to be independent of SO_2 and

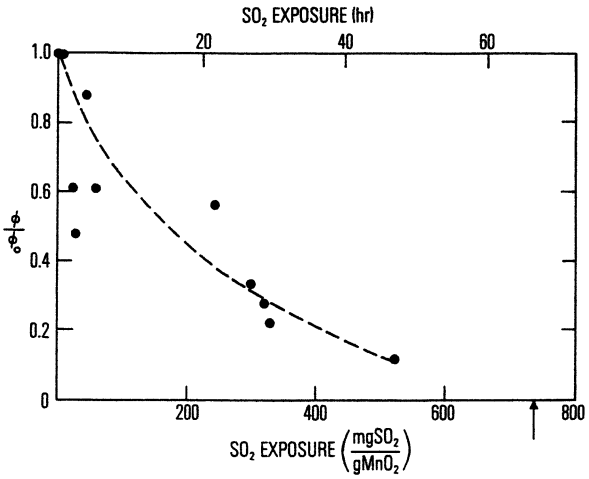

Figure 26. Decrease in collision efficiency (uptake coefficient) as a function of SO_2 exposure on manganese oxide. (Reprinted from *Atmos. Environ. 12*, pp 1633−1641; H. S. Judeikis, T. B. Stewart, and A. G. Wren, Laboratory studies of the heterogeneous reactions of SO_2. Copyright 1978 Elsevier.)

O_2 concentrations and were also unaffected by changes in relative humidity and total pressure. It was then concluded that the removal of SO_2 by the heterogeneous reaction is first order with respect to SO_2 concentration. The uptake coefficient was also found to be independent of the thickness of the sample, indicating that only the outer layer of the particles was reacting, although it is important to note that no systematic study of sample thickness was presented.

As exposure to SO_2 continued, the rate of adsorption was found to decrease until the surface showed no further reactivity toward SO_2. Figure 26 shows the decrease in collision efficiency of SO_2 reaction on MnO_2 upon continued SO_2 exposure. The capacity of each solid for SO_2 removal was calculated and in most cases was found to increase when relative humidity increased. In addition, under humidified conditions, the decrease of the rate of adsorption with time was more gradual than under dry conditions.

MnO_2 showed an increase to nearly 7 monolayers at 95% relative humidity. Wet chemical and XPS analyses determined that SO_2 quantitatively converted to adsorbed sulfate except in the case of Al_2O_3, for which little sulfur of any kind was detected, suggesting that SO_2 did not adsorb to Al_2O_3 to any great extent.

To probe regeneration of a saturated sample, fly ash that had been reacted with SO_2 was washed with water to remove the sulfate ion. The washing process resulted in a sample that was once again reactive toward gas-phase SO_2. In another experiment, a sample of fly ash that had been reacted with SO_2 until the surface was completely saturated was then exposed to ammonia gas. The uptake coefficient after exposure to ammonia was restored to ∼50% of its initial value. Because the fly ash samples were thought to have already been exposed to SO_2 in the flue gas of the power plants where they were collected, the rates of removal for these materials were quite low and were considered to be lower limits. It is also noted that the fly ash samples may have some

organic fraction that is not quantified; thus, the rates do not reflect uptake onto clean, fresh material.

In 1989, Mamane and Gottlieb performed bulk- and single-particle analyses on minerals that had been reacted with SO_2 to provide quantitative information about their conversion to sulfate and to provide direct proof for sulfate formation.[196] Samples of cement and clay soil were studied under different mineral loadings and times of exposure at constant relative humidity and SO_2 concentration. Bulk analysis showed that for the chosen mineral loadings the amount of sulfate formed was proportional to mineral mass. Capacity for sulfate formation for each of the mineral samples was determined. SO_2 adsorption capacities extended from 75 to 150 mg of sulfate g^{-1} of mineral under the reaction conditions reported in that study. SEM and EDX analyses of individual particles before and after reaction with SO_2 were performed. The analyses showed that before reaction, mineral particles were composed of primarily elements found in the Earth's crust including Mg, Al, Si, K, Ca, and Fe. Analysis revealed that 75% of the minerals was composed predominately of aluminosilicates with the remainder as carbonates. Conversely, the cement particles were mainly carbonates (60%), and the remaining composition was identified as gypsum, chlorides, and silicates, all present in equal amounts. After reaction, it was found that the S/Si and S/Ca ratios in the soil sample increased appreciably. However, the carbonate minerals in a cement sample showed a negligible increase in sulfur content, whereas the silicate portion did. The carbonate minerals were thought to have previously reacted to saturation in flue gases; therefore, no increase in sulfur was observed during the experiments. It was concluded from both bulk and individual particle analyses that not all minerals reacted with SO_2 under the reaction conditions employed.

In later studies, the mechanism and kinetics of the heterogeneous reaction of SO_2 with minerals was further examined by Goodman et al.[168] and Usher et al.[181] Using α-Al_2O_3 and MgO as model dust compounds, the surface after reaction with SO_2 was characterized through transmission FT-IR. Results of the FT-IR experiments showed that absorption bands in the infrared could be assigned to vibrational modes of sulfite and bisulfite on the surface. A negative feature in the hydroxyl region (3200−3500 cm^{-1}) indicated that surface hydroxyl groups were either lost or involved in hydrogen bonding at the surface during reaction. It was suggested that the surface-coordinated sulfite and bisulfite formed when SO_2 reacted with basic oxide anions (O^{2-}) or hydroxyl groups (OH^-) on the surface according to the following reactions:

$$O^{2-}(a) + SO_2(g) \rightarrow SO_3^{2-}(a) \quad (28)$$

$$OH^-(a) + SO_2(g) \rightarrow HSO_3^-(a) \quad (29)$$

$$\text{or} \quad 2OH^-(a) + SO_2(g) \rightarrow SO_3^{2-}(a) + H_2O \quad (30)$$

The irreversibility of the reaction of SO_2 with alumina as observed here was in contrast to what was observed by Judeikis et al.,[243] who noted the lack of sulfur content on samples examined with XPS, suggesting that the reaction of SO_2 with the alumina surface was reversible.

The surface coverages for SO_2 uptake on α-Al_2O_3 and MgO were determined to be $(1.5 \pm 0.3) \times 10^{14}$ and $(3.5 \pm 0.6) \times 10^{14}$ molecules cm^{-2}, respectively, at saturation. For α-Al_2O_3, this coverage corresponds to a capacity of 2.2 mg of SO_2 g^{-1} of oxide. On MgO, a coverage 4×10^{14} molecules cm^{-2} corresponds to a capacity of ~5.6 mg of SO_2 g^{-1} of oxide, which is comparable to what was determined by Judeikis et al.[243] for MgO at 0% RH. However, it should be noted that the surface areas may be different for the samples used by Judeikis et al., making a direct comparison difficult.

Because adsorbed water may be important in atmospheric reactions, the role of water adsorption on sulfite-coated particles of MgO and α-Al_2O_3 was investigated.[168] Particles that had been reacted with SO_2 to saturation were then exposed to water vapor as a function of increasing relative humidity between 1 and 93% RH. Besides the appearance of the bending mode of adsorbed water, only small changes were observed in the infrared spectra of sulfited Al_2O_3 as a function of relative humidity. When sulfite-saturated MgO was exposed to water, several new spectral features at 1110 and 957 cm^{-1} were apparent in the spectrum and were assigned to the vibrational modes of sulfate. When the water was removed by evacuation, absorption bands at 1138 and 970 cm^{-1} remained, indicating a likely mixture of surface-coordinated SO_3^{2-} and SO_4^{2-}. An estimated 5−10% of the initial sulfite was converted to sulfate upon exposure to H_2O. Further investigation of the oxidation of sulfite in Usher et al. showed that sulfite could be oxidized quantitatively to sulfate in the presence of ozone.[181]

Usher et al. also investigated the heterogeneous kinetics of SO_2 uptake on a range of mineral oxide compounds as well as an authentic sample from a loess region in China using a Knudsen cell reactor.[181] Additionally, the oxidation of SO_2 on selected oxides was explored with transmission FT-IR spectroscopy. Uptake of SO_2 onto the oxide and dust samples, at an SO_2 pressure of 4 μTorr, scaled linearly with sample mass, demonstrating that diffusion to underlying layers occurred. Initial uptake coefficients were calculated for each sample through the linear mass regime method[178] and ranged from 10^{-7} to 10^{-4} (1×10^{-7} being an estimated upper limit for SiO_2, which exhibited no observable reactivity, and 5.1×10^{-4} for MgO).

The loess sample yielded a relatively low initial uptake coefficient of $(3 \pm 1) \times 10^{-5}$. The reactivity of the loess was thought to reflect its chemical composition. EDX analysis showed that the bulk China loess was composed of (excluding C and O) 48% Si, 22% Ca, 10% of both Al and Fe, and small amounts of K, Ti, and Mg as well (6, 2, and 1%, respectively). The X-ray maps displayed in Figure 27 show an aggregate of particles with an inhomogeneous distribution of the elements. If one considers the uptake of an authentic dust sample to be additive, that is, uptake

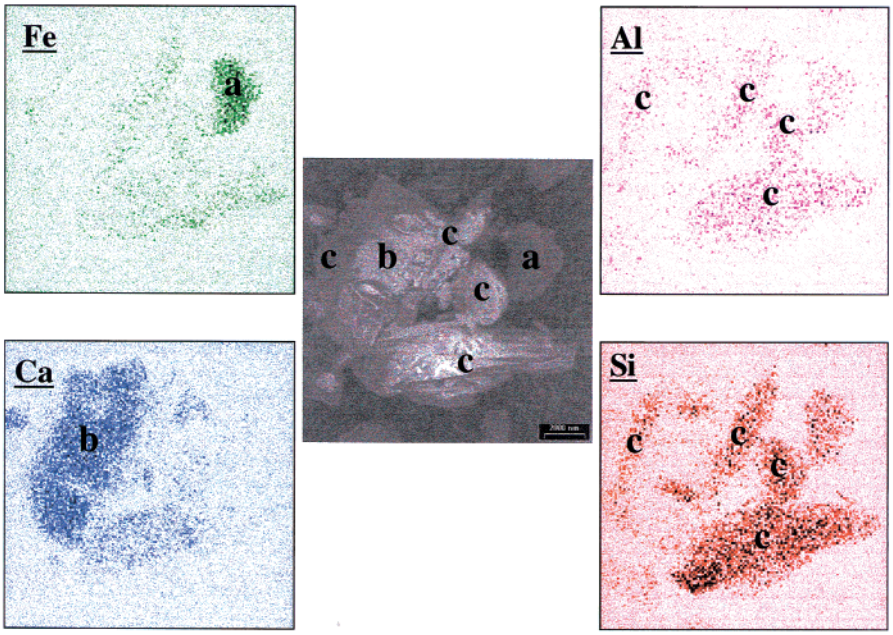

Figure 27. SEM image and EDX map of a particle aggregate of a China loess sample. The sample shows iron particles that are enriched with iron and calcium as well as aluminum silicates. The heterogeneous uptake of SO_2 on the loess sample was investigated. (Reproduced with permission from *J. Geophys. Res. 107*, D23, DOI 10.1029/2002JD002051; C. R. Usher, H. Al-Hosney, S. Carlos-Cuellar, and V. H. Grassian, A laboratory study of the heterogeneous uptake and oxidation of sulfur dioxide on mineral dust particles. Copyright 2002 American Geophysical Union.)

onto dust is a sum of the reactivity of its individual components, then

$$\gamma_{\text{loess}} = \Sigma_i f_i \gamma_i \tag{31}$$

where f_i is the fraction of the ith component (as determined by EDX in this case) and γ_i is the measured uptake coefficient for that component. The calculated value determined from the individual reactivities measured for pure oxides (carbonate in the case of calcium) and the elemental fractions agreed well with the experimentally determined uptake coefficient; that is, the uptake calculated from the individual components was determined to be $(4 \pm 2) \times 10^{-5}$, which compares well with the experimental value of $(3 \pm 1) \times 10^{-5}$. It should be noted this analysis assumes that all components of the loess sample have similar surface areas and are all present as oxides (and one carbonate). Thus, caution should be taken in extending these results to general cases. However, the results imply that chemical specificity of dust samples may be very important and should be taken into account in models that determine the impact of the presence of dust in the troposphere.

The importance of the heterogeneous pathway versus homogeneous loss mechanisms was assessed on the basis of comparing the lifetimes of gas-phase reactions to the rates of the heterogeneous reaction. At most aerosol densities, the heterogeneous loss of SO_2 (with γ between 10^{-4} and 10^{-5} as measured in this study) is competitive with gas-phase mechanisms in urban, dust, and maritime aerosol distributions, suggesting that even under dry conditions, the heterogeneous reaction of SO_2 will affect SO_2 partitioning in the troposphere.

Using DRIFTS, Ullerstam et al. investigated the oxidation of SO_2 on mineral dust by ozone.[265] Authentic dust samples from the Cape Verde Islands (dust with origins in the Sahara Desert) were exposed to gas mixtures of SO_2 in helium or SO_2 and O_3 in helium. The changes to the surface were followed with IR spectroscopy, whereas the amount of sulfate formed during the experiments was determined by ion chromatography.

First, the particles, which were known to have water adsorbed to the surface that was not completely removed by pretreatment, were exposed to only SO_2. The absorption bands observed at 1240 and 2450 cm^{-1} were attributed to sulfate. Ion chromatography showed both sulfite and sulfate, with sulfite arising from dissolved physisorbed SO_2. Another sample of dust particles was exposed to a mixture of SO_2 and O_3. In addition to absorption bands observed in the SO_2 in helium mixture, an absorption at 1714 cm^{-1} and a loss at 2800 cm^{-1} were observed in the spectrum as well (Figure 28). These additional features are due to the oxidation and loss of organic contaminants present on the native dust surface. The other difference observed when ozone was present in the gas mixture was the increased intensity of the peak at 1240 cm^{-1}, and thus the increase in the amount of adsorbed sulfate, as the experiment progressed. It was proposed that the increased production of sulfate came about from the surface-catalyzed oxidation of physisorbed SO_2 in the presence of ozone.

The importance of water vapor was also recognized in this investigation, and the effect of relative humidity on sulfate formation was examined. Samples exposed first to the SO_2/O_3 mixture were then exposed to 80% RH. When the water was pumped away, no major changes were observed in the spectra. The sample was also treated to alternating exposures of SO_2/O_3 and H_2O, and although no spectral changes

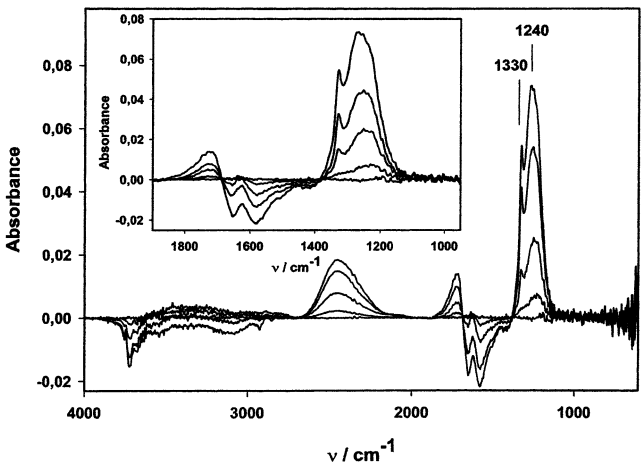

Figure 28. Difference infrared spectra recorded as a function of time of the reaction of mineral dust and SO_2 in the presence of ozone. The inset shows an expanded version of the region between 950 and 1700 cm^{-1}. (Reproduced with permission from *Phys. Chem. Chem. Phys. 4*, pp 4694−4699; M. Ullerstam, R. Vogt, S. Langer, and E. Ljungström. Copyright 2002 PCCP Owner Societies.)

were observed, the total sulfate formed increased by 47%.

Further analysis of the data showed that the reaction was approximately first-order in SO_2 and zero-order in O_3. It was also found that more than simply the top layer of the samples reacted and that diffusion of the reactant gas into the samples occurred.[178,180,181] The reactive uptake coefficient γ was determined according to the equation

$$\gamma = {}^1/_4 \times \mathrm{d}[SO_4{}^{2-}]/\mathrm{d}t/Z \quad (32)$$

where

$$Z = A_{\mathrm{surf}}[SO_2]\nu_{SO_2} \quad (33)$$

where ν_{SO_2} is the gas-phase mean speed of the SO_2 molecules and A_{surf} is the reactive surface area of the sample. γ values obtained in this study using both geometric and BET surface areas as the reactive surface were reported for varying experimental concentrations of SO_2 and O_3. The values of $\gamma SO_{2(\mathrm{geometric})}$ were in the mid-10^{-3} range, whereas $\gamma_{SO_2(\mathrm{BET})}$ values were in the mid-10^{-7} range. The mechanism of reaction is thought to occur through two main steps:

$$\{\mathrm{MeOOH}\} + SO_2(g) \rightarrow \{\mathrm{MeOOH}\cdots SO_2\} \quad (34)$$

which describes the reversible adsorption of SO_2 to active sites with hydroxyl groups on the surface (Me = metal component), and

$$\{\mathrm{MeOOH}\cdots SO_2\} + O_3 \rightarrow \{\mathrm{MeO}\cdots HSO_4\} + O_2 \quad (35)$$

which describes the irreversible oxidation of adsorbed SO_2 to sulfate by ozone. On the basis of the reaction kinetics, adsorption of SO_2 is the rate-determining step (reaction 34), most likely to form a surface sulfite/bisulfite species as described in reactions 28−30, followed by collision with ozone and immediate subsequent oxidation.

The natural origin of the samples studied makes the results of these experiments particularly relevant to atmospheric processes. With some assumptions as to atmospheric conditions and using calculated reactive uptake coefficients (both geometric- and BET-area derived), calculations demonstrated that for geometric calculated values, 46 mg m^{-3} sulfate could form during 13 days in the atmosphere if surface saturation is not an issue. In contrast, using BET-area calculated values, the sulfate formed would be only 0.0005 mg m^{-3}, a negligible value. The value for $\gamma_{SO_2(\mathrm{geometric})}$ would lead to a loss of 12 ppb of SO_2 in 13 days, on par with a loss of SO_2 due to homogeneous oxidation by OH radicals. According to Ullerstam et al.,[265] the uptake coefficient determined for O_3 uptake by surfaces with adsorbed SO_2 showed that O_3 loss by this process could approach values of O_3 loss that were observed in the ACE-2 campaign, indicating the heterogeneous conversion of SO_2 to sulfate by O_3 may be important.

The heterogeneous uptake kinetics of other sulfur oxides such as SO_3 and H_2SO_4 has yet to be investigated. However, as described below, phase transitions of sulfate coatings have been measured.

2.2.2. Sulfate Coatings [H_2SO_4, NH_4HSO_4, and $(NH_4)_2SO_4$] on Mineral Dust

A great deal of study has gone into the analysis of atmospheric particles, and it is often found that many of the particles collected in the field contain sulfate coatings. Andreae et al. observed a mixture of silicates and sulfates in marine aerosols collected over the equatorial Pacific between Ecuador and Hawaii.[266] The presence of mineral material in the marine atmosphere was thought to have occurred through cloud mixing and that the sulfate coating on the particles occurred by in-cloud processes, by which reactions of mineral particles and H_2SO_4 could deposit sulfate on the surface of the particle. Sulfate was also found in particles collected in and above Israel and above the Mediterranean Sea.[112] Among the particles analyzed, sulfate was found together with silicon, implying an interaction with sulfate and minerals originating from the desert regions. Proposed sources of these mixed sulfate−mineral particles included coagulation of sulfate particles [possibly NH_4HSO_4, $(NH_4)_2SO_4$, or H_2SO_4] and desert mineral aerosols or deposition of sulfate onto the mineral particles, where the oxidation of SO_2 to sulfate could occur on the surface possibly through mechanisms described under section 2.2.1. Buseck and Posfai have also noted the prevalence of mineral particles associated with hygroscopic sulfate, which can act as cloud condensation nuclei.[24] Field studies performed in China in 2000[267] and 2001[268] analyzed the composition of the particles collected in Qingdao and Xianghe, respectively. Particles collected in Xianghe were found to contain sulfuric acid on the basis of SEM micrographs. However, in Qingdao, sulfuric acid particles were not detected, and it was concluded that any sulfuric acid possibly formed through the oxidation of SO_2 would be neutralized by surface-adsorbed or gas-phase NH_3 present in the troposphere at the time of the measurements.

It is apparent that dust particles can accumulate thick sulfate coatings during their residence in the troposphere. The consequence of sulfate-coated particles is that they may influence the climate by scattering solar radiation, as noted above.[102] However, the phase of the coating on the particles can affect light-scattering properties. Laboratory and modeling studies have shown that ammonium sulfate particles with mineral inclusions can induce heterogeneous nucleation at a relative humidity higher than that found for homogeneous nucleation.[269] Sulfate coatings on the mineral particles were produced by flowing a gas mixture of SO_3, NH_3, and H_2O with the mineral inclusion that served as a substrate. Changes of the sulfate-coated inclusion, as a function of decreasing relative humidity, were observed using FT-IR. Whereas pure ammonium sulfate effloresces at 35 ± 2% RH, internally mixed particles [i.e., an oxide particle as the core coated with $(NH_4)_2SO_4$] with an Al_2O_3 core effloresced at 57 ± 2% RH, with a ZrO_2 core effloresced at 59 ± 2% RH, and with a TiO_2 core effloresced at 65 ± 2% RH. As the water content of the system decreased, the spectra changed such that the peaks corresponding to sulfate became less liquid-like, indicating SO_4^{2-} adsorbed to the oxide surfaces after the efflorescence relative humidity was passed. On the basis of the results of this study, the acidity of the TiO_2 surface that accommodated the negative charge of the sulfate anion was thought to be the reason it was the most effective heterogeneous nucleus.

Additional studies by Martin and co-workers further examine the effects of metal oxide cores on the efflorescence of ammonium sulfate particles.[270,271] In these studies, a variety of solid particles, including hematite, corundum, mullite, rutile and anatase TiO_2, and baddeleyite, were used to simulate the types of cores that may be present in the atmosphere. Some of the minerals investigated were more effective as heterogeneous nuclei for crystallization than others. Two hypotheses were proposed. The first hypothesis attempted to correlate the strength of the chemisorbed sulfate to the dust and the efficacy of the mineral to induce crystallization. The second hypothesis related the crystal structures between crystalline sulfate and the crystalline structure of the mineral surface. The first hypothesis could not adequately describe the results, whereas the second better matched the laboratory observations. Specifically, both hematite and corundum, with similar crystal structures, were efficient heterogeneous nuclei. TiO_2 particles were also found to have good epitaxial fits as compared to other oxides. The results were then described in the framework of an active site model. The active site model suggested that epitaxial matching is in fact a strong indication of heterogeneous nucleation activity.[270] In the active site model, corundum and hematite induced nucleation with similar efficacies, whereas other compounds such as mullite and baddeleyite were relatively poorer. In the case of hematite, the model showed that the crystallizing sulfate was highly ordered on the surface, binding to every other iron atom with two sulfate species bound to each iron. However, this was not observed spectroscopically, suggesting that perhaps the configuration between the sulfate and the surface during crystallization differed somehow after crystallization and drying had occurred, when the spectra were recorded. Another possibility not suggested by these authors is that iron oxide surfaces reconstruct under ambient conditions and are not well represented by bulk-terminated surface structures.

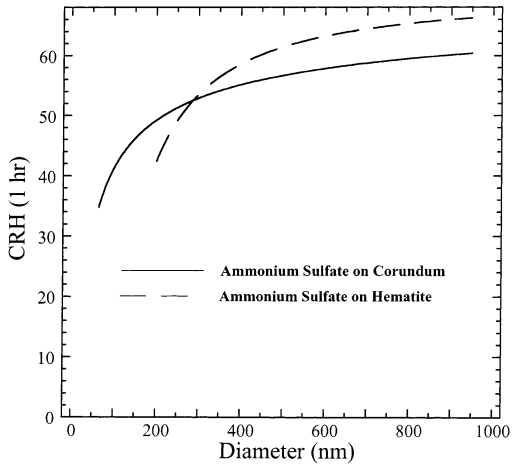

Figure 29. Plot of the heterogeneous crystallization relative humidities (CRH) of aqueous ammonium sulfate coated on mineral dust inclusions. The lines in the plot are for two different mineral dust inclusions, α-Al_2O_3 and α-Fe_2O_3, and are represented by the governing polynomials found from laboratory studies (based on studies by Martin et al.[272]).

The critical relative humidity at which the phase of the ammonium sulfate coating changes from aqueous to crystalline is approximated in a series of polynomials developed by Martin et al. and is dependent on the type of particle inclusion[272]

$$\mathrm{CRH} = 71.6 - 235(0.36)^{\mathrm{Log}D_c} \quad D_c \geq 65\ \mathrm{nm} \qquad (36)$$

$$\mathrm{CRH} = 70 - 25000(0.052)^{\mathrm{Log}D_h} \quad D_h \geq 65\ \mathrm{nm} \qquad (37)$$

where CRH is the crystallization relative humidity (or efflorescence), D_c is the diameter (nm) of a corundum core particle, and D_h is the diameter (nm) of a hematite core particle. These polynomials are plotted in Figure 29 for ammonium sulfate with corundum and hematite mineral inclusions. As was the case for ammonium nitrate coatings, the heterogeneous nuclei (mineral inclusions) regulated the relative humidity of the phase transition. It was found that as particle size increased, the crystallization or efflorescence relative humidity also increased. This was also observed by Onasch et al., who found that the efflorescence relative humidity increased with particle diameter and the nucleation rate was dependent upon the surface area (size) of the inclusion.[273] From the results of these studies, it is clear not only that mineral inclusions provide a surface on which sulfate coatings can form but also that the mineral dust particle itself will influence the phase of the sulfate coating.

Table 7. Summary of Laboratory Studies Reviewed under Section 2.2

reactive species	sample(s)	technique	measurements	reference
SO_2	NaCl, $CaCO_3$, Fe_2O_3, Fe_3O_4, Cr_2O_3, PbO, PbO_2, V_2O_5, CaO, Al_2O_3	colorimetry, scintillation counting (radiotracing)	reaction rates, reaction product identification	Urone et al., 1968 (ref 263)
SO_2, H_2S	γ-Al_2O_3, NaOH-doped γ-Al_2O_3, sodium Y zeolite, hydrogen Y zeolite	IR	surface adsorption, reaction mechanism	Deo et al., 1971 (ref 245)
SO_2	CaO	IR	surface adsorption, reaction mechanism	Low et al., 1971 (ref 246)
SO_2	MgO	IR	surface adsorption, reaction mechanism	Goodsel et al., 1972 (ref 248)
SO_2	MgO	IR	surface adsorption, reaction mechanism	Schoonheydt and Lunsford, 1972 (ref 247)
SO_2	Fe_2O_3	nephelometry, desorption and precipitation of SO_2	reaction rates, reaction product identification	Chun and Quon, 1973 (ref 244)
SO_2	γ-Al_2O_3	IR	surface adsorption, reaction mechanism	Chang, 1978 (ref 250)
SO_2	SiO_2, $SiO_2-Al_2O_3$	IR, ESCA, EPR	surface adsorption, reaction mechanism	Davis and Lunsford, 1978 (ref 249)
SO_2	MgO, Fe_2O_3, Mohave fly ash, Al_2O_3, MnO_2, Cholla fly ash, River bend fly ash, Shawnee fly ash, Louisville fly ash, PbO, charcoal, NaCl	flow reactor, wet chemistry ($BaCl_2/NO_3$ precipitation), XPS	reaction rates; reaction product identification; collision efficiencies (uptake coefficients)	Judeikis et al., 1978 (ref 243)
SO_2, H_2S	γ-Al_2O_3	IR, volumetric adsorption	surface adsorption, reaction mechanism	Karge and Dalla Lana, 1984 (ref 252)
SO_2	γ-Al_2O_3	FT-IR, EPR	surface adsorption, reaction mechanism	Datta et al., 1985 (ref 253)
SO_2	Al_2O_3, TiO_2 (anatase)	IR	surface adsorption, reaction mechanism	Saur et al., 1986 (ref 254)
SO_2	"local soil" (~75% aluminosilicates,25% carbonates) cement (~60% carbonates; gypsum, chlorides, silicates remainder)	SEM/EDX, TEM, wet chemistry	reaction product identification	Mamane and Gottlieb, 1989 (ref 196)
SO_2	MgO, CeO_2, ZrO_2, $MgAl_2O_4$, TiO_2 (anatase), TiO_2 (rutile), Al_2O_3, Na-doped Al_2O_3	TPD, IR thermogravimetric analysis	surface adsorption, reaction mechanism	Waqif et al., 1992 (ref 257)
SO_2	γ-Al_2O_3, Na-doped γ-Al_2O_3	DRIFTS, thermogravimetric analysis	surface adsorption, reaction mechanism	Mitchell et al., 1996 (ref 255)
$(NH_4)_2SO_4$	Al_2O_3, TiO_2, ZrO_2	FT-IR	efflorescence and deliquescence of ammonium sulfate particles	Han and Martin, 1999 (ref 269)
SO_2	α-Al_2O_3, MgO	Knudsen cell, FT-IR	uptake coefficients, surface adsorption, reaction mechanism	Goodman et al., 2001 (ref 168)
$(NH_4)_2SO_4$	hematite, corundum	DRIFTS, modeling	efflorescence and deliquescence of ammonium sulfate particles	Martin et al., 2001 (ref 271)
$(NH_4)_2SO_4$	corundum, hematite, mullite, rutile and anatase TiO_2, baddeleyite	DRIFTS, epitaxial modeling	efflorescence and deliquescence of ammonium sulfate particles	Martin et al., 2001 (ref 270)
SO_2, O_3	Saharan dust	DRIFTS	uptake coefficients, surface adsorption, reaction mechanism	Ullerstam et al., 2002 (ref 265)
SO_2	α-Al_2O_3, α-Fe_2O_3, CaO, $CaCO_3$, TiO_2, SiO_2, China loess	Knudsen cell, FT-IR	uptake coefficients, surface adsorption, mechanism	Usher et al., 2002 (ref 181)

2.2.3. Summary of Sulfur Dioxide Studies

A summary of the studies described in this section on sulfur oxides is compiled in Table 7. These studies show that SO_2 itself is taken up by mineral dust and the oxidation of SO_2 on the surface of mineral dust by ozone is a viable route for sulfate formation, although other oxidants may also play a role, and future studies should address this issue. The role of adsorbed water and the chemistry of other sulfur oxides such as SO_3 should be further explored in laboratory studies. Sulfate coatings on mineral dust undergo efflorescence (crystallization) at different relative humidities depending on the size of the mineral dust inclusion and the mineralogy of the inclusion.

2.3. Ozone

Although stratospheric ozone shields the surface of the Earth from the harmful UV components of solar radiation, in the troposphere, ozone is a notable pollutant and irritant. Specifically, it is an important constituent in photochemical smog and can cause harmful effects to vegetation[274−276] and human health.[277−279] Ozone is present in the troposphere

through downward transport from the stratosphere and is produced through the oxidation of hydrocarbons by HO_x and NO_x (see Figure 10). Background concentrations of ozone currently range from 20 to 40 ppb in the remote troposphere.[102] These background concentrations have been increasing since preindustrial times. Because ozone is a greenhouse gas, this increase in concentration has resulted in a global radiative forcing contribution within the range of 0.28−0.49 W m^{-2}.[280] Furthermore, ozone concentrations are projected to increase ~5 ppm by the year 2030 and potentially >20 ppm by 2100.[281] In urban areas where there are large NO_x sources, ozone can be present in high concentrations ranging from 100 to 400 ppb[102] and pose a serious air pollution challenge.

The primary gas-phase loss mechanism for ozone in the troposphere is photolysis, which accounts for ~75% of its tropospheric loss, with the rest occurring mainly by reaction with HO_2.[102] However, recent modeling studies have shown that ozone concentrations are lowered in regions of high dust events,[148] suggesting that interaction of O_3 with solid material suspended in the troposphere may present another viable loss route. This acknowledgment has spurred recent inspections of O_3 interactions with mineral compounds, which are built on the foundations of a few studies that examined the reaction of O_3 with metal oxides for applications to the field of catalysis.[282,283] Although direct ozone interactions may be important, indirect effects through the loss of ozone precursors may also play a role.

2.3.1. Ozone Uptake on Mineral Dust

Several field studies measuring both trace gas-phase species as well as aerosol species have reported low ozone mixing ratios in regions concurrently containing high mass concentrations of mineral dust particulates.[284−286] Probably the most notable example of this anticorrelation was observed by de Reus et al. in 1997 during the ACE-2 campaign over the vicinity of the Canary Islands.[286] Specifically in this investigation, a high concentration of mineral dust was detected within an air parcel traveling between an altitude of 2 and 6 km (Figure 30, left panel), and the vertical profile through this air parcel showed a marked decrease in the concentration of ozone as compared to concentrations at altitudes above and below this dust layer (Figure 30, right panel). Through the use of a box-model simulation, it was determined that the dust surface provided a sink for the direct removal of ozone, causing a maximum of 50% ozone depletion, agreeing with profiles from the field data, but it was noted that there was large uncertainty attributed to the uncertainty in the value of the reactive uptake coefficient.

Prior to the model predictions reported by de Reus et al., several investigations tried to address the effects that heterogeneous reactions on mineral dust have on tropospheric ozone levels with the use of chemistry box models.[284,287] In 1996, Dentener et al. used a global three-dimensional model for evaluating the direct loss of ozone due to heterogeneous reactions with mineral dust, based on measurements of deposition rates to soils, sand, and other terrestrial surfaces.[148] Using a value of the reactive uptake coefficient of 2×10^{-4} as an upper limit, O_3 loss would approach 20% in regions of high dust concentrations, whereas with the use of a "best guess" reactive uptake coefficient of 5×10^{-5}, 2−6% ozone loss would be due to direct O_3−dust interaction. However, there was high uncertainty in this prediction due to the lack of information on the reactive uptake of ozone onto mineral surfaces, a point also reiterated by Jacob several years later and discussed in the Introduction of this review.[8]

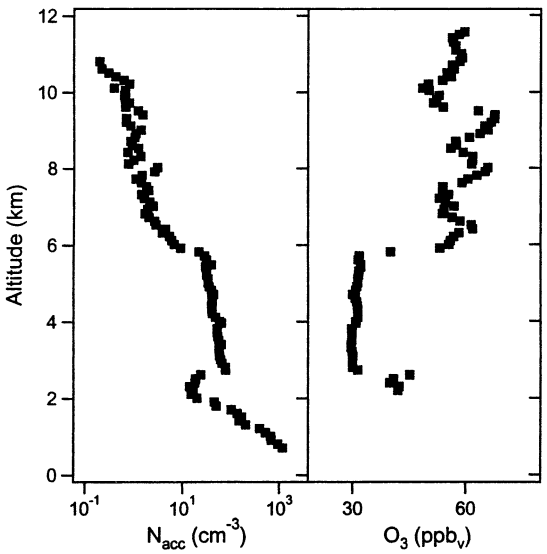

Figure 30. Altitude profiles for total number of accumulation mode particles between 0.11 and 3.5 mm (left panel), N_{acc}, and ozone observed (right panel) from flight measurements over the Canary Islands on July 8, 1997. Ozone and particle number concentrations were averaged over 100 m altitude intervals. Panels a and d from the original figure are not shown. (Reproduced with permission from *J. Geophys. Res. 105*, D12, pp 15263−15275; M. de Reus, F. Dentener, A. Thomas, S. Borrmann, J. Ström, and J. Lelieveld, Airborne Observations of Dust Aerosol over the North Atlantic Ocean During ACE 2: Indications for Heterogeneous Ozone Destruction. Copyright 2000 American Geophysical Union.)

To better understand the observations from field studies and model analyses, the focus shifts to laboratory investigations concerning the reaction of ozone with mineral oxides and mineral dust compounds. A preliminary laboratory study by Suzuki et al. investigated some of the salient details of O_3−dust interactions.[288] Although this investigation did not offer much quantitative rate information or suggest a mechanism, the relative results showed fundamentally the variations in reactivity for various mineral oxides. Using a UV absorption monitor, the authors reported the relative O_3 reactivity of silica, α-Fe_2O_3, Fe_3O_4, α-Al_2O_3, and natural sea sand collected in Japan, which was further separated into an "iron sand" component to compare with the selected iron oxide compounds and a "remainder sand" component. For the reaction on natural sand, the decomposition rate decreased with decreasing ozone concentrations and increased proportionally with increasing volume of sand. At the highest experimental

concentration of ozone, the decomposition rate was initially fast before slowing to a much lower steady-state value; however, the decomposition rate was nearly constant throughout the exposure at the lowest concentration of ozone. Additionally, the iron sand had a reactivity similar to that of Fe_3O_4, a major component in the iron sand, and decomposed O_3 at a faster rate than the natural sand and the remainder sand, suggesting that iron oxide as Fe_3O_4 more effectively destroys ozone than the other phases present in the sand. It was concluded that the iron-containing compounds had an ozone decomposition rate superior to those of alumina and silica model compounds.

In a report by Klimovskii et al., O_3 decomposition kinetics on γ-Al_2O_3 was measured.[289] A reactive uptake coefficient of 10^{-4} was calculated using the geometric area as the surface area of the sample. It was also observed that as the ozone concentration decreased, there was a simultaneous increase in the pressure of O_2.[289] A mechanism was proposed based on one suggested earlier by Golodets[290]

$$O_3(g) + (\ ) \rightarrow O(a) + O_2 \quad (38)$$

$$O_3(g) + O(a) \rightarrow 2O_2(g) + (\ ) \quad (39)$$

where ( ) represents an active surface site, such as anion vacancies, with reaction 39 being the rate-determining step. The resulting net reaction for ozone destruction would be

$$2O_3(g) \rightarrow 3O_2(g) \quad (40)$$

Moreover, the authors note that adsorbed oxygen, O(a), can also combine to form O_2

$$O(a) + O(a) \rightarrow O_2(g) + 2(\ ) \quad (41)$$

which also would account for the observed production of oxygen.

In a series of investigations, Alebic-Juretic et al. studied ozone reactions on environmentally and atmospherically relevant compounds including silica gel, alumina, calcite, TiO_2, Saharan sand, wood ash, coal fly ash, pollen, and sodium halides.[291−293] Using a fluidized-bed reactor, ozone uptake on these various samples was studied and the data were evaluated on the basis of three observations or criteria. Criterion 1 was the initial decrease in ozone concentration when a reactive sample was present. Criterion 2 was the ozone concentration at steady state for the different compounds. Criterion 3 was the time required to attain steady state.

Using criterion 1 to evaluate the first investigation, wood ash proved to be the most effective at decomposing ozone as 14% of the initial ozone passed through the reactor, indicating that >80% of the ozone was being destroyed.[291] When only the initial decrease in ozone concentration was considered, the relative reactivities of various compounds were ranked as

wood ash > silica gel = alumina > Saharan sand > calcite

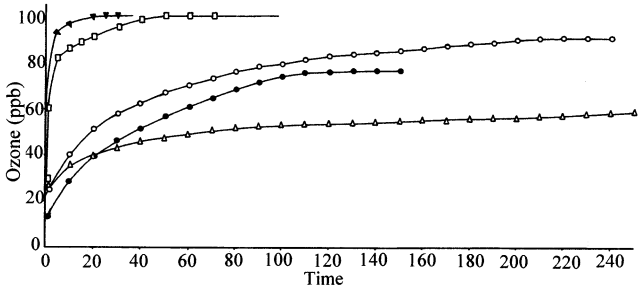

Figure 31. Ozone destruction capabilities of various particles as demonstrated by a plot of ozone concentration as a function of time. Particles examined include Al_2O_3 (△), wood ash (●), silica gel (○), Saharan sand (□), and calcite (▼). (Reproduced with permission from ref 291. Copyright 1992 Wiley-VCH.)

Similar results were obtained in the second investigation that focused on the ozone reaction with coal fly ash, pollen, TiO_2, silica gel, and sodium halides, with coal fly ash being less effective than wood ash according to criterion 1.[292] However, according to criterion 2, the relative efficiency for ozone removal by the various compounds at steady state was found to be

Al_2O_3 > wood ash > silica gel > Saharan sand = calcite[291]

At steady state, the concentration detected at the output flow of the fluidized-bed reactor loaded with Al_2O_3 was 58% of the initial ozone concentration, whereas after a certain time period, Saharan sand and calcite were found not to decrease ozone concentrations very much. Comparison of the samples according to criterion 3 gave the relative efficiency of ozone destruction as

silica gel = alumina > wood ash > Saharan sand > calcite

where silica gel and alumina took the longest (200 min) to reach steady-state reactivity and, in the other extreme, calcite took only 20 min to reach steady state.[291] In the extreme case for the second study, the coal fly ash reacted for nearly 10 h before reaching steady state.[292] Figure 31 displays a plot of ozone concentration as a function of exposure time for several of these surfaces. The results demonstrate that many types of surfaces can destroy ozone, with the oxides and coal and wood ash (with significant mineral oxide and/or carbon content) serving as the most effective samples in this investigation. Therefore, on the basis of these results and the sheer abundance of particles in the troposphere, such as Saharan sand, the observed reactivity toward ozone suggests that these surfaces could be a significant sink for ozone in the troposphere.

The effect of surface area was also examined for the mineral oxide samples (silica gel and TiO_2).[292] TiO_2 samples with different specific surface areas and masses but similar total surface area required the same time period to reach steady state. In the case of samples of a high-surface-area SiO_2, as the sample mass (and thus total surface area) increased, the time to reach steady state increased proportionally.

These observations suggest that sample composition and surface area are important. Overall in this investigation, rate constants or possible reaction mechanisms were not reported, but the authors suggested that the ozone destruction process is not a simple one that can be described by first-order kinetics.

The kinetics and mechanism of ozone destruction on various types of solid particulates were considered later by Alebic-Juretic et al. using the results of experiments performed in the above-mentioned studies.[293] It was stated that the elimination of ozone from an air stream is not a straightforward process. Rather, the process was described as involving the adsorption to a surface and successive chemical and/or catalytic transformations at the active sites until they are fully occupied and/or activated, which was observed experimentally through the loss of ozone and the gradual decrease in the effectiveness of a particular substance to remove ozone. In most cases, the process cannot be described by first-order kinetics; rather, Alebic-Juretic et al.[291,292] compared these reactions on powders to investigations of ozone on soot,[294] which presented a similar rapid initial loss of O_3 followed by a slower rate of ozone reaction. The process including steps where a swift initial decomposition is followed by slower reactions with surface species and inactivation of reactive surface sites is consistent with that observed by Klimovskii et al. and described by eqs 40 and 41.[289]

Michel et al. measured the reactive uptake of ozone onto powders chosen as models for atmospheric dust and a sample of authentic dust.[176,177] Using a Knudsen cell reactor, the loss of O_3 to a powder sample was measured with a mass spectrometer as a function of time. The mass spectral signal intensity dropped and remained relatively flat for the majority of samples tested regardless of sample mass, as demonstrated for an iron oxide sample in the upper panel of Figure 32. This response was atypical compared to previous Knudsen cell investigations involving other reactive species, in which an initial drop is observed followed by a distinct rise back to the baseline, indicating the complete saturation of the sample surface for thin samples of small mass. Samples of Saharan sand and China loess behaved in part like samples observed in previous Knudsen studies, where a rapid initial drop was observed, followed by a partial recovery toward the baseline; however, the signal never reached the baseline, instead leveling out to some flatter steady-state value similar to what was observed in other investigations.[288,291] The difference between the authentic dusts and the mineral oxide compounds was thought to be caused by possible organic contaminants on the authentic samples, which may react to a greater extent with the ozone.[295]

Initial uptake coefficients for the oxide samples, based on the BET surface area of the powders, were reported as $(5 \pm 3) \times 10^{-5}$ for SiO_2, $(8 \pm 5) \times 10^{-5}$ for α-Al_2O_3, and $(1.8 \pm 0.7) \times 10^{-4}$ for α-Fe_2O_3. The greater reactivity of the iron oxide is in agreement with what was observed by Suzuki et al.[288] The value obtained for alumina is considerably greater than

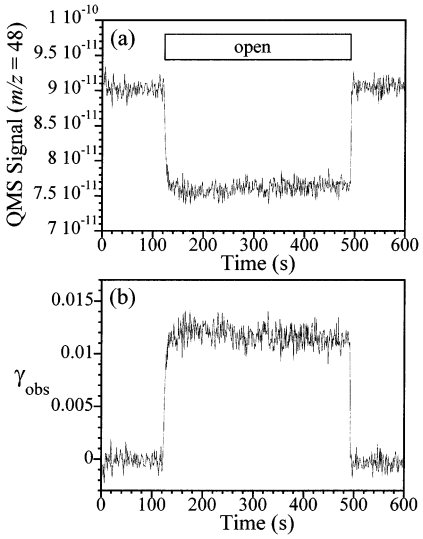

Figure 32. Knudsen cell data for the uptake of ozone (8 ppb) on α-Fe_2O_3 (10.9 mg) at 295 K: (a) mass spectral signal (m/z 48) as a function of time with the rectangular box representing when the sample was exposed to ozone; (b) γ_{obs} calculated from the data plotted in (a) as a function of time. (Reprinted with permission from *Atmos. Environ. 37*, pp 3201−3211; A. E. Michel, C. R. Usher, and V. H. Grassian, Reactive uptake of ozone on mineral oxides and mineral dust. Copyright 2003 Elsevier.)

what was determined by Hanning-Lee et al., who calculated a much lower uptake coefficient of 2×10^{-10} for another alumina phase, γ-Al_2O_3, at 22 °C.[296] The authentic dust samples resulted in uptake values of $4 \pm 2 \times 10^{-6}$ for sieved Saharan sand, $2.7 \pm 0.9 \times 10^{-5}$ for China loess and $6 \pm 3 \times 10^{-5}$ for ground Saharan sand. Differences in the reactive uptake coefficient for Saharan sand were attributed to differences in sample treatment, as the grinding process may have created reactive sites not originally present on native sand and sieving may have changed the elemental composition of the particles in the sample by concentrating certain mineral phases and excluding others. Therefore, the reactive uptake coefficient obtained for ground sand was considered as an upper limit. Ultimately, the calculation of ozone molecules lost per unit BET surface area of sample confirmed that many more O_3 molecules were destroyed than can reasonably be accommodated on the surface, which Michel et al. provides as evidence for a catalytic mechanism.

In a second study by Michel et al. expanded upon the first report to include the reactivity of a clay compound (kaolinite) as a model for mineral dust and the pressure, time, and temperature dependencies of the reaction of ozone on mineral compounds.[177] The initial uptake of ozone onto the clay compound was $(3 \pm 1) \times 10^{-5}$, which is on the order of the values that were determined for the authentic mineral compounds reported in the previous study. The initial uptake of ozone onto α-Fe_2O_3 and α-Al_2O_3 was studied as a function of ozone partial pressure between 3 and 30 μTorr (corresponding to 2− ppb); however, neither compound displayed a significant dependence of initial γ within the experimental ozone pressure. This indicated that the adsorption of ozone to the surface is a first-order process in this pressure

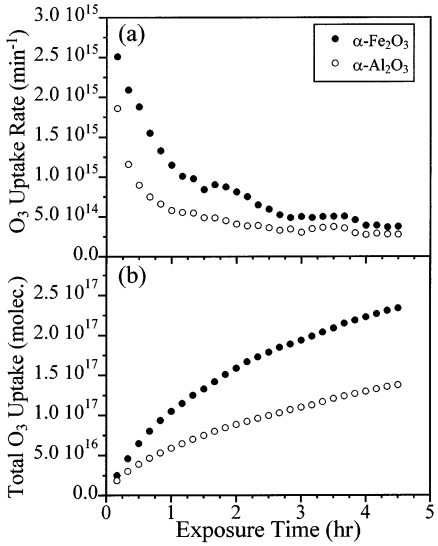

Figure 33. (a) Ozone uptake rate and (b) total ozone uptake of α-Fe_2O_3 (6.6 mg) and α-Al_2O_3 (6.0 mg) as a function of time exposed to 18 and 24 ppb of ozone, respectively. (Reprinted with permission from *Atmos. Environ. 37*, pp 3201−3211; A. E. Michel, C. R. Usher, and V. H. Grassian, Reactive uptake of ozone on mineral oxides and mineral dust. Copyright 2003 Elsevier.)

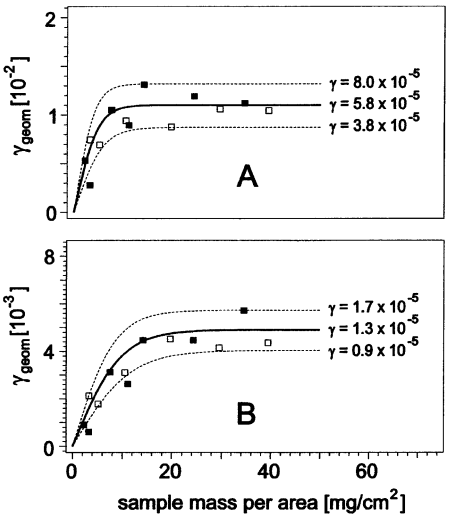

Figure 34. Plot of the (A) initial and (B) steady-state geometric uptake coefficients for the reaction of ozone (2.8×10^{11} cm^{-3}) with Saharan sand versus normalized sample mass. Samples were prepared by dispersion with either ethanol (■) or water (□), and the data were fit with a pore diffusion model (solid lines, uncertainty shown with dashed lines). (Reproduced with permission from ref 173. Copyright 2003 European Geosciences Union.)

range. The dependence of initial reactive uptake coefficient on temperature was examined in order to probe the energy of activation for the reaction and showed a weak temperature dependence of $\gamma_{o,BET}$ for α-Al_2O_3 corresponding to an activation energy of 7 ± 4 kJ mol^{-1}. Similar activation energies were reported in catalysis studies.[297,298]

To confirm the catalytic nature of the ozone reaction with mineral oxides, the dependence of the reactive uptake on ozone exposure time was measured in experiments with α-Al_2O_3, α-Fe_2O_3, and Saharan sand, whereby each sample was exposed to ozone for extended periods of time (4.5 h of the mineral oxides and 0.6 h for the Saharan sand). For the mineral oxides, the capacity to decompose ozone decreased over the initial 2−3 h, and after this time, the decomposition settled into steady-state uptake with no indication that the rate of ozone uptake would approach zero, as displayed in Figure 33. Under steady-state conditions, uptake values for α-Fe_2O_3 and α-Al_2O_3 were 2.2×10^{-5} and 7.6×10^{-6}, respectively. This decrease of ~90% of the initial uptake is significant, but the samples continued to take up ozone, on the order of 3×10^{14} molecules min^{-1}, with a total O_3 consumption of between 1×10^{17} and 2.5×10^{17} molecules (Figure 33). This decrease in the efficiency of mineral oxides to decompose ozone agrees with previous reports of ozone destruction by metal oxides for catalysis investigations[282,298,299] and by Alebic-Juretic et al. with similar mineral oxides.[291−293] The sample of Saharan sand also exhibited a considerable decrease in reactivity over time, and with expectations that the sand would continue reacting in the same manner as the mineral oxides, the extrapolated value for 4.5 h of exposure time was estimated to be 6×10^{-6}. Michel et al. concluded that the catalytic nature of the reaction of ozone on mineral particles may make this heterogeneous reaction important to tropospheric chemistry in comparison with other ozone loss mechanisms.

Uptake of O_3 onto mineral dust was also studied by Hanisch and Crowley.[173] In that report, the reaction of ozone with Saharan sand from the Cape Verde Islands was investigated as a function of sample treatment and ozone concentration using a Knudsen reactor. A quick initial drop was observed in the ozone signal followed by a recovery somewhat toward the baseline to a nonzero steady-state value, which is similar to the authentic dust samples explored in the Knudsen cell study of Michel et al.[176,177] and with other methods utilized by Suzuki[288] and Alebic-Juretic.[291−293] Also in agreement with Michel et al., Hanisch and Crowley reported that the ozone uptake was dependent on the mass of the sample as shown in Figure 34. Therefore, to take mass dependence into account, the reported reactive uptake coefficients were calculated with a pore diffusion model. Additionally, the reactive uptake coefficient was dependent on the ozone concentration, and at lower ozone concentrations, the reactive uptake coefficients were an order of magnitude greater than those at higher concentrations and ranged from 2.2×10^{-6} to 4.8×10^{-5}. These values are in relatively good agreement with the reactivity determined for Saharan sand with a similar ozone concentration by Michel et al.[176] For comparison, Hanisch and Crowley reacted different dusts with ozone, including Arizona Test Dust, Chinese dust from the Taklamakan Desert, and several clay minerals; however, only the results derived from the geometric surface area were reported, which were found to be comparable to the geometric γ for Saharan dust.

On the basis of the reported results, possible mechanisms of ozone destruction on the sand surface were discussed. An ozone molecule attaches to an active surface site through a terminal oxygen atom

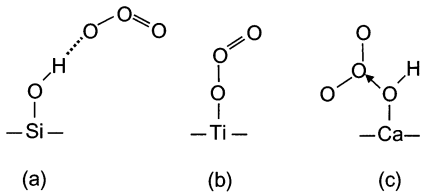

Figure 35. Orientations of adsorbed ozone on mineral oxide surfaces including (a) SiO_2, (b) TiO_2, and (c) CaO. Schematic based on studies by Bulanin et al.[301−303]

and dissociates into gas-phase O_2 and a surface-bound O atom. Either this O atom can react with another incoming ozone molecule to produce two gas-phase O_2 molecules or the O atoms can migrate at appropriate temperatures and also react to form O_2. In the experiments done by Hanisch and Crowley discussed above, O_2 was observed as a product, whereas it could not be detected due to the high background of O_2 in experiments by Michel et al.[176] The values for γ as determined here would be in the lower limit of values that might make O_3 loss on dust surfaces important (as proposed by Dentener et al.,[148] with $\gamma > 10^{-5}$), but because photochemical processes would be faster during the day, the authors suggested this mechanism may have importance at night.

In addition to laboratory studies that explored the kinetics of reactive uptake of ozone onto mineral oxide surfaces, several laboratory studies were initiated to exclusively examine the mechanism of O_3 adsorption onto various oxides at low temperatures. Ozone adsorption onto several metal oxides, including SiO_2, TiO_2, and CaO, was investigated by Bulanin et al. in order to probe the interaction between ozone and the acidic and basic moieties of metal oxides and to elucidate the mechanism and sites of ozone adsorption.[300−303] Specifically, using SiO_2, a relatively neutral oxide by nature, Bulanin et al. investigated the interaction of ozone with surface hydroxyl groups.[300] Perturbations of the OH stretching region of the IR spectrum indicated extensive hydrogen bonding of the ozone to the surface OH groups. However, the bands that would indicate O_3 physisorbed to other sites overlapped with the bands indicative of H-bonded O_3; thus, a weaker physisorption state could not be distinguished. Despite this complication, physisorbed O_3 was thought to influence the H-bonded complexes at higher ozone coverages. Experimental evidence with isotopically labeled O_3 indicated that O_3 adsorbs through a terminal oxygen atom, as depicted in Figure 35a, rather than through the central atom. The adsorption of a terminal oxygen to the acidic proton of a hydroxyl group demonstrates the basic nature of the terminal oxygen, which acts as an electron donor to the proton forming the hydrogen bond.

To further examine the basic characteristics of ozone, TiO_2 was used as the substrate in another investigation whereby the TiO_2 was pretreated in three ways to control the strength of different Lewis acid sites.[301] Ozone was exposed to a sample that was completely hydroxylated, a sample that had been evacuated at 300 K, and one that had been evacuated at 773 K. In the case of the completely hydroxylated sample, evidence for weakly adsorbed ozone was observed by bands at 1034 and 1108 cm^{-1} in the infrared spectrum along with shifts in the OH stretching region.

For the more strongly bound O_3 molecules, it was found through isotopic substitution of ozone that ozone adsorbs to metal cation sites through a terminal oxygen (see Figure 35b). This molecular adsorption occurs at what was defined by Bulanin et al. as weaker Lewis acid sites, which were identified through adsorption studies of carbon monoxide, a probe molecule. However, for samples that had been heated to 773 K, O_3 adsorbs to the surface through stronger adsorption sites. At the strongest sites, no molecular adsorption was detected; instead, the O_3 molecules can distort and dissociate on the surface, forming molecular oxygen and an O atom incorporated into the surface. A third report by the same authors confirmed these findings, in which similar molecular adsorptions occur for ozone on cationic Lewis acid sites on ZrO_2, MgO, and CeO_2; however, on Al_2O_3 and ZnO, molecular adsorption on Lewis acid sites was not detected, indicating their strength was sufficient to actually dissociate ozone.[302]

The strength of Lewis acid sites on alumina was also investigated by Thomas et al., who tracked O_3 dissociation by monitoring a pressure increase in the reaction chamber.[304] The products of the decomposition were shown to be molecular oxygen (through the pressure increase in the chamber) and surface O atoms (shown by computer simulations) as described in reaction 38. IR results yielded evidence of weakly bound O_3 on the alumina surface but no bands corresponding to molecular O_3 at strong Lewis acid sites. Importantly, when the reactive sites in the sample were completely poisoned through adsorption of pyridine, no ozone decomposition occurred, but partial recovery of the reactive surface was observed when some of the pyridine was pumped away. Thus, the Lewis acid sites were proven to be reactive centers for decomposition of ozone, and the reactive sites on alumina are strong enough that molecular adsorption does not occur even at low temperatures.

Conversely, to reveal the acidic properties of ozone, its adsorption to a basic oxide, CaO, was examined.[303] CaO does not exhibit Lewis acidity and its hydroxyl groups do not form even weak hydrogen bonds with basic molecules. Therefore, it was anticipated that the adsorption to a basic oxide would demonstrate the acidic characteristics of ozone and that its adsorption would occur through a mechanism different from that on acidic oxides. Experiments were carried out similarly to those on TiO_2, where O_3 was exposed to CaO that had been completely hydrated, partially dehydrated (pumped at 723 K), and very dehydrated (pumped at 973 K).

At high degrees of hydration, weakly adsorbed O_3 was observed in the infrared spectrum with bands measured at 1035, 1106, and 2106 cm^{-1}, corresponding to ν_3, ν_1, and $\nu_1 + \nu_3$ modes of adsorbed O_3. CaO treated at 723 K showed the same set of absorptions and an unperturbed OH region; that is, no hydrogen bonding was observed. CaO pretreated at 973 K yielded similar bands at slightly different positions and a band at ~812 cm^{-1} that increased with

exposure time. The band at 812 cm^{-1} was due to the chemisorption of O_3 to basic sites, but the exact mechanism and species involved is speculative. One possibility is the formation of a peroxy species on the surface, possibly through the initial formation of an unstable O_4^{2-} complex. For the sample pretreated at 973 K, perturbations of the OH stretching region with the introduction of O_3 indicated some degree of interaction with hydroxyl groups. The surface OH groups do not donate a proton; rather, the ozone molecule through its central atom can interact with the oxygen atom of the hydroxyl group. Therefore, the central oxygen on the ozone molecule can act as a Lewis acid, accepting electrons donated by the oxygen of the hydroxyl group (see Figure 35c).

O_3 adsorption on another basic oxide, MgO, was studied by Berlier et al. with IR spectroscopy at 77 K.[305] The microcrystalline MgO powder was characterized as having a prevalence of (001) faces, which contained five-coordinate Mg^{2+} ions. At steps and edges, four-coordinate Mg^{2+} and O^{2-} ions were present, whereas three-coordinate Mg^{2+} ions were present at corners. The four-coordinate Mg^{2+} was said to exhibit enhanced Lewis acidity, whereas the O^{2-} on steps and edges would act as a medium-strong Lewis base. In the infrared spectrum, four bands of interest appeared between 1000 and 1150 cm^{-1} and were characterized as two sets of two correlated peaks. The correlated bands at 1110 and 1024 cm^{-1} were assigned to stretching modes of ozone physisorbed through a terminal oxygen to five-coordinate Mg^{2+} sites on (001) surface terraces. Assignment of the two correlated bands at 1140 and 1038 cm^{-1} was less straightforward and tentatively assigned to stretching modes of O_3 attached weakly to defect sites on edges and steps, the sites of enhanced Lewis acidity.

Thus, these various studies that utilized infrared spectroscopy to probe the surface interactions between ozone and mineral oxides showed the flexibility of ozone to act as either an acidic or basic molecule depending on the nature of the surface to which it adsorbs and the presence of hydroxyl groups on those surfaces. Importantly, these factors determine the orientation of the adsorbed ozone on the surface or whether the ozone dissociates immediately upon the surface, as demonstrated by the strong acidic sites of alumina. A fundamental understanding of the adsorption mechanism of ozone onto single-component oxide surfaces is necessary to elucidate the uptake mechanism and understand the catalytic nature of the ozone reaction with more complicated mineral dust particles that were described in the first part of this section. Because tropospheric dust particles contain various combinations of different mineral phases under various humidity conditions, future investigations involving reactions with ozone are needed that probe the surface adsorption of ozone onto multicomponent (i.e., combinations of acidic and basic) oxide samples to determine if a specific adsorption mechanism dominates others for samples containing a variety of surface sites. In addition, it is very important that future laboratory studies investigate the uptake of ozone on mineral oxide and dust samples in the presence of water vapor at tropospherically relevant relative humidities.

2.3.2. Ozone Uptake on Processed or Atmospherically Aged Mineral Dust

It is clear from studies involving single-particle analysis that mineral aerosol in the troposphere contains various surface coatings.[160,192,306] This is because as the dust particles are transported through the troposphere from source regions, they will come into contact with any number of trace compounds and react to yield material irreversibly adsorbed on the surface. Particles that contain coatings of nitrate, sulfate, or organic matter will exhibit different reactivities toward other trace gases, and the chemistry that takes place between the coating of the particle and gas-phase species can change the fate of the particle by altering its optical properties through differences in hygroscopicity or chemical composition or by affecting its ability to act as a cloud condensation nucleus. Consequently, the interaction of processed mineral particles with ozone has been probed as one example of how the surface chemical properties of atmospherically aged mineral particles can be altered and affected through prior exposure to other gas-phase compounds.

Grøntoft observed the decomposition of ozone on various indoor surfaces including the reaction of ozone on concrete floor tiles, a surface containing a variety of mineral oxide species.[295] A concrete floor tile was exposed to 40 ppb of ozone for >2 days, followed by repeat exposures 6 and 7 months after the initial experiment. Observations showed that the deposition rate to the surface decreased between the first, second, and third experiments. The deposition to the surface never reached a steady state by the end of the first experiment, although it approached it by the end of the second experiment and relatively quickly reached a steady state in the third. The data correlated well with a first-order model, which supports the supposition that the heterogeneous reaction of ozone with solid surfaces is first-order under these conditions of constant humidity and pH. However, the decrease in deposition rate from the first to third exposures may imply a second-order nature of the reaction. Grøntoft notes that possible oxidation of an organic contaminant would explain the fast initial deposition rates compared to later rates; thus, aging of the surface may be an important process.

The reaction of ozone with laboratory-processed particles was also examined recently by Usher et al.[182] Mineral oxide particles representative of mineral dusts were pretreated ex situ with either a reactive inorganic or organic species and then reacted with ozone in a Knudsen cell. Changes in the reactivity of the oxide particles toward ozone were observed, and these changes were dependent upon the nature of the pretreatment.

The Usher et al. investigation explored the processing of surfaces with reactive inorganic species prior to any ozone reaction. Specifically, particles of α-Al_2O_3 were first exposed to either HNO_3 vapor or SO_2 gas to result in coatings of nitrate and sulfite. On the basis of coverage measurements made previ-

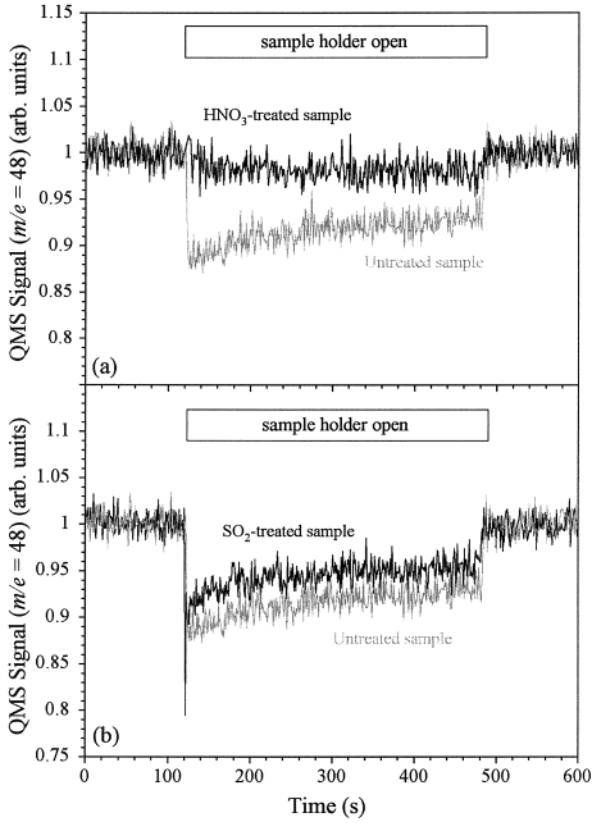

Figure 36. Normalized mass spectral signal for the uptake of ozone onto (a) α-Al_2O_3 (5.6 mg) pretreated with HNO_3 (dark signal) as compared to untreated α-Al_2O_3 (4.5 mg, gray scale) and (b) α-Al_2O_3 (4.9 mg) pretreated with SO_2 (dark signal) as compared to the untreated α-Al_2O_3 (gray scale).

ously,[168,184] the surface was characterized as partially coated by the HNO_3 or SO_2, also leaving alumina sites that may be available for reaction with ozone. Therefore, uptake of ozone onto these treated surfaces was a function of the reactivity of ozone with both the coating and the bare oxide.

Particles containing a nitrate coating exhibited an ~70% decrease in reactivity as compared to the pure Al_2O_3 surface [γ value down to $(3.4 \pm 0.6) \times 10^{-5}$ from $(1.2 \pm 0.4) \times 10^{-4}$]. For example, panel a in Figure 36 clearly shows the initial signal drop, indicating the uptake of ozone, was significantly decreased for the nitrate-coated powder compared to untreated alumina. This result coincides with what is anticipated for a surface coated in a fully oxidized species, which is not expected to undergo further reaction with an oxidant such as ozone. Because the surface was not fully covered in NO_3^-, there was still some uptake observed as ozone reacted with the bare alumina reactive sites. In contrast, particles pretreated with SO_2 to yield surface SO_3^{2-} exhibited enhanced reactivity, shown in Figure 36b, toward ozone as compared with pure Al_2O_3; the initial reactive uptake coefficient increased ~30% [up to $(1.6 \pm 0.2) \times 10^{-4}$]. The SO_3^{2-} groups on the surface were available for oxidation by ozone, and this reaction represents a mechanism for the oxidation of SO_2 on surfaces to form sulfate.

In addition to aging of aerosol by the presence of inorganic species, Usher et al. probed the processing of mineral dust with organic coatings through monitoring the reaction of ozone with particles of SiO_2 that were functionalized with either octenyltrichlorosilane or octyltrichlorosilane. When the particles were coated with the alkyl compound, the mass spectral signal within the Knudsen apparatus showed the anticipated result of decreased reactivity toward ozone. With a coverage of $(2 \pm 1) \times 10^{14}$ aliphatic molecules cm^{-2} on the surface of the SiO_2 particles, the reactivity decreased ~40% [γ from $(5 \pm 1) \times 10^{-5}$ to $(3 \pm 1) \times 10^{-5}$] from that of unreacted SiO_2. Because there were still active sites available for reaction with ozone, these sites accounted for the observed uptake in the signal, given that alkane species are unreactive toward ozone. On the other hand, the reactivity of alkene-functionalized silica was increased by 40% [initial γ up to $(7 \pm 2) \times 10^{-5}$]. The initial uptake value onto this surface was a combination of uptake by reactive double bonds and reactive sites on the bare silica surface.

The Knudsen cell technique is capable of measuring the loss of the reactant and any gas-phase products that may evolve. In the case of the reaction with the alkene-coated silica, the signal at *m/e* 29 showed the production of a species that fragments into CHO^+ and was assigned to the fragmentation of formaldehyde (CH_2O) rather than formic acid (HCOOH) on the basis of results obtained by Thomas et al.[307] To determine the nature of the surface species that remained after reaction of the organic coatings with ozone, solid-state ^{13}C NMR was employed. Comparison of alkene spectra, displayed on the left of Figure 37, before and after reaction with ozone, showed a decrease in the intensity of the peaks due to loss of the double-bond carbons (113 and 139 ppm) accompanied by an increase in the peak corresponding to the formation of a methyl group (10 ppm). No peaks due to carbons bonded to oxygen atoms were observed, indicating that no carbonyl remained, or at least carbonyl was not detectable with solid-state ^{13}C NMR. The mechanism of reaction, based on the NMR results, is similar to that proposed by Thomas et al.[307] and is depicted on the right of Figure 37. The ozone initially attacks the double bond, forming the ozonide, which decomposes to form formaldehyde (observed in the gas phase in Knudsen experiments) and a Criegee intermediate. The Criegee intermediate then rearranges on the surface and decomposes, yielding carbon dioxide in the gas phase and a surface-bound alkyl chain. Carbon dioxide was not observed in the Knudsen cell, possibly because the rearrangement and decomposition of the Criegee intermediate may be too slow to allow for detection of the gas-phase CO_2 in this instrument.

Rudich and co-workers considered the reaction of ozone with organic compounds bound to glass surfaces as proxies for organic aerosol.[307,308] The kinetics and mechanism of the ozone reaction with surface-bound olefinic and aliphatic compounds were investigated using FT-IR spectroscopy and a cylindrical flow reactor coupled to a chemical ionization mass spectrometer (CIMS). To examine the uptake kinetics of ozone to organic-coated surfaces, the glass surfaces

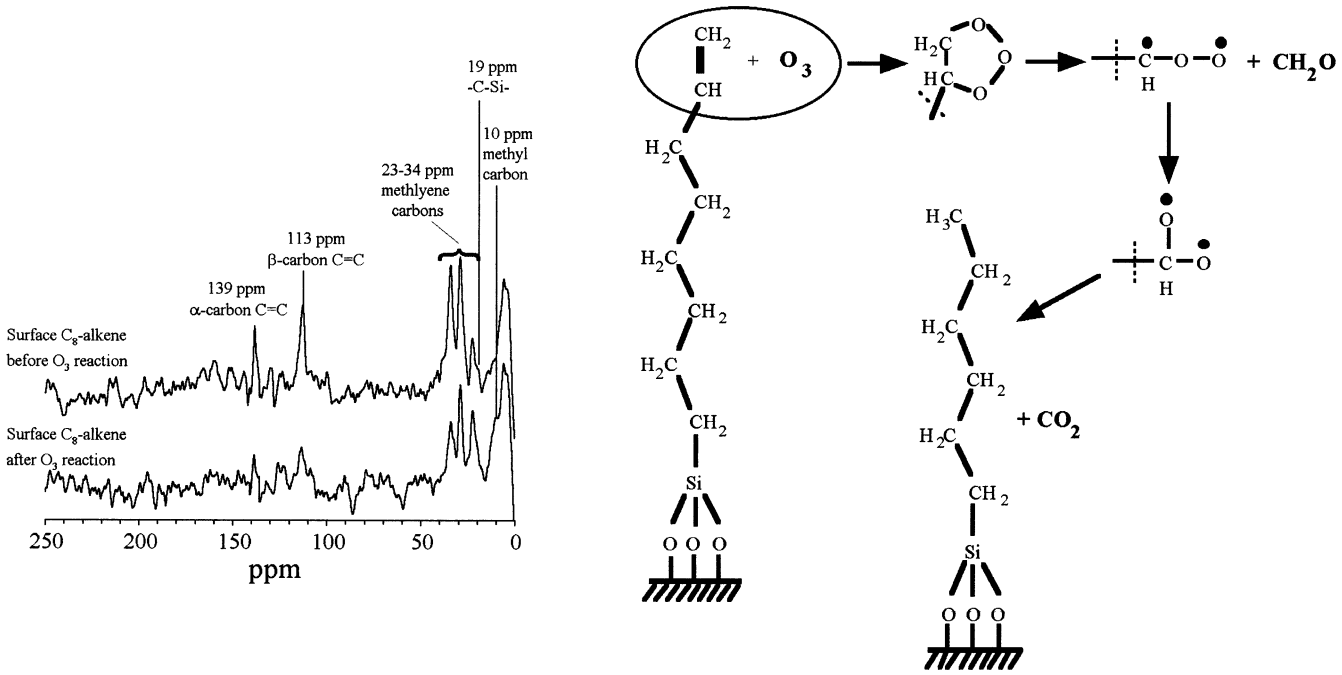

Figure 37. Solid-state ^{13}C NMR spectra of C_8-alkene-functionalized SiO_2 before and after reaction with ozone and a schematic of the mechanism of ozone reaction with surface-bound alkene. Bold lettering indicates gas-phase species.

of the cylindrical flow reactor were coated with self-assembled monolayers prepared from organosilanes with either terminal methyl end groups (octadecyltrichlorosilane, octyltrichlorosilane, and methyltrichlorosilane) or terminal vinyl end groups (octenyltrichlorosilane and allyltrichlorosilane) and then exposed to ozone.[308] Uptake coefficients were measured on the basis of the loss of ozone when the surface was exposed. The reactive uptake coefficients for the aliphatic compounds, as well as uncoated glass, were very small, $<3 \times 10^{-6}$. For the glass coated with the alkene-containing samples, uptake values were obtained between 1.2×10^{-4} and 2.7×10^{-4}, depending on the temperature and length of the olefin chain. When the reacted alkene samples were again exposed to ozone, negligible uptake was observed, on the order of $<3 \times 10^{-6}$, consistent with the aliphatic compounds. IR spectra of the alkene system before and after reaction show the loss of the double bond.

The uptake of ozone onto organic-coated surfaces was further probed by Thomas et al. in a study that examined the surface-bound and gas-phase products of ozone reaction with monolayers prepared from allyltrichlorosilane, octenyltrichlorosilane, and octyltrichlorosilane on glass slides and glass beads.[307] Species monitored in the gas-phase included O_3, CO, CO_2, formic acid (HCOOH), and formaldehyde (CH_2O). It was found that when fresh monolayer surfaces of allyl- and octenyltrichlorosilane were exposed to ozone and consumed the double bond, CH_2O was a gas-phase product, as well as CO and CO_2 of varying yields depending on the surface studied. A very low yield of HCOOH was observed only when the reaction took place with the allyl monolayer at low ozone pressures. Attenuated total reflection (ATR)-IR spectroscopy directly observed the decrease in absorptions within the monolayers due to the C−H stretching associated with the terminal double bond and the increase in absorption due to carbonyl stretching. Features in the spectrum after ozone reaction showed the presence of terminal methyl groups. A peak at 1705 cm^{-1} indicated the formation of a carbonyl, and a peak at 1650 cm^{-1} was assigned to an H-bonded carbonyl species. Thus, it was concluded that a combination of a carboxylic acid and methyl groups terminated the organic chains.

On the basis of the gas-phase and surface-bound products that were observed, the following mechanism for ozone reaction with surface organic containing a double bond was proposed. The ozone initially inserts into the double bond, generating a primary ozonide that can rearrange, stabilize, or decompose into a Criegee intermediate (CHOO biradical). In one decomposition scheme, the Criegee intermediate is released into the gas phase, leaving an aldehyde functionality on the surface. The Criegee intermediate can undergo other reactions that will lead to products such as those observed in the gas phase in these experiments. Alternatively, through a second scheme, formaldehyde is released to the gas phase while the Criegee intermediate remains bound to the surface. This surface-bound intermediate species can decompose in several ways, leading to the formation of a carbonyl or carboxylic acid or carbon dioxide and an alkane. The formation of formaldehyde, as observed in these experiments, will have important implications in gas-phase tropospheric chemistry, because formaldehyde is an important source of HO_x. The nature of the surface-bound product will affect the hygroscopicity of the particle, possibly altering the optical properties of the particle.

Both the inorganic and organic coatings on mineral oxides described in this section were rather simple models of aging processes that occur in the troposphere. Atmospheric aerosols may have coatings of

Table 8. Summary of Laboratory Studies Reviewed under Section 2.3

reactive species	sample(s)	technique	measurements	reference
O_3	SiO_2, α-Al_2O_3, α-Fe_2O_3, Fe_3O_4, sea sand	UV absorption	relative reactivity measurements, kinetics	Suzuki et al., 1979 (ref 288)
O_3	γ-Al_2O_3	mass and thermal desorption spectroscopy, luminescence	uptake coefficients, kinetics	Klimovskii et al., 1983 (ref 289)
O_3	silica gel, Al_2O_3, calcite, NaCl, Saharan sand, wood ash	fluidized-bed reactor	relative reactivity measurements	Alebic-Juretic et al., 1992 (ref 291)
O_3	SiO_2	FT-IR	surface adsorption, reaction mechanism	Bulanin et al., 1994 (ref 300)
O_3	TiO_2	FT-IR	surface adsorption, reaction mechanism	Bulanin et al., 1995 (ref 301)
O_3	SiO_2, TiO_2, MgO, ZrO_2, CeO_2, Al_2O_3, ZnO	FT-IR	surface adsorption, reaction mechanism	Bulanin et al., 1995 (ref 302)
O_3	coal fly ash, pollen, TiO_2, silica gel, NaCl, NaBr, NaI	fluidized-bed reactor	relative reactivity measurements, kinetics	Alebic-Juretic et al., 1997 (ref 292)
O_3	CaO	FT-IR	surface adsorption, reaction mechanism	Bulanin et al., 1997 (ref 303)
O_3	γ-Al_2O_3	FT-IR, quantum chemistry calculations	surface adsorption, reaction mechanism	Thomas et al., 1997 (ref 304)
O_3	silica gel, alumina, wood ash, coal ash, Saharan sand, calcite	fluidized-bed reactor	kinetics	Alebic-Juretic et al., 2000 (ref 293)
O_3	alkane-coated (octadecyltrichlorosilane, octyltrichlorosilane, methyltrichlorosilane) and alkene-coated (octenyltrichlorosilane, allyltrichlorosilane) glass surfaces	FT-IR, flow tube reactor	surface characterization, uptake coefficients, kinetics	Moise and Rudich, 2000 (ref 325)
O_3	allyltrichlorosilane, octenyltrichlorosilane, and octyltrichlorosilane on glass beads and slides	FT-IR, ATR−IR	surface and product characterization, reaction mechanism	Thomas et al., 2001 (ref 307)
O_3	α-Al_2O_3, α-Fe_2O_3, SiO_2, Saharan sand, China loess	Knudsen cell	uptake coefficients, kinetics	Michel et al., 2002 (ref 176)
O_3	MgO	FT-IR	surface adsorption, reaction mechanism	Berlier et al., 2002 (ref 305)
O_3	concrete tiles, activated carbon cloth	deposition chamber	deposition velocities, kinetics	Grøntoft, 2002 (ref 295)
O_3	Saharan sand, Arizona test dust, Chinese dust, kaolinite, illinite, Ca-montmorillonite, palygorskite	Knudsen cell	uptake coefficients, kinetics	Hanisch and Crowley, 2003 (ref 173)
O_3	α-Al_2O_3, α-Fe_2O_3, SiO_2, kaolinite, Saharan sand, China loess	Knudsen cell	uptake coefficients, kinetics	Michel et al., 2003 (ref 177)
O_3	nitric acid- and sulfur dioxide-coated α-Al_2O_3, octenyltrichlorosilane and octyltrichlorosilane functionalized SiO_2	Knudsen cell, ^{13}C MAS NMR	uptake coefficients, reaction mechanism	Usher et al., 2003 (ref 182)

varying thickness possibly containing multiple components. However, it is clear through the changes in reactivity demonstrated with these laboratory-processed particles that knowledge of the history of mineral particles is necessary when their impact on tropospheric chemistry is assessed. It is clear that the gas-particle interaction will depend on the nature of the molecular coating of the particle. Under section 2.4, possible reactions of organics on mineral dust are discussed. The uptake of organics will result in organic-coated mineral dust particles with reactivity different from that of the uncoated particle.

2.3.3. Summary of Ozone Studies

The ozone studies reviewed in this section are compiled in Table 8 with a listing of the reactive gas, surface, and techniques used in each study along with the reference citation. From the studies reviewed here, it is important to note that uptake onto clean oxide surfaces was found to be catalytic, and under dry conditions the reactive sites were determined to be Lewis acid sites. However, what constitutes the reactive site under atmospheric conditions is still under question. Through experiments in pretreating oxide samples, it was found that if Lewis acid sites were not available for reaction, inorganic and organic coatings on mineral dust particles may provide important reactive centers. Further studies under atmospherically relevant conditions of relative humidity and with authentic dust samples are necessary to better understand the capability of mineral dust to react directly with ozone and the impacts that these reactions may have.

2.4. Organic Compounds

In addition to the ubiquitous presence of trace inorganic compounds in the troposphere, such as those described in the previous sections, there are also numerous volatile and semivolatile organic compounds (VOCs and SOCs, respectively) in the Earth's atmosphere. Sources of organics in the atmosphere have biogenic and anthropogenic origins

in both marine and continental environments. In marine environments, biological processes are responsible for the emission of organic matter, as unsaturated fatty acids present in lipid compounds are released through ocean sprays and transported into the troposphere.[309−313] Over land in nonurban areas, aerosols can contain a variety of carbon compounds—aliphatic hydrocarbons, alcohols, and aromatics—which arise from biogenic emissions.[314−317] In urban areas, organic matter is mainly released directly into the troposphere through anthropogenic means such as cooking meat, automobile exhaust, leaf abrasions, wood smoke, and natural gas combustion.[318−322] Specifically, oleic acid is found to be a significant component of organic matter found in the troposphere and has been used in laboratory experiments as a model for organic aerosol.[308,323,324] Several studies probing the interaction of ozone on surface-bound organic material indicate that the sites of unsaturation in fatty acid compounds act as reactive centers for ozone, producing formaldehyde in the gas phase as well as other gas-phase and surface-bound products.[307,308,323,325]

Organic material in the troposphere can be present as purely condensed particulates or as coatings on other particulates such as liquid droplets or solid cores. In the particulate phase, organics are often found mixed with sulfates. For example, Buseck and Posfai showed that ammonium sulfate particles can have coatings of organic material, which were easily observed in TEM micrographs after electron-beam sublimation of the ammonium sulfate.[24] Internal mixtures of organics and sulfates were commonly found in individual particle mass spectra during the Atlanta SuperSite project field study.[160] FT-IR spectra of dust particles collected in Germany showed definitive bands for aliphatic CH and CH_2 groups, although the organic component of the particles could not be further identified.[326] Recently a study of the composition of aerosols in the eastern Mediterranean found carboxylic, dicarboxylic, and keto acids in particles and suggested their origin might arise not only from gas-to-particle conversion but also from heterogeneous reactions on pre-existing particles.[327]

Most relevant to this review is the fact that organic material found in the troposphere is often associated with dust particles.[24,328−330] In the Atlanta SuperSite project, particles containing mineral components (Al, Si, Fe, Ca, and their oxides) were found to also contain water-soluble organic acids.[160] Russell et al. mapped the composition of organic coatings on aerosol particles using soft X-ray techniques and found that dust samples contained Ca^{2+}, CO_3^{2-}, R(C═O)-OH, and R(C═O)R in a shell-like structure of aragonite $CaCO_3$ encapsulated by organic layers.[327] The presence of carboxylic acids and ketones is consistent with the typical families of organic compounds, which are often found as coatings. Using gas chromatography combined with thermal desorption, Falkovich and Rudich identified nearly 100 semivolatile organic compounds in a NIST Urban Dust standard (SRM1649a).[331]

The transport of organic pollutants in the atmosphere will be strongly affected by their tendency to adsorb to aerosol particles or to terrestrial surfaces. It is thought that the adsorption of organics to the surface of minerals is an important process.[332] Despite the growing evidence of organic material associated with mineral dust, there is scant information about how the organic material came to be associated with the mineral particles. Additional knowledge of heterogeneous processes, such as reactions on the surface of mineral dust aerosol, could identify effective sinks and provide a greater understanding of the earth−atmosphere system. Similar to studies conducted for inorganic gases, there are questions as to with what species, what processes, what rates, and through what mechanisms these organic reactions occur. The potential importance of organic material on particles in affecting how the particle contributes to tropospheric chemistry and climate makes the continued study of the origin of organics and organic coatings a worthy endeavor. In addition to forming organic coatings on mineral particles, the removal of volatile organic compounds via adsorption onto dust surfaces and the potential desorption of volatile organic compounds may also impact the photochemical oxidant cycle. This facet of the chemistry, that is, revolatilization or desorption of organics, has received little attention. This section will attempt to review the current knowledge of the heterogeneous chemistry of organic compounds with mineral dust.

2.4.1. Carbonyl Compounds

A study by Grosjean et al. identified at least 23 carbonyl species in the troposphere in the Los Angeles, CA, area including formaldehyde, acetaldehyde, and acetone, the three most commonly measured carbonyls.[333] Such carbonyl species have significant functions in the photochemical oxidant cycle by acting as sources for peroxy radicals and peroxyacetylnitrates (PAN).[102] These three carbonyls account for 28% of the total OH removal capacity by carbonyl compounds. In addition, the total OH removal capacity of these carbonyls was estimated to be 4 times higher than that due to observed levels of toluene and isopentane, the two most abundant hydrocarbons in urban air. Recent studies have shown the presence and importance of carbonyls in regional[334] and clean marine[335] air. Lee et al. assessed the role of formaldehyde as a peroxy radical source in the Nashville SOS'95 summer experiment, where it accounted for 20% of the radicals during high sun conditions and >60% during early morning and late afternoon.[336] On the global scale, Singh et al. estimated that photolysis of acetone, one of the most dominant VOC species in the middle to upper troposphere, represents a significant source of PAN and free radicals.[337] Model calculations have suggested that in the upper troposphere loss of acetone by photolysis provides a HO_x source which is 5 times greater than that due to the $O(^1D) + H_2O$ reaction.[338,339] Similar reactions of other abundant, higher carbon number carbonyls are expected to play an analogous role.

Laboratory studies have investigated the interaction of carbonyl compounds such as formaldehyde and acetone with sulfuric acid aerosols,[340−346] but

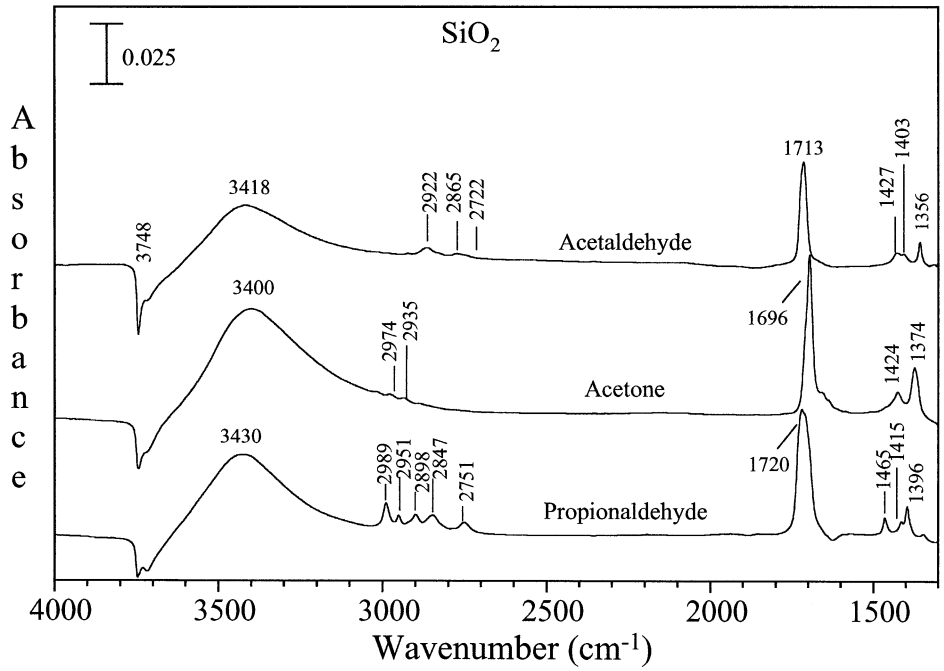

Figure 38. Transmission FT-IR spectra of acetaldehyde, acetone, and propionaldehyde adsorbed on SiO_2 particles in the presence of 10 mTorr (1 ppm) of the carbonyl vapor at 298 K. (Reproduced with permission from *J. Geophys. Res. 106*, D6, pp 5517−5529; P. Li, K. A. Perreau, E. Covington, C. H. Song, G. R. Carmichael, and V. H. Grassian, Heterogeneous reactions of volatile organic compounds on oxide particles of the most abundant crustal elements: surface reactions of acetaldehyde, acetone, and propionaldehyde on SiO_2, Al_2O_3, Fe_2O3, TiO_2, and CaO. Copyright 2001 American Geophysical Union.)

information about reactions of such compounds on mineral surfaces of tropospheric relevance is extremely limited. In 2001, Li et al. combined both laboratory studies and modeling analysis to investigate the reactions of several carbonyl compounds on the surface of mineral oxides.[175] Acetone, acetaldehyde, and propionaldehyde were reacted with α-Al_2O_3, TiO_2, α-Fe_2O_3, SiO_2, and CaO. The surface adsorption process was probed by spectroscopic techniques (transmission FT-IR and diffuse reflectance UV−vis spectroscopy) and a Knudsen cell in order to gain insight into the mechanism of VOC adsorption onto mineral particles and the kinetics of this adsorption. Both surface-bound and gas-phase products were identified in this study.

It was found that on SiO_2 particle surfaces, the organics adsorbed molecularly through hydrogen-bonding interactions with surface hydroxyl groups in a nonreactive and reversible fashion. The FT-IR data in Figure 38 show the spectra of acetaldehyde, acetone, and propionaldehyde adsorbed on SiO_2. It is important to note that these spectra were recorded at an equilibrium pressure of the carbonyl vapor. All absorptions due to the vapor phase were subtracted from the spectra shown in Figure 38. The most intense band in all of the spectra appeared near 1700 cm^{-1} and was assigned to the stretching motion of the carbonyl group. The frequencies of the absorption bands in the infrared spectra for these molecules adsorbed on SiO_2 were similar to those reported for the gas or liquid phase by the National Institute of Standards and Technology, suggesting that these molecules weakly adsorb on SiO_2. The decrease in intensity of the band at 3748 cm^{-1}, associated with the isolated OH groups, and a concomitant growth of a band at lower frequency near 3420 cm^{-1} suggest that there is a hydrogen-bonding interaction between the carbonyl compound and the surface hydroxyl groups.[347−349] Upon evacuation of the carbonyl vapor, the bands in the SiO_2 spectrum disappeared, indicating that these molecules are weakly and reversibly adsorbed to the surface of the SiO_2 particles.

A similar conclusion was drawn in the study by Carlos-Cuellar et al. examining the reaction of formaldehyde on SiO_2.[350] Formaldehyde is an important precursor to HO_x in the troposphere, and any heterogeneous interactions it may have with aerosol could potentially affect HO_x levels, especially if it is removed from the troposphere. The reaction of formaldehyde on SiO_2 was found to be reversible, and peaks observed in the presence of the gas phase that corresponded to weakly adsorbed formaldehyde were removed completely upon evacuation of the gas phase.

For the other oxides investigated by Li et al. (α-Al_2O_3, TiO_2, α-Fe_2O_3, SiO_2, and CaO), adsorption of the carbonyl compounds was found to be irreversible.[175] In fact, the spectra shown in Figure 39 of acetaldehyde, acetone, and propionaldehyde adsorbed on α-Al_2O_3 were recorded after evacuation of the carbonyl vapor. It was determined that these carbonyl compounds, acetaldehyde, acetone, and propionaldehyde, could undergo Aldol condensation reactions to form higher molecular weight carbonyl compounds on the surface of α-Al_2O_3 and the other oxides except for SiO_2. This can be seen in the infrared spectra; for example, infrared absorption bands between 1500 and 1675 cm^{-1} in the spectrum of acetaldehyde adsorbed on alumina (shown in Figure 39) were consistent with crotonaldehyde on

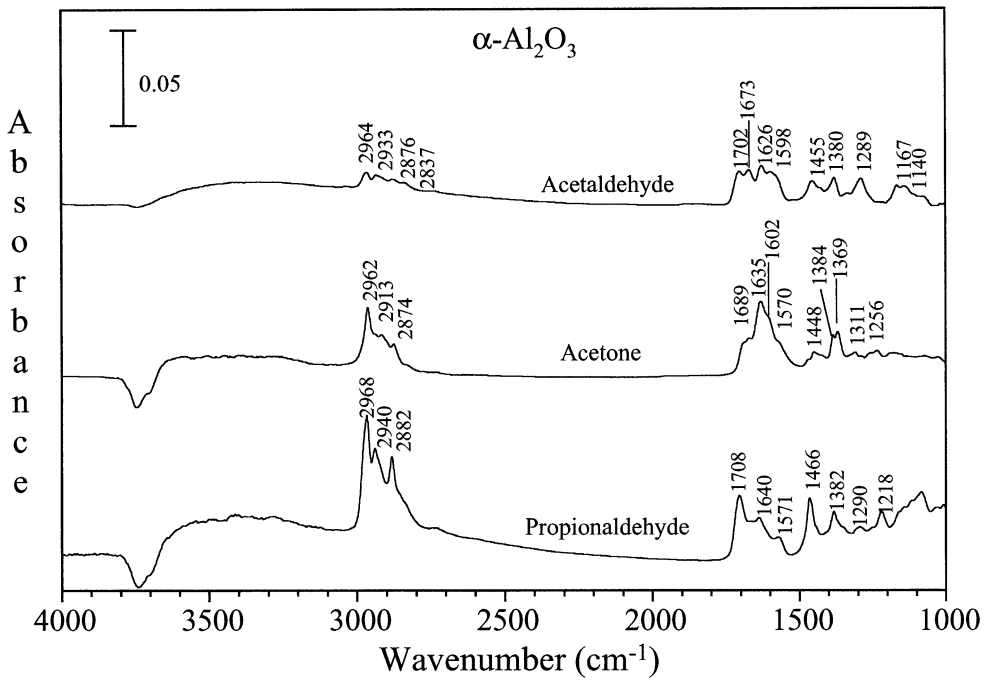

Figure 39. Transmission FT-IR spectra of acetaldehyde, acetone, and propionaldehyde adsorbed on α-Al_2O_3 particles after evacuation of ~10 mTorr (1 ppm) of the carbonyl vapor at $T = 298$ K. (Reproduced with permission from *J. Geophys. Res. 106*, D6, pp 5517−5529; P. Li, K. A. Perreau, E. Covington, C. H. Song, G. R. Carmichael, and V. H. Grassian, Heterogeneous reactions of volatile organic compounds on oxide particles of the most abundant crustal elements: surface reactions of acetaldehyde, acetone, and propionaldehyde on SiO_2, Al_2O_3, Fe_2O3, TiO_2, and CaO. Copyright 2001 American Geophysical Union.)

the surface. Propionaldehyde and acetone also underwent condensation reactions to form mesityl oxide (acetone reaction) and 2-methyl-2-pentenal (propionaldehyde reaction), and the spectra shown in Figure 39 are consistent with these products. These higher molecular weight compounds strongly adhere to the mineral oxide surface.

The kinetics of heterogeneous uptake were also measured. Initial uptake coefficients corrected for BET surface area were determined to be in the ranges of 2.9×10^{-6} to 3×10^{-4} for acetaldehyde, 6.2×10^{-6} to 3.6×10^{-4} for acetone, and 1.1×10^{-5} to 5.9×10^{-4} for propionaldehyde on these oxide surfaces from Knudsen cell experiments. It was observed that SiO_2 particles typically were the least reactive (lowest uptake coefficients compared to other oxides, α-Al_2O_3, TiO_2, α-Fe_2O_3, and CaO), consistent with the infrared data which showed weak adsorption to the surface. After initial uptake of the carbonyl, it was found that for the reactive oxides where Aldol condensation took place, small amounts (<1% of the total carbonyl taken up) of condensation product desorbed into the gas phase. Pressure dependence experiments on the uptake of acetaldehyde and formation of crotonaldehyde on CaO revealed first-order kinetics in acetaldehyde pressure for the uptake of acetaldehyde and second-order kinetics in acetaldehyde pressure for crotonaldehyde (CH_3-CHCHCHO) formation. The second-order kinetics are expected on the basis of the reaction mechanism

$$CH_3CHO(g) \rightarrow CH_3CHO(a) \quad (42)$$

$$CH_3CHO(a) + CH_3CHO(a) \rightarrow CH_3CHCHCHO(a) + H_2O(a) \quad (43)$$

$$CH_3CHCHCHO(a) \rightarrow CH_3CHCHCHO(g) \quad (44)$$

The heterogeneous reaction of carbonyl compounds on dust surfaces may also act as sources of secondary organic aerosol mass. Because these reactions may contribute to the secondary organic aerosol mass, it is important to understand the reaction mechanism. A mechanism for these reactions is shown in Figure 40. To evaluate the potential loss of carbonyl species (acetaldehyde, acetone, propionaldehyde, and formaldehyde) to mineral dust surfaces versus other known gas-phase loss mechanisms, a modeling analysis was performed by Li et al.[175] The results of this analysis are displayed in Figure 41. A plot of the calculated mass transfer coefficient versus uptake is shown in Figure 41 as a function of the aerosol distribution (lines in plots). These coefficients were calculated using eq 1 given under section 1.4.1. The calculated rates for gas-phase chemistry and photochemistry are shown in a double-*y* axes plot, where the rate constants and an estimate of the lifetime of the carbonyl (including formaldehyde, acetaldehyde, and acetone) for reaction with different gas-phase compounds were calculated by assuming a concentration of the reactant partner. Comparison of the rates of heterogeneous loss in different regions of the troposphere with the gas-phase and photolysis rates in those same regions showed that in the middle and upper troposphere, heterogeneous loss is comparable to gas-phase processes, on the basis of the uptake values discussed in Li et al. However, it was suggested that the critical importance of the heterogeneous uptake of carbonyls onto the surface of dust

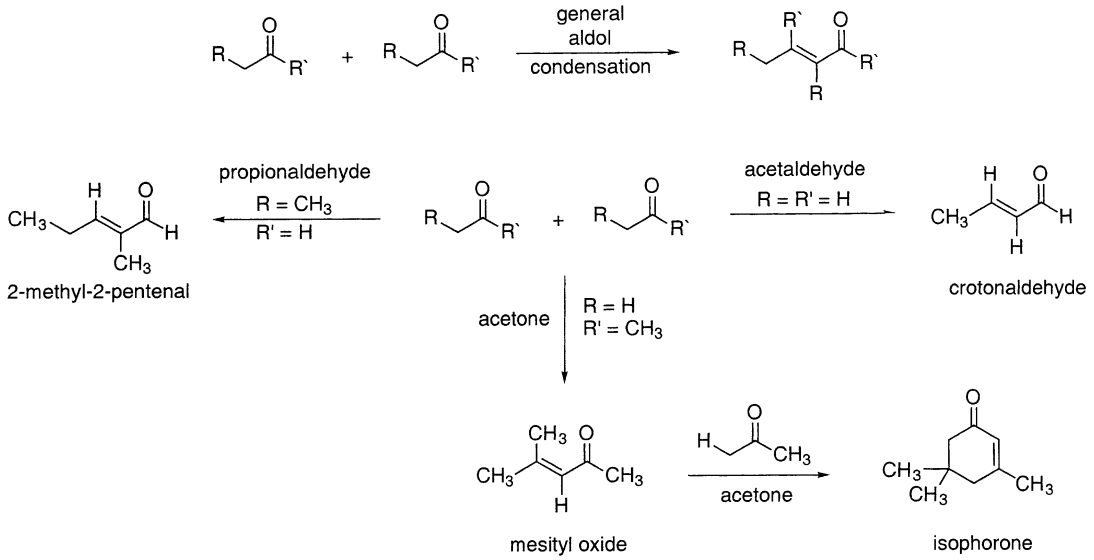

Figure 40. Reaction diagram showing the possible surface products that can form following Aldol condensation reactions of acetaldehyde, acetone, and propionaldehyde on oxide particles with acidic or basic properties. (Reproduced with permission from *J. Geophys. Res. 106*, D6, pp 5517−5529; P. Li, K. A. Perreau, E. Covington, C. H. Song, G. R. Carmichael, and V. H. Grassian, Heterogeneous reactions of volatile organic compounds on oxide particles of the most abundant crustal elements: surface reactions of acetaldehyde, acetone, and propionaldehyde on SiO_2, Al_2O_3, Fe_2O3, TiO_2, and CaO. Copyright 2001 American Geophysical Union.)

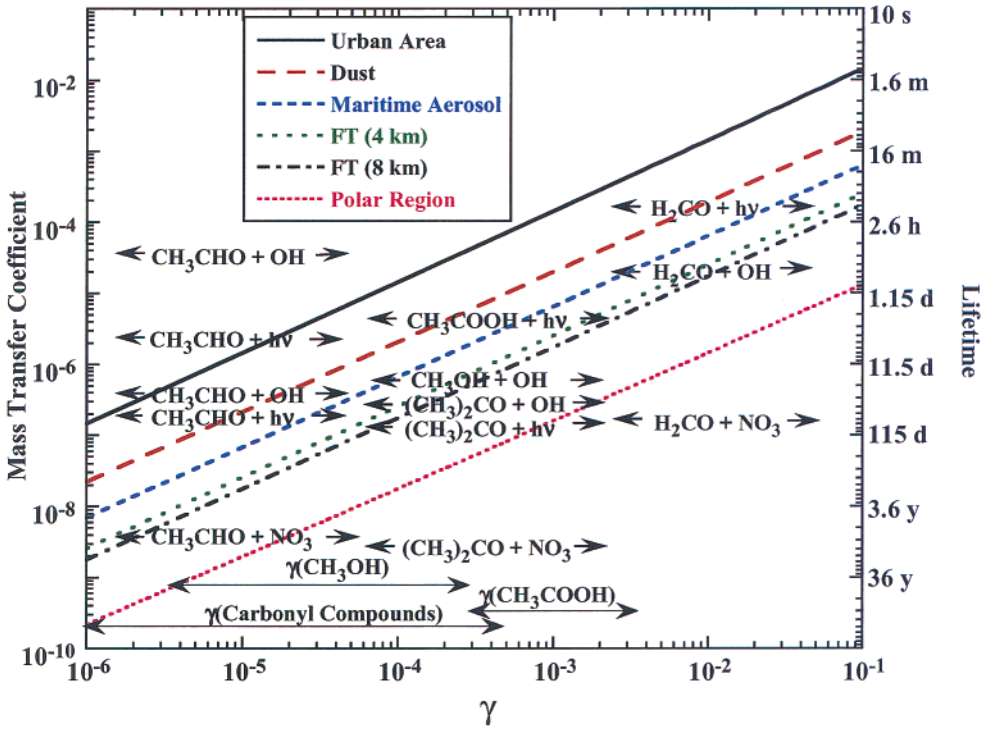

Figure 41. Calculated mass transfer coefficients as a function of the heterogeneous uptake γ (measured values of γ are indicated by the lines on the bottom of the graph). Different gas-phase loss mechanisms are also shown. This diagram shows that under certain conditions loss rates of these carbonyl compounds through heterogeneous uptake are comparable to other loss rate mechanisms. (Reproduced with permission from *J. Geophys. Res. 106*, D6, pp 5517−5529; P. Li, K. A. Perreau, E. Covington, C. H. Song, G. R. Carmichael, and V. H. Grassian, Heterogeneous reactions of volatile organic compounds on oxide particles of the most abundant crustal elements: surface reactions of acetaldehyde, acetone, and propionaldehyde on SiO_2, Al_2O_3, Fe_2O3, TiO_2, and CaO. Copyright 2001 American Geophysical Union.)

would depend on the fate of the surface-adsorbed carbonyl and whether it remains on the surface. The net effect would be to decrease HO_x production from these carbonyl compounds; however, if they further react, the impact on HO_x production may be greater or lesser.

2.4.2. Alcohols

There have been few studies of the uptake of alcohols on mineral dust or mineral dust proxies as related to the atmosphere. Methanol, in particular, is of great interest because it is a globally abundant

VOC with poorly understood sources and removal processes.[351] The 1997 Subsonic Assessment (SASS) Ozone and Nitrogen Oxide Experiment (SONEX) discovered large differences between atmospheric concentrations and estimated sources of methanol.[351] Understanding this discrepancy is important to atmospheric science because methanol has been linked to upper tropospheric NO_x and HO_x cycles.[351,352]

In Carlos-Cuellar et al., the uptake of methanol onto mineral oxides was investigated.[350] Transmission FT-IR spectroscopy was also utilized to examine the changes to the mineral oxide surface after reaction with the alcohol. The uptake of methanol onto α-Fe_2O_3 and α-Al_2O_3 was found to be mostly irreversible, with $<1-15\%$ desorption observed when the sample was opened to an evacuated system. In contrast, the adsorption onto SiO_2 was found to be largely reversible, similar to what was observed for carbonyl compounds as discussed in the previous subsection.

Initial values of the uptake coefficient were reported for the various oxides and determined from mass-dependent uptake data and are as follows: $(1.9 \pm 0.4) \times 10^{-4}$ (α-Fe_2O_3), $(1.0 \pm 0.7) \times 10^{-4}$ (α-Al_2O_3), and $(4 \pm 2) \times 10^{-6}$ (SiO_2). The uptake of methanol to the surface decreased as the reaction occurred, indicating the surface saturated with adsorbed methanol. Saturation coverage was determined using the Knudsen cell by exposing the sample to methanol until no further uptake was observed. α-Fe_2O_3 and α-Al_2O_3 yielded similar coverage values of $(2 \pm 1) \times 10^{13}$ molecules cm^{-2}, whereas the coverage on SiO_2 was 2 orders of magnitude lower, $(1.1 \pm 0.5) \times 10^{11}$ molecules cm^{-2}.

The implications for the adsorption of alcohol species onto mineral aerosol depend on the competitiveness of the heterogeneous reaction with homogeneous removal routes. When the rates of the heterogeneous reactions measured in this study in terms of a pseudo-first-order mass transfer constant (as done for the carbonyl studies discussed above) were expressed, comparison of the heterogeneous removal to gas-phase and photolysis losses over a range of aerosol size distributions and particle densities showed that the uptake of methanol onto surfaces may be competitive in urban, dust, and maritime aerosol distributions, given the above values of the uptake coefficients measured here (see Figure 41). This implies that in such regions, loss to aerosol surfaces may be a significant process for alcohol removal in the troposphere.

2.4.3. Organic Acids

Another class of oxygenated organic compounds of atmospheric interest is organic acids. Although there is some question as to all of the sources of organic acids, such as acetic acid in the atmosphere, it is known that both primary and secondary sources of acetic acid exist.[353] Acetic acid is one of the most abundant carboxylic acids in the troposphere. Concentrations of acetic acid reported in the literature vary by location, season, and time of day (from 0.05 to 16 ppbv of gas-phase acetic acid)[354] but are usually higher during the day, during the dry season, and in urban areas. Primary sources include anthropogenic emissions from biomass combustion and vehicular emissions and biogenic emissions from soil and vegetation.[354] Secondary sources consist of the photochemical oxidation of chemical precursors, such as the reaction of isoprenes and monoterpenes with ozone.[354] Removal processes for acetic acid in the troposphere principally comprise wet and dry deposition and, to a smaller extent, the reaction with OH radicals in the upper troposphere.[354] Single-particle and spectrochemical studies have shown that there are many tropospheric particles that contain organic acids.[160,327]

To elucidate a possible route to the coating of atmospheric particles with organic acids, heterogeneous uptake of acetic acid onto mineral oxide surfaces was also studied by Carlos-Cuellar et al.[350] Heterogeneous uptake of acetic acid on α-Fe_2O_3, α-Al_2O_3, and SiO_2 is greater than the uptake of methanol and formaldehyde. Specifically, both the rate of the reaction, as determined from the initial uptake coefficient, and the extent of the reaction, as determined from the surface saturation coverage, were greater for acetic acid than for methanol and the carbonyl compounds. The reversibility/irreversibility of acetic acid uptake was probed using transmission FT-IR. Spectra for iron oxide and alumina in the absence of the gas phase showed that features that correspond to surface-bound acetate remained. In contrast to the 100% reversible adsorption of methanol on SiO_2, acetic acid adsorption is partially irreversible on SiO_2.

The relevance of this loss mechanism as compared to gas-phase and photolysis processes in the troposphere were compared using the same analysis as for methanol and the carbonyl compounds, where the lifetime of acetic acid due to the heterogeneous process was compared to the lifetime due to gas-phase reactions (see Figure 41). In urban, dust, and maritime distributions, acetic acid loss to aerosol surface is competitive with gas-phase losses assuming uptake rates measured by Carlos-Cuellar et al. The heterogeneous loss of acetic acid indicates that the interaction of organic acids with mineral particles in the troposphere may have significant implications for the balance of such organic compounds, as well as compounds whose existence depends on them.

2.4.4. Other Semivolatile Organic Compounds

In a series of papers by Goss and co-workers, the adsorption of a series of SOCs was systematically studied on mineral oxides, clays, and carbonates.[355−357] Adsorption coefficients, K, normalized for surface area, were reported in these studies. The adsorption coefficient was defined as

$$K = \frac{\text{mg of substance/surface area of sorbent } (cm^2)}{\text{mg of substance/volume of gas } (cm^3)} \quad (46)$$

Importantly, in these studies the effects of temperature and relative humidity were investigated in detail. It was determined that for the adsorption of a series of organics on α-Al_2O_3, $CaCO_3$, and α-Fe_2O_3,

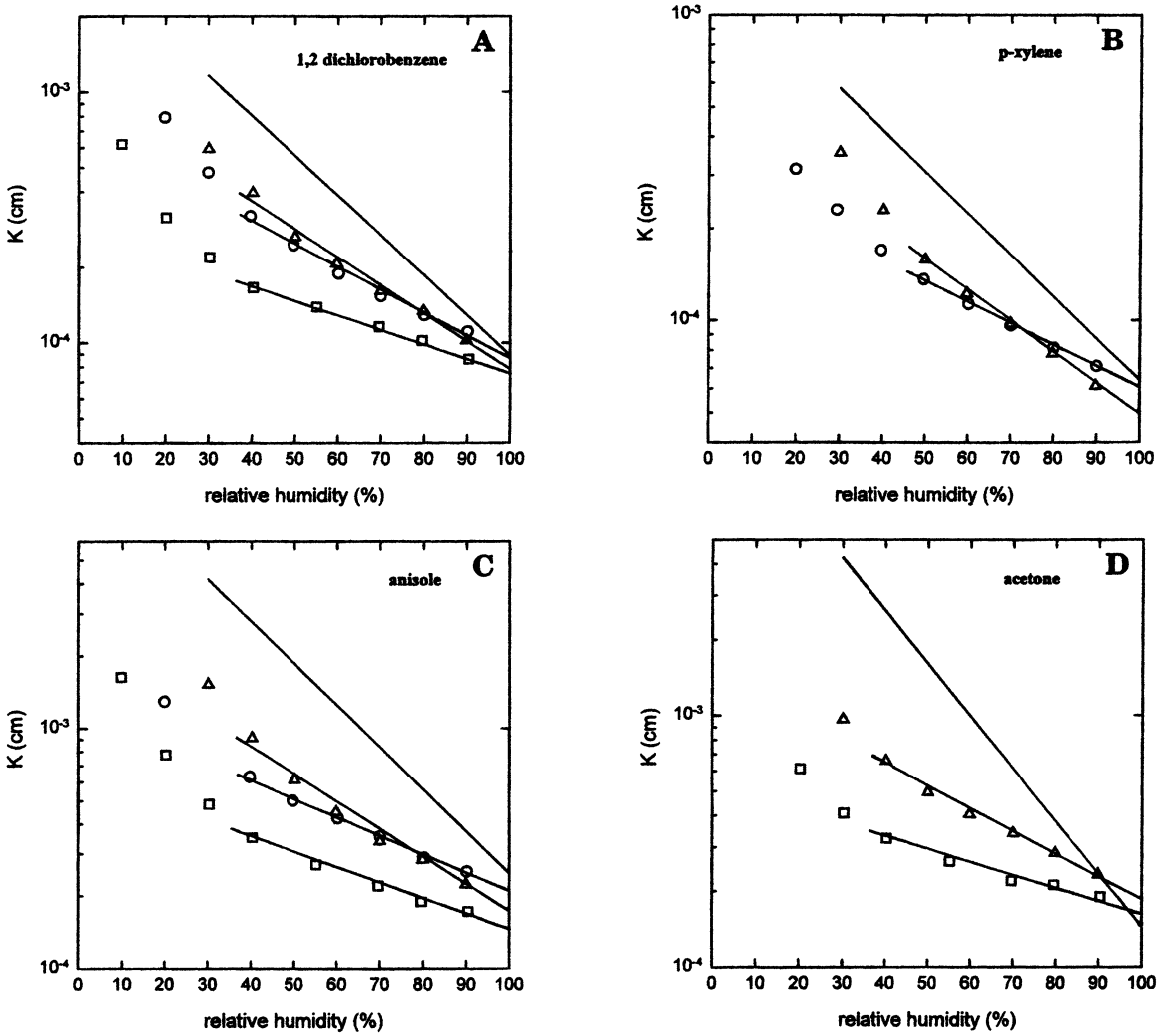

Figure 42. Adsorption coefficients determined at 60.5 °C, as a function of relative humidity for different minerals and compounds: (□) α-Al_2O_3; (○) $CaCO_3$; (△) α-Fe_2O_3; solid lines with no data points are fits to the data for quartz and kaolinite. (Reprinted with permission from ref 357. Copyright 1996 American Chemical Society.)

the effect of relative humidity on the gas adsorption coefficient could be described by the following equation for >30% RH

$$\ln K = \ln A - C(100 - \mathrm{RH}) \qquad (47)$$

where A represents the adsorption coefficient at 100% RH and C describes the extent of change of ln K with relative humidity. The value of A was nearly independent of the different minerals, suggesting that the mineral provided only a support for the water and did little else. The value of C was found to depend on the mineral, therefore reflecting the fact that at lower relative humidity the mineral itself was involved in the adsorption process. Figure 42 shows the adsorption coefficients for 1,2-dichlorobenzene, *p*-xylene, anisole, and acetone as a function of relative humidity on three different minerals. It can be seen from the slopes of the fitted lines that the effects of relative humidity are quite large. The adsorption coefficient in all cases decreased by ~1 order of magnitude over the 10−90% RH range.

In a later study by Goss, a conceptual model for the adsorption of organic compounds to liquid and solid surfaces was put forth.[358] The model took into account the interactions between the adsorbate and the surface and approximated the interactions at the surface as functional forms of van der Waals and acid−base interactions. This semiempirical model provided fairly good predictions; however, there were several limitations noted as well due to the difficulty in estimating surface parameters to describe the solid interface. Despite these limitations and difficulties, in a later study by Goss and Schwarzenbach, the same model was used to quantify the effect of relative humidity on the adsorption of organic compounds on mineral oxides.[332]

In a manner similar to the studies by Goss and coworkers, Jang and Kamens investigated a series of SOCs on Arizona road dust in an outdoor Teflon-film chamber.[359] Partitioning coefficients were determined for a series of SOCs including anthracene and pyrene. The partitioning coefficient, K_p, was defined as

$$\log K_p = \log \frac{F}{A \times \mathrm{TSP}} \qquad (48)$$

where F is the particle-phase concentration of the organic in units of ng m^{-3}, A is the gas-phase concentration in units of ng m^{-3}, and TSP is the

Table 9. Summary of Laboratory Studies Reviewed under Section 2.4

reactive species	sample(s)	technique	measurements	reference
n-hexane, *trans*-1,2-dichloroethylene, cyclohexane, dichloromethane, trichloroethylene, chloroform, 1,1,1-trichloroethane, tetrachloroethylene, benzene, *n*-octane, toluene, 1,2-dichloroethane, chlorobenzene, *m*-xylene, *p*-xylene, 1,3-dichlorobenzene, 1,2-dichlorobenzene, 1,3,5-trichlorobenzene, 2,3-benzofuran, diethyl ether, acetonitrile, methanol, anisole	Ca-kaolinite, Na-kaolinite, Ca-bentonite	GC	retention of vapors as measure of sorption capability of samples	Goss, 1993 (ref 355)
n-octane, *n*-nonane, *n*-decane, toluene, *p*-xylene, *o*-xylene, ethylbenzene, propylbenzene, chlorobenzene, 1,2-dichlorobenzene, 1,4-dichlorobenzene, 1,2,3,4-tetrachlorobenzene, naphthalene, anisole, pyridine, ethanol, ethyl acetate, acetone, diethyl ether	$CaCO_3$, α-Al_2O_3, α-Fe_2O_3	GC	retention of vapors as measure of sorption capability of samples	Goss and Eisenreich, 1996 (ref 357)
fluorene, phenanthrene-d_{10}, anthracene, anthracene-d_{10}, fluoranthene, pyrene, pyrene-d_{10}, benz[*a*]anthracene, 9-methylanthracene, heptadecane-d_{36}, nonadecane-d_{40}, eicosane-d_{42}, tricosane-d_{48}, dodecanoic acid, 4-biphenylcarbaldehyde, 9-phenanthrenecarbaldehyde, 9,10-anthraquinone, 3,5-dimethylphenol, 2-isopropylphenol, BHT, nonylphenol, 9-nitroanthracene	Arizona road dust	smog chamber, GC-MS, FT-IR	surface adsorption, reaction product identification	Jang and Kamens, 1999 (ref 359)
acetone, acetaldehyde, propionaldehyde	Al_2O_3, TiO_2, α-Fe_2O_3, SiO_2, CaO	Knudsen cell, FT-IR diffuse reflectance UV−vis	uptake coefficients, reaction product identification, surface adsorption	Li et al., 2001 (ref 175)
formaldehyde, methanol, acetic acid	SiO_2, α-Fe_2O_3, α-Al_2O_3	Knudsen cell, FT-IR	uptake coefficients, surface adsorption; reaction product identification	Carlos-Cuellar et al., 2003 (ref 350)

concentration of total suspended particulate matter in the atmosphere in units of mg m^{-3}. To better understand partitioning of SOCs on hydrated and dehydrated (i.e., baked) Arizona road dust, physicochemical properties of the SOCs were used to describe both specific and nonspecific interactions with the dust. The K_p values were better predicted when solute−solvation parameters were included rather than only vapor pressures.

2.4.5. Summary of Organic Compound Studies

The laboratory studies on organic compounds discussed under section 2.4 are summarized in Table 9, where the reactive gas, surface, and techniques used in each experiment along with the reference citation are given. The studies on organic compounds described above represent an important step in understanding the interaction between mineral dust and SOCs. A further understanding of the partitioning of organic SOCs is needed. In addition, adsorption isotherms and equilibrium coverages should be measured as a function of relevant tropospheric conditions of temperature and relative humidity. This will require both macroscopic measurements, such as the ones described above, and molecular spectroscopic measurements. Given the limited data set presented here, further studies on the interaction of organic compounds on authentic mineral dust samples are necessary.

3. Recommended Future Directions

In this section, several recommendations are made to further our understanding of reactions on mineral dust in the troposphere. A discussion of ways to improve the incorporation of reactions on dust into atmospheric chemistry models is presented. There is also a discussion concerning how laboratory studies could be improved to better represent the complexity of the atmosphere. Finally, a few suggestions for field measurements are also made.

3.1. Recommended Future Directions in Modeling Studies and Modeling Analysis

As discussed in the Introduction section (section 1.4), in the atmospheric chemistry modeling work of Dentener et al.,[148] surface reaction kinetics describing the uptake of trace atmospheric gases on dust was done in a relatively simplistic manner with respect to the surface chemistry involved. The model assumed that the uptake rate on the mineral dust was equal to the product of a rate constant, *k*, and the

gas concentration. The rate constant contains the number density of particles at a given radius, the uptake coefficient, and a gas-particle diffusion correction. However, constraints, such as consideration of surface saturation effects, were not included in the earlier models.

Since the atmospheric chemistry modeling work by Dentener et al.,[148] there have been a substantial number of laboratory studies and field measurements involving heterogeneous reactions on mineral dust. These studies, described under section 2 of this review, indicate that the surface chemistry is more complex than that described in the earlier modeling study. Several improvements in modeling analysis have been made since Dentener et al. For example, in Underwood et al., surface saturation effects for the reaction of nitrogen dioxide and nitric acid on mineral oxides and mineral dusts were considered in a box-model analysis.[180] In that study, the number of molecules adsorbed on the dust surface was calculated as the uptake proceeded. Once the surface coverage reached its maximum value, as determined by laboratory experiments on these systems, the heterogeneous reaction pathway was shut down. In another study by Song and Carmichael, heterogeneous uptake of gases onto alkaline aerosol was considered using a kinetic model that included thermodynamic constraints.[187] Further discussion of these issues and others was given in Song et al., including a very general examination of site specificity for reactions on mineral dust as well as the regeneration and poisoning of sites on an aerosol dust surface.[360] Other recent modeling studies have also included the influence of mineral dust on tropospheric chemistry.[361−363]

Although reactions of trace gases on dust were considered in a more complex manner in these later modeling studies, it is essential that even more details of surface reaction mechanisms be incorporated into atmospheric chemistry models if these models are to accurately describe the chemistry of the troposphere. In the next subsection, different mechanisms for heterogeneous chemistry of trace atmospheric gases on dust particles are discussed. These mechanisms provide molecular level insight into potentially important tropospheric reactions that can be incorporated into atmospheric chemistry models. Many of these mechanisms have been observed in laboratory studies, as discussed in detail under section 2 of this review.

3.1.1. Chemical Scenarios for Surface Reaction Mechanisms on Mineral Dust

In 1997, Ravishankara described heterogeneous and multiphase reactions as reactions that take place on solid and liquid surfaces, respectively.[4] For reactions on solids, reactions were described as being surface area limited with no diffusion occurring into the bulk of the solid. In the case of liquids, reactions were proposed to be surface area or volume limited, depending on the diffusional characteristics of the system. From the laboratory studies described herein, it is clear that for reactions on solid surfaces, specifically those that involve mineral dust, the situation is more complicated than that described by Ravishankara.[4] In this section, several chemical scenarios for heterogeneous reaction mechanisms involving solid surfaces in the atmosphere, with an emphasis on mineral dust, are examined. The key mechanistic features of each scenario are highlighted, so depending on the specific gas and mineral dust reaction, the appropriate mechanism(s) can be incorporated into atmospheric chemistry models.

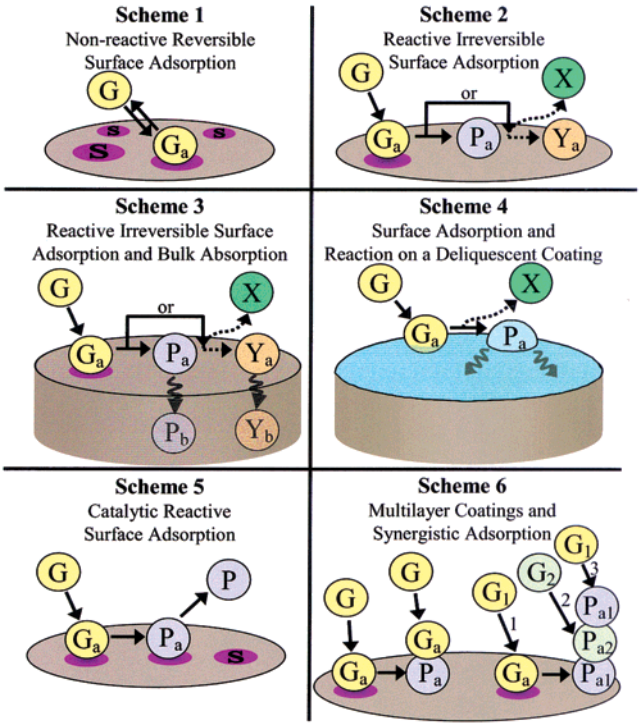

Figure 43. Different reaction schemes for uptake of gases on mineral dust. Various chemical components include surface sites (S), gas-phase reactants (G), and product species (P, X, and Y), which can be released into the gas phase, adsorbed to the surface (subscripted a), and/or incorporated into the bulk (subscripted b). Numbers located along arrows represent sequential reactions, whereas subscripted numbers signify different species of the same phase (i.e., G_1 is a different reactant gas from G_2). These schemes can be incorporated into atmospheric chemistry models. See text for further details.

Generalized schemes for different reaction mechanisms are shown in Figure 43. Scheme 1 represents the nonreactive reversible adsorption of a gas, G, taken up by a surface according to

$$G + \text{site} \leftrightarrows G(a) \qquad (49)$$

Assuming a simple Langmuir-type adsorption mechanism, the coverage of G on the surface, θ, will depend on the pressure of G in the atmosphere, the temperature, and the Langmuir equilibrium constant, K. The equilibrium constant is defined as the ratio of the rate of adsorption onto surface sites divided by the rate of desorption. This type of interaction for the adsorption onto stratospheric particles has been previously discussed by Tabazadeh and Turco.[364] Under steady-state conditions, the equilibrium coverage is given as

$$\theta = \frac{KP}{1 + KP} \quad (50)$$

and the uptake coefficient, γ, is related to the coverage according to the equation

$$\gamma = \gamma_0(1 - \theta) \quad (51)$$

Thus, the uptake coefficient will be coverage- and time-dependent as the surface approaches an equilibrium coverage. It is important to note that Scheme 1 also implies that in some cases as the particle is transported in the atmosphere from region to region the adsorbed gas will be released from the particle; that is, there will be desorption from the surface when there is a decrease in the pressure of that species in the surrounding gas phase. Therefore, mineral dust potentially represents a viable way to transport molecules through the atmosphere and can be a source of gas-phase pollutants. This may be especially important in the case of semivolatile organic compounds.

Scheme 2 in Figure 43 represents the reversible adsorption of a gas molecule followed by surface reaction, with and without the formation of gas-phase products, according to the reaction

$$G(g) + \text{site} \leftrightarrows G(a) \rightarrow P(a) \quad (52a)$$

or

$$G(g) + \text{site} \leftrightarrows G(a) \rightarrow Y(a) + X(g) \quad (52b)$$

In this case, a constraint on the adsorption needs to be considered because as surface sites become blocked in this mechanism by surface-bound products (P or Y, with and without the formation of gas-phase products), the reaction should cease. This case was considered in earlier work by Tabazadeh and Turco[364] and more recently in greater detail by Ammann et al.[365] In Ammann et al., observed uptake coefficients on solid surfaces were parametrized in terms of reversible adsorption followed by surface reaction with a surface site that could be, for example, a preadsorbed molecule. Ammann et al. also showed that the coverage, and therefore time-dependent uptake, could effectively model laboratory data. This model was specifically applied to reactions of ozone with organic-coated soot and organic aerosol but should be applicable to mineral dust chemistry as well.

Scheme 3 in Figure 43 represents the reversible adsorption of a gas molecule followed by surface reaction, with and without the formation of gas-phase products, and absorption of the product into the bulk of the surface. In this case, surface sites are regenerated and the reactivity of the mineral dust particle will be constrained by the total volume of the particle and not just the number of available surface sites.

Scheme 4 in Figure 43 represents surface adsorption of a gas molecule on a deliquescent film coating the dust particle, followed by solvation into the aqueous phase, diffusion, and reaction within the film, with and without the formation of gas-phase products. In this case, the uptake may potentially be described by gas uptake on an aqueous droplet of similar composition. The modeling of gas uptake into aqueous droplets has been described in detail by Jacob,[8] and a discussion of this is given under section 1.4.2 of this review.

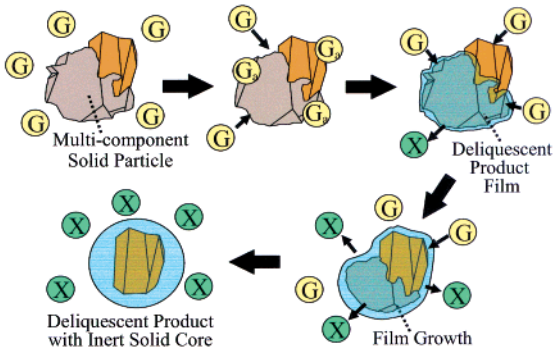

Figure 44. Pictorial representation of how a particle may change as it is processed in the atmosphere. In this case, a multicomponent solid particle is converted into a liquid droplet as the reaction proceeds and one of the components reacts. This has been observed in laboratory studies for calcium carbonate particles upon reaction with nitric acid even at low relative humidity.[186,367]

Scheme 5 represents a catalytic reaction. In this case, the modeling analysis described in Dentener et al. and discussed under section 1.4.1 is applicable; that is, the rate of the reaction can be described to continuously occur in the atmosphere without saturation. However, it should be noted that even for catalytic reactions, such as ozone destruction on mineral dust, the reactive uptake coefficient decreases over time until a steady-state uptake coefficient is reached, as some of the more reactive sites become less active over time.

Scheme 6 represents an even greater level of complexity whereby multilayer coatings can form on the surface and synergistic adsorption can also occur; that is, an adsorbed molecule may assist in the adsorption of another molecule by providing a reactive site (e.g., adsorbed C=C for ozone reaction) or a medium (e.g., adsorbed H_2O for HNO_3 uptake). Multilayer coatings and synergistic adsorption was considered by Mozurkewich in his work on modeling adsorption and chemistry important in polar stratospheric clouds.[366] The reader is referred to that paper for additional details.

The discussion above examines different schemes that may be needed in atmospheric chemistry models depending on the details of how a particular gas interacts with mineral dust. It is important to increase the level of sophistication of reaction mechanisms involving heterogeneous reactions on mineral dust. However, it should be noted that the details about the nature of reactive sites on a tropospheric particle, the nature of the particle surface, and how the particle reactivity changes over time as the particle ages in the atmosphere are not explicitly presented in the discussion above.

An example of how the reactivity of a particle can change over time is demonstrated in Figure 44, whereby the displayed particle reacts such that the product formed deliquesces at low relative humidity. One case specifically described by this behavior is the reaction of nitric acid and calcium carbonate, given in eq 15 of section 2.1.1. For this reaction, the product

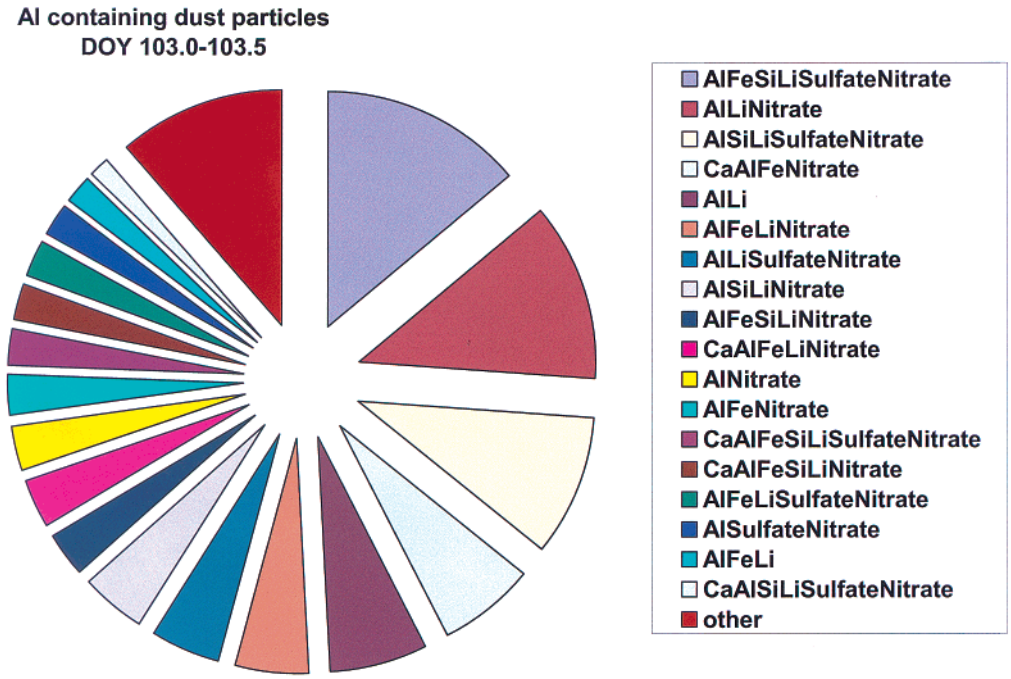

Figure 45. ATOFMS data for aluminum particles collected during the ACE-Asia field campaign (DOY 103.0−103.5). The particles are classified and sorted according to different types. The data are shown in a pie graph and represent the complexity of mineral dust particles containing aluminum in the troposphere. (Courtesy of Guazzotti et al., ref 369.)

calcium nitrate deliquesces at a relative humidity of <20%.[186,367] In this case, the particle will be transformed from a solid to a liquid droplet as it is transported and aged in the atmosphere. Initially, as the deliquescent product layer begins to build up, the reactive uptake coefficient will be time dependent as the phase of the particle changes.

From the discussion above, several specific recommendations for improving modeling analysis are made here. The first recommendation is to increase the level of detail incorporated into atmospheric chemistry models with respect to heterogeneous reactions on solid surfaces as described in Schemes 1−6 above. The second recommendation, which is complementary to the first recommendation, is to include mineralogy and chemical composition of the dust into the models. The models that take into account heterogeneous chemistry on mineral dust must go beyond representing the dust as just a size distribution. It is clear from section 2 that quartz (SiO_2), for example, will react very differently from other minerals, such as calcite ($CaCO_3$). Source apportionment and the mineralogy of dust from various dust sources such as the two major source regions—the Sahara and Gobi Deserts—should be incorporated into models. This idea is currently implemented in models that describe climate forcing due to dust aerosol.[31,81,121] To a first approximation, the atmospheric chemistry models can consider the dust as an external mixture of the various components. The abundance of each is weighted by its fractional component. Of course, more details could be included, such as the size fractionation of different components of dust, which was discussed in the Introduction under section 1.2.1.

Last, it would be useful to model changes of the mineral aerosol as it is processed in the atmosphere. Specifically, can models accurately track dust plumes as they age in the atmosphere by encountering air masses with different chemical constituents and account for the changing surface chemical characteristics (nitrate-coated, organic-coated, etc.)?

3.2. Recommended Future Directions in Laboratory Studies

It is clear that there are difficulties in measuring heterogeneous reaction rates on particles present as bulk powders. As already discussed under section 2, it is preferable to measure uptake on isolated particles and not bulk powders to remove large uncertainties in bulk powder measurements due to diffusion of gas into the powder and, therefore, better define the available surface area. This is especially important when diffusion and surface saturation occur on the same time scale.[368] Laboratory studies can be further improved by focusing on methods and techniques for studying the chemistry of individual particles. The difficulty here lies in the fact that single-particle techniques or methods are not sensitive enough to detect surface coverages on the order of ≤1 monolayer. Single-particle methods that have probed heterogeneous reactions thus far have been used to study liquid organic aerosol and reactions that occur within the bulk of the particle. Therefore, the first recommendation is to further develop single-particle analysis for laboratory studies to probe the heterogeneous chemistry of trace atmospheric gases with individual particles. A follow-up recommendation is to investigate the reactivity of various authentic dust sources to determine differences in their reactivities and to try to connect these differences to the chemistry of the individual particles as a function of composition and size in the dust sources. These studies should be combined with single-particle analy-

sis, and thus, the different reactive components of the dust can be understood.

The third recommendation is to perform laboratory studies under conditions of relative humidity, temperature, and pressure of the reactant gas that are most relevant to the atmosphere. Included in this recommendation is that the complexity of the atmosphere, in terms of the multiple components present in air masses, should also be simulated in laboratory studies. For example, water has been shown to play a key role in reactions on tropospheric particles, but are there other gas-phase components in the troposphere that are similarly influential in affecting the reactivity of mineral aerosol? It is also important to note that there are some concerns in extrapolating experiments done at high partial pressures to the lower partial pressures at which trace gases are typically found. The reasons for these concerns include the nonlinear relationship between surface coverage and pressures due to adsorbate−adsorbate interactions and contributions from gas-phase dimers at higher pressure (e.g., N_2O_4).

3.3. Recommended Future Directions in Field Measurements

It is difficult to give recommendations for field measurements at this time as several very large field campaigns have been completed within the past 1−2 years and the data are currently being analyzed and submitted for publication. For example, several special journal issues dedicated to Trace-P and ACE-Asia, two field campaigns that took place in spring 2001, are being prepared for publication. Figure 45 displays some of these recent data, specifically single-particle mass spectrometry (ATOFMS) analysis of mineral aerosol from the ACE-Asia field study.[369] The data, represented as a pie graph, show many different types of aluminum-containing particles. It is clearly seen from the single-particle data that the composition of mineral dust is quite complex and diverse.

One recommendation for field campaigns is to make measurements of *both* the aerosol and gas phase as accurately as possible. The second recommendation is to further improve single-particle analysis such that quantitative information can be obtained.[323] In addition, as discussed in laboratory studies above, improving the sensitivity of single-particle analysis to achieve monolayer surface sensitivity will help unravel the complexity of the surfaces of mineral dust aerosol. The final recommendation for field studies is for the establishment of additional continuous aerosol monitoring sites and/or their data reported, as has been done in a few cases.[21] This will provide additional and complementary data to the large field campaigns that occur on a very sporadic basis.

4. Acknowledgments

We thank Zev Levin, Kimberly Prather, and Sergio Guazzotti for providing us with original figures. We gratefully acknowledge the National Science Foundation and the Department of Energy for financial support.

5. References

(1) Kolb, C. E.; Worsnop, D. R.; Zahniser, M. S.; Davidovits, P.; Keyser, L. F.; Leu, M.-T.; Molina, M. J.; Hanson, D. R.; Ravishankara, A. R. *Adv. Ser. Phys. Chem.* **1995**, *3*, 771.
(2) Molina, M. J.; Molina, L. T.; Kolb, C. E. *Annu. Rev. Phys. Chem.* **1996**, *47*, 327.
(3) Andreae, M. O.; Crutzen, P. J. *Science* **1997**, *276*, 1052.
(4) Ravishankara, A. R. *Science* **1997**, *276*, 1058.
(5) Kreidenweis, S. M. In *Perspectives in Environmental Chemistry*; Macalady, D. L., Ed.; Oxford University Press: New York, 1998.
(6) De Haan, D. O.; Brauers, T.; Oum, K.; Stutz, J.; Nordmeyer, T.; Finlayson-Pitts, B. J. *Int. Rev. Phys. Chem.* **1999**, *18*, 343.
(7) Hemminger, J. C. *Int. Rev. Phys. Chem.* **1999**, *18*, 387.
(8) Jacob, D. J. *Atmos. Environ.* **2000**, *34*, 2131.
(9) Grassian, V. H. *Int. Rev. Phys. Chem.* **2001**, *20*, 467.
(10) Grassian, V. H. *J. Phys. Chem. A* **2002**, *106*, 860.
(11) Reid, J. P.; Sayer, R. M. *Sci. Prog.* **2002**, *85*, 263.
(12) Haywood, J.; Boucher, O. *Rev. Geophys.* **2000**, *38*, 513.
(13) IPCC. *Climate Change 2001: The Scientific Basis. Contribution of Working Group I to the Third Assessment Report of the Intergovernmental Panel on Climate Change*; Cambridge University Press: Cambridge, U.K., 2001.
(14) Sokolik, I. N.; Winker, D. M.; Bergametti, G.; Gillette, D. A.; Carmichael, G.; Kaufman, Y. J.; Gomes, L.; Schütz, L.; Penner, J. E. *J. Geophys. Res.* **2001**, *106*, 18015.
(15) Kohfeld, K. E.; Harrison, S. P. *Earth-Sci. Rev.* **2001**, *54*, 81.
(16) Pye, K. *Aeolian Dust and Dust Deposits*; Academic: Orlando, FL, 1987.
(17) Goudie, A. S.; Middleton, N. J. *Earth-Sci. Rev.* **2001**, *56*, 179.
(18) Prospero, J. M. In *The Impact of Desert Dust Across the Mediterranean*; Guerzoni, S., Chester, R., Eds.; Kluwer: Dordrecht, The Netherlands, 1996.
(19) Prospero, J. M. In *Particle Flux in the Ocean*; Ittekkot, V., Schafer, P., Honjo, S., Depetris, P. J., Eds.; Wiley: Chichester, U.K., 1996; Vol. SCOPE Report 57.
(20) Prospero, J. M. *Proc. Natl. Acad. Sci. U.S.A.* **1999**, *96*, 3396.
(21) Prospero, J. M. *J. Geophys. Res.* **1999**, *104*, 15917.
(22) Duce, R. A. In *Aerosol Forcing of Climate*; Charlson, R. J., Heintzenberg, J., Eds.; Wiley: Chichester, U.K., 1995.
(23) Andreae, M. O. In *World Survey of Climatology—Future Climates of the World: A Modelling Perspective*; Henderson-Sellers, A., Ed.; Elsevier: Amsterdam, The Netherlands, 1995; Vol. 16.
(24) Buseck, P. R.; Pósfai, M. *Proc. Natl. Acad. Sci. U.S.A.* **1999**, *96*, 3372.
(25) Buseck, P. R.; Jacob, D. J.; Pósfai, M.; Li, J.; Anderson, J. R. *Int. Geol. Rev.* **2000**, *42*, 577.
(26) Wedepohl, K. H. *Geochim. Cosmochim. Acta* **1995**, *59*, 1217.
(27) Berry, L. G.; Mason, B.; Dietrich, R. V. *Mineralogy*, 2nd ed.; W. H. Freeman: New York, 1983.
(28) Anthony, J. W.; Bideaux, R. A.; Bladh, K. W.; Nichols, M. C. *Handbook of Mineralogy*; Mineral Data Publishing: Tucson, AZ, 1995.
(29) Glaccum, R. A.; Prospero, J. M. *Mar. Geol.* **1980**, *37*, 295.
(30) Betzer, P. R.; Carder, K. L.; Duce, R. A.; Merrill, J. T.; Tindale, N. W.; Uematsu, M.; Costello, D. K.; Young, R. W.; Feely, R. A.; Breland, J. A.; Bernstein, R. E.; Greco, A. M. *Nature* **1988**, *336*, 568.
(31) Sokolik, I. N.; Toon, O. B. *J. Geophys. Res.* **1999**, *104*, 9423.
(32) Molinaroli, E. In *The Impact of Desert Dust Across the Mediterranean*; Guezoni, S., Chester, R., Eds.; Kluwer: Dordrecht, The Netherlands, 1996.
(33) Chester, R.; Elderfield, H.; Griffin, J. J.; Johnson, L. R.; Padgham, R. C. *Mar. Geol.* **1972**, *13*, 91.
(34) Caquineau, S.; Gaudichet, A.; Gomes, L.; Magonthier, M.-C.; Chatenet, B. *Geophys. Res. Lett.* **1998**, *25*, 983.
(35) Sarnthein, D.; Thiede, J.; Pflaumann, U.; Erlenkeuser, H.; Futterer, D.; Koopman, B.; Lange, H.; Seibold, E. In *Geology of the Northwest African Continental Margin*; von Rad, U., Hinz, K., Sarnthein, M., Seibold, E., Eds.; Springer: Berlin, Germany, 1982.
(36) Claquin, T.; Schulz, M.; Balkanski, Y. J. *J. Geophys. Res.* **1999**, *104*, 22243.
(37) Schütz, L. In *Paleoclimatology and Paleometeorology: Modern and Past Patterns of Global Atmospheric Transport*; Leinen, M., Sarnthein, M., Eds.; Kluwer: Dordrecht, The Netherlands, 1989.
(38) Rahn, K. A.; Borys, R. D.; Shaw, G. E.; Schütz, L.; Jaenicke, R. In *Saharan Dust: Mobilization, Transport and Deposition*; Morales, C., Ed.; Wiley: Chichester, U.K., 1979; Vol. SCOPE Report 14.
(39) Guieu, C.; Thomas, A. J. In *The Impact of Desert Dust Across the Mediterranean*; Guerzoni, S., Chester, R., Eds.; Kluwer: Dordrecht, The Netherlands, 1996.

(40) Güllü, G. H.; Ölmez, I.; Tuncel, G. In *The Impact of Desert Dust Across the Mediterranean*; Guerzoni, S., Chester, R., Eds.; Kluwer: Dordrecht, The Netherlands, 1996.
(41) Eltayeb, M. A. H.; Injuk, J.; Maenhaut, W.; Van Grieken, R. E. *J. Atmos. Chem.* **2001**, *40*, 247.
(42) Gomes, L.; Gillette, D. A. *Atmos. Environ.* **1993**, *27A*, 2539.
(43) Formenti, P.; Andreae, M. O.; Lange, L.; Roberts, G.; Cafmeyer, J.; Rajta, I.; Maenhaut, W.; Artaxo, P.; Lelieveld, J. *J. Geophys. Res.* **2001**, *106*, 14919.
(44) Prospero, J. M.; Olmez, I.; Ames, M. *Water, Air, Soil Pollut.* **2001**, *125*, 291.
(45) Chiapello, I.; Bergametti, G.; Chatenet, B.; Bousquet, P.; Dulac, F.; Santos Soares, E. *J. Geophys. Res.* **1997**, *102*, 13701.
(46) Silva, P. J.; Carlin, R. A.; Prather, K. A. *Atmos. Environ.* **2000**, *34*, 1811.
(47) Bory, A. J.-M.; Biscaye, P. E.; Svensson, A.; Grousset, F. E. *Earth Planet. Sci. Lett.* **2002**, *196*, 123.
(48) Basile, I.; Grousset, F. E.; Revel, M.; Petit, J. R.; Biscaye, P. E.; Barkov, N. I. *Earth Planet. Sci. Lett.* **1997**, *146*, 573.
(49) Biscaye, P. E.; Grousset, F. E.; Revel, M.; Van Der Gaast, S.; Zielinski, G. A. *J. Geophys. Res.* **1997**, *102*, 26765.
(50) Grousset, F. E.; Biscaye, P. E. In *Paleoclimatology and Paleometeorology: Modern and Past Patterns of Global Atmospheric Transport*; Leinen, M., Sarnthein, M., Eds.; Kluwer: Dordrecht, The Netherlands, 1989.
(51) Grousset, F. E.; Parra, M.; Bory, A.; Martinez, P.; Bertrand, P.; Shimmield, G.; Ellam, R. M. *Quat. Sci. Rev.* **1998**, *17*, 395.
(52) Mizota, C.; Matsuhisa, Y. *Geoderma* **1995**, *66*, 313.
(53) Rognon, P.; Coudé-Gaussen, G.; Revel, M.; Grousset, F. E.; Pedemay, P. *Sedimentology* **1996**, *43*, 359.
(54) Kurtz, A. C.; Derry, L. A.; Chadwick, O. A. *Geochim. Cosmochim. Acta* **2001**, *65*, 1971.
(55) Aléon, J.; Chaussidon, M.; Marty, B.; Schütz, L.; Jaenicke, R. *Geochim. Cosmochim. Acta* **2002**, *66*, 3351.
(56) Wagenbach, D.; Preunkert, S.; Schafer, J.; Jung, W.; Tomadin, L. In *The Impact of Desert Dust Across the Mediterranean*; Guerzoni, S., Chester, R., Eds.; Kluwer: Dordrecht, The Netherlands, 1996.
(57) Perry, K. D.; Cahill, T. A.; Eldred, R. A.; Dutcher, D. D.; Gill, T. E. *J. Geophys. Res.* **1997**, *102*, 11225.
(58) Prospero, J. M.; Glaccum, R. A.; Nees, R. T. *Nature* **1981**, *289*, 570.
(59) Talbot, R. W.; Andreae, M. O.; Berresheim, H.; Artaxo, P.; Garstang, M.; Harriss, R. C.; Beecher, K. M.; Li, S. M. *J. Geophys. Res.* **1990**, *95*, 16955.
(60) Swap, R.; Garstang, M.; Greco, S.; Talbot, R.; Kållberg, P. *Tellus* **1992**, *44B*, 133.
(61) Franzen, L. G.; Hjelmroos, M.; Kallberg, P.; Brorstrom-Lunden, E.; Juntto, S.; Savolainen, A.-L. *Atmos. Environ.* **1994**, *28*, 3587.
(62) Franzen, L. G.; Hjelmroos, M.; Kållberg, P.; Rapp, A.; Mattsson, J. O.; Brorstrom-Lunden, E. *Weather* **1995**, *50*, 313.
(63) Ganor, E.; Foner, H. A.; Brenner, S.; Neeman, E.; Lavi, N. *Atmos. Environ.* **1991**, *25*, 2665.
(64) Ganor, E.; Foner, H. A. In *The Impact of Desert Dust Across the Mediterranean*; Guerzoni, S., Chester, R., Eds.; Kluwer: Dordrecht, The Netherlands, 1996.
(65) Alpert, P.; Ganor, E. *J. Geophys. Res.* **2001**, *106*, 18275.
(66) Jaffe, D.; Anderson, T.; Covert, D.; Kotchenruther, R.; Trost, B.; Danielson, J.; Simpson, W.; Berntsen, T.; Karlsdottir, S.; Blake, D.; Harris, J.; Carmichael, G.; Uno, I. *Geophys. Res. Lett.* **1999**, *26*, 711.
(67) Husar, R. B.; Tratt, D. M.; Schichtel, B. A.; Falke, S. R.; Li, F.; Jaffe, D.; Gasso, S.; Gill, T.; Laulainen, N. S.; Lu, F.; Reheis, M. C.; Chun, Y.; Westphal, D.; Holben, B. N.; Gueymard, C.; McKendry, I.; Kuring, N.; Feldman, G. C.; McClain, C.; Frouin, R. J.; Merrill, J.; DuBois, D.; Vignola, F.; Murayama, T.; Nickovic, S.; Wilson, W. E.; Sassen, K.; Sugimoto, N.; Malm, W. C. *J. Geophys. Res.* **2001**, *106*, 18317.
(68) McKendry, I. G.; Hacker, J. P.; Stull, R.; Sakiyama, S.; Mignacca, D.; Reid, K. *J. Geophys. Res.* **2001**, *106*, 18361.
(69) Tratt, D. M.; Frouin, R. J.; Westphal, D. L. *J. Geophys. Res.* **2001**, *106*, 18371.
(70) VanCuren, R. A.; Cahill, T. A. *J. Geophys. Res.* **2002**, *107*, 10.1029/2002JD002204.
(71) Jaffe, D.; McKendry, I.; Anderson, T.; Price, H. *Atmos. Environ.* **2003**, *37*, 391.
(72) Darzi, M.; Winchester, J. W. *J. Geophys. Res.* **1982**, *87*, 1251.
(73) Bodhaine, B. A. *J. Geophys. Res.* **1983**, *88*, 10753.
(74) Parrington, J. R.; Zoller, W. H.; Aras, N. K. *Science* **1983**, *220*, 195.
(75) Braaten, D. A.; Cahill, T. A. *Atmos. Environ.* **1986**, *20*, 1105.
(76) Zieman, J. J.; Holmes, J. L.; Connor, D.; Jensen, C. R.; Zoller, W. H.; Hermann, D. M.; Parrington, J. R.; Gordon, G. E. *J. Geophys. Res.* **1995**, *100*, 25.
(77) Holmes, J.; Zoller, W. *Tellus* **1996**, *48B*, 83.
(78) Perry, K. D.; Cahill, T. A.; Schnell, R. C.; Harris, J. M. *J. Geophys. Res.* **1999**, *104*, 18521.
(79) Jonas, P.; Charlson, R.; Rodhe, H. In *Climate Change*; Fiocco, G., Ed.; Cambridge University Press: Cambridge, 1995.
(80) Tegen, I.; Fung, I. *J. Geophys. Res.* **1994**, *99*, 22897.
(81) Sokolik, I. N.; Toon, O. B. *Nature* **1996**, *381*, 681.
(82) Sheehy, D. P. *Ambio* **1992**, *21*, 303.
(83) Henderson-Sellers, A. In *World Survey of Climatology- -Future Climates of the World: A Modelling Perspective*; Henderson-Sellers, A., Ed.; Elsevier: Amsterdam, 1995; Vol. 16.
(84) Gomes, L.; Bergametti, G.; Coudé-Gaussen, G.; Rognon, P. *J. Geophys. Res.* **1990**, *95*, 13927.
(85) Alfaro, S. C.; Gaudichet, A.; Gomes, L.; Maille, M. *J. Geophys. Res.* **1997**, *102*, 11239.
(86) Marticorena, B.; Bergametti, G. *J. Geophys. Res.* **1995**, *100*, 16415.
(87) Pereira, E. B.; Setzer, A. W.; Gerab, F.; Artaxo, P. E.; Pereira, M. C.; Monroe, G. *J. Geophys. Res.* **1996**, *101*, 23983.
(88) Husar, R. B.; Prospero, J. M.; Stowe, L. L. *J. Geophys. Res.* **1997**, *102*, 16889.
(89) Durkee, P. A.; Nielsen, K. E.; Smith, P. J.; Russell, P. B.; Schmid, B.; Livingston, J. M.; Holben, B. N.; Tomasi, C.; Vitale, V.; Collins, D.; Flagan, R. C.; Seinfeld, J. H.; Noone, K. J.; Ostrom, E.; Gasso, S.; Hegg, D.; Russell, L. M.; Bates, T. S.; Quinn, P. K. *Tellus* **2000**, *52B*, 484.
(90) Diaz, J. P.; Exposito, F. J.; Torres, C. J.; Herrera, F.; Prospero, J. M.; Romero, M. C. *J. Geophys. Res.* **2001**, *106*, 18403.
(91) Ozsoy, E.; Kubilay, N.; Nickovic, S.; Moulin, C. *J. Geophys. Res.* **2001**, *106*, 18439.
(92) Coudé-Gaussen, G.; Rognon, P.; Bergametti, G.; Gomes, L.; Strauss, B.; Gros, J. M.; Le Coustumer, M. N. *J. Geophys. Res.* **1987**, *92*, 9753.
(93) Moulin, C.; Guillard, F.; Dulac, F.; Lambert, C. E. *J. Geophys. Res.* **1997**, *102*, 16947.
(94) Legrand, M.; Plana-Fattori, A.; N'Doume, C. *J. Geophys. Res.* **2001**, *106*, 18251.
(95) Falke, S. R.; Husar, R. B.; Schichtel, B. A. *J. Air Waste Manage. Assoc.* **2001**, *51*, 1579.
(96) Moulin, C.; Gordon, H. R.; Banzon, V. F.; Evans, R. H. *J. Geophys. Res.* **2001**, *106*, 18239.
(97) Viana, M.; Querol, X.; Alastuey, A.; Cuevas, E.; Rodriguez, S. *Atmos. Environ.* **2002**, *36*, 5861.
(98) NASA/Goddard Spaceflight Center, 2003; http://visibleearth.nasa.gov.
(99) Herman, J. R.; Bhartia, P. K.; Torres, O.; Hsu, C.; Seftor, C.; Celarier, E. *J. Geophys. Res.* **1997**, *102*, 16911.
(100) Chiapello, I.; Prospero, J. M.; Herman, J. R.; Hsu, N. C. *J. Geophys. Res.* **1999**, *104*, 9277.
(101) Cakmur, R. V.; Miller, R. L.; Tegen, I. *J. Geophys. Res.* **2001**, *106*, 18287.
(102) Seinfeld, J. H.; Pandis, S. N. *Atmospheric Chemistry and Physics: from Air Pollution to Climate Change*; Wiley: New York, 1998.
(103) Coudé-Gaussen, G. In *Paleoclimatology and Paleometeorology: Modern and Past Patterns of Global Atmospheric Transport*; Leinen, M., Sarnthein, M., Eds.; Kluwer: Dordrecht, The Netherlands, 1989.
(104) Alfaro, S. C.; Gaudichet, A.; Gomes, L.; Maille, M. *Geophys. Res. Lett.* **1998**, *25*, 991.
(105) Chatenet, B.; Marticorena, B.; Gomes, L.; Bergametti, G. *Sedimentology* **1996**, *43*, 901.
(106) Ginoux, P.; Chin, M.; Tegen, I.; Prospero, J. M.; Holben, B.; Dubovik, O.; Lin, S.-J. *J. Geophys. Res.* **2001**, *106*, 20255.
(107) Xuan, J.; Sokolik, I. N. *Atmos. Environ.* **2002**, *36*, 4863.
(108) Liu, S. C.; Trainer, M.; Carroll, M. A.; Hubler, G.; Montzka, D. D.; Norton, R. B.; Ridley, B. A.; Walega, J. G.; Atlas, E. L.; Heikes, B. G.; Huebert, B. J.; Warren, W. *J. Geophys. Res.* **1992**, *97*, 10463.
(109) Chatfield, R. B. *Geophys. Res. Lett.* **1994**, *21*, 2705.
(110) Fan, S.-M.; Jacob, D. J.; Mauzerall, D. L.; Bradshaw, J. D.; Sandholm, S. T.; Blake, D. R.; Singh, H. B.; Talbot, R. W.; Gregory, G. L.; Sachse, G. W. *J. Geophys. Res.* **1994**, *99*, 16867.
(111) Singh, H. B.; Herlth, D.; Kolyer, R.; Salas, L.; Bradshaw, J. D.; Sandholm, S. T.; Davis, D. D.; Crawford, J.; Kondo, Y.; Koike, M.; Talbot, R.; Gregory, G. L.; Sachse, G. W.; Browell, E.; Blake, D. R.; Rowland, F. S.; Newell, R.; Merrill, J.; Heikes, B.; Liu, S. C.; Crutzen, P. J.; Kanakidou, M. *J. Geophys. Res.* **1996**, *101*, 1793.
(112) Levin, Z.; Ganor, E.; Gladstein, V. *J. Appl. Meteorol.* **1996**, *35*, 1511.
(113) Li, X.; Maring, H.; Savoie, D.; Voss, K.; Prospero, J. M. *Nature* **1996**, *380*, 416.
(114) Tegen, I.; Lacis, A. A.; Fung, I. *Nature* **1996**, *380*, 419.
(115) Moulin, C.; Lambert, C. E.; Dulac, F.; Dayan, U. *Nature* **1997**, *387*, 691.
(116) Alpert, P.; Kaufman, Y. J.; Shay-El, Y.; Tanre, D.; da Silva, A.; Schubert, S.; Joseph, J. H. *Nature* **1998**, *395*, 367.
(117) Miller, R. L.; Tegen, I. *J. Climate* **1998**, *11*, 3247.
(118) Arimoto, R.; Balsam, W.; Schloesslin, C. *Atmos. Environ.* **2000**, *36*, 89.
(119) Fouquart, Y. B.; Bonnell, G.; Brogniez, G.; Buriez, J. C.; Smith, L.; Morcrette, J. J.; Cerf, A. *J. Appl. Meteorol.* **1987**, *26*, 38.

(120) Claquin, T.; Schulz, M.; Balkanski, Y.; Boucher, O. *Tellus* **1998**, *50B*, 491.
(121) Sokolik, I. N.; Toon, O. B.; Bergstrom, R. W. *J. Geophys. Res.* **1998**, *103*, 8813.
(122) Quijano, A. L.; Sokolik, I. N.; Toon, O. B. *J. Geophys. Res.* **2000**, *105*, 12207.
(123) Rudich, Y.; Khersonsky, O.; Rosenfeld, D. *Geophys. Res. Lett.* **2002**, *29*, 10.1029/2001GL016055.
(124) Yin, Y.; Wurzler, S.; Levin, Z.; Reisin, T. G. *J. Geophys. Res.* **2002**, *107*, 10.1029/2001JD001544.
(125) DeMott, P. J.; Rogers, D. C.; Kreidenweis, S. M. *J. Geophys. Res.* **1997**, *102*, 19575.
(126) Hung, H.-M.; Malinowski, A.; Martin, S. T. *J. Phys. Chem. A* **2003**, *107*, 1296.
(127) Charlson, R. J.; Schwartz, S. E.; Hales, J. M.; Cess, R. D.; Coakley, J. A.; Hansen, J. E.; Hofmann, D. J. *Science* **1992**, *255*, 423.
(128) Eschenbacher, W. L.; Kullman, G. J.; Gomberg, C. C. In *Patty's Industrial Hygiene*, 5th ed.; Harris, R. L., Ed.; Wiley: New York, 2000; Vol. 1.
(129) Ross, M.; Nolan, R. P.; Langer, A. M.; Cooper, W. C. *Rev. Mineral.* **1993**, *28*, 361.
(130) Richards, R. *Mineral. Mag.* **2003**, *67*, 129.
(131) Wagner, J. C.; McConnochie, K.; Gibbs, A. R.; Pooley, F. D. In *Environmental Interactions of Clays*; Parker, A., Rae, J. E., Eds.; Springer: Berlin, Germany, 1998.
(132) Dogan, M. *Environ. Geol.* **2002**, *41*, 571.
(133) Levin, S.; Herbert, R.; Skloot, G.; Szeinuk, J.; Teirstein, A.; Fischler, D.; Milek, D.; Piligian, G.; Wilk-Rivard, E.; Moline, J. *Am. J. Ind. Med.* **2002**, *42*, 545.
(134) *Fed. Regist.* **1997**, 40 CFR Part 50.
(135) Prospero, J. M.; Nees, R. T.; Uematsu, M. *J. Geophys. Res.* **1987**, *92*, 14.
(136) Muhs, D. R.; Bush, C. A.; Stewart, K. C.; Rowland, T. R.; Crittenden, R. C. *Quat. Res.* **1990**, *33*, 157.
(137) Zhuang, G.; Duce, R. A.; Kester, D. R. *J. Geophys. Res.* **1990**, *95*, 16207.
(138) Zhu, X.; Prospero, J. M.; Savoie, D. L.; Millero, F. J.; Zika, R. G.; Saltzman, E. S. *J. Geophys. Res.* **1993**, *98*, 9039.
(139) Zhu, X. R.; Prospero, J. M.; Millero, F. J. *J. Geophys. Res.* **1997**, *102*, 21297.
(140) Martin, J. H.; Fitzwater, S. E. *Nature* **1988**, *331*, 341.
(141) Walsh, J. J.; Steidinger, K. A. *J. Geophys. Res.* **2001**, *106*, 11597.
(142) Fung, I. Y.; Meyn, S. K.; Tegen, I.; Doney, S. C.; John, J. G.; Bishop, J. K. B. *Global Biogeochem. Cycles* **2000**, *14*, 281.
(143) Zhuang, G.; Yi, Z.; Duce, R. A.; Brown, P. R. *Global Biogeochem. Cycles* **1992**, *6*, 161.
(144) Spokes, L. J.; Jickells, T. D.; Lim, B. *Geochim. Cosmochim. Acta* **1994**, *58*, 3281.
(145) Desboeufs, K. V.; Losno, R.; Vimeux, F.; Cholbi, S. *J. Geophys. Res.* **1999**, *104*, 21287.
(146) Desboeufs, K. V.; Losno, R.; Colin, J. L. *Atmos. Environ.* **2001**, *35*, 3529.
(147) Shinn, E. A.; Smith, G. W.; Prospero, J. M.; Betzer, P.; Hayes, M. L.; Garrison, V.; Barber, R. T. *Geophys. Res. Lett.* **2000**, *27*, 3029.
(148) Dentener, F. J.; Carmichael, G. R.; Zhang, Y.; Lelieveld, J.; Crutzen, P. J. *J. Geophys. Res.* **1996**, *101*, 22869.
(149) Preszler Prince, A.; Wade, J. L.; Grassian, V. H.; Kleiber, P. D.; Young, M. A. *Atmos. Environ.* **2002**, *36*, 5729.
(150) Lovejoy, E. R.; Hanson, D. R. *J. Phys. Chem.* **1995**, *99*, 2080.
(151) Mozurkewich, M.; McMurry, P. H.; Gupta, A.; Calvert, J. G. *J. Geophys. Res.* **1987**, *92*, 4163.
(152) Hanson, D. R.; Burkholder, J. B.; Howard, C. J.; Ravishankara, A. R. *J. Phys. Chem.* **1992**, *96*, 4979.
(153) van Doren, J. M.; Watson, L. R.; Davidovits, P.; Worsnop, D. R.; Zahniser, M. S.; Kolb, C. E. *J. Phys. Chem.* **1990**, *94*, 3265.
(154) Hanson, D. R.; Lovejoy, E. R. *Geophys. Res. Lett.* **1994**, *21*, 2401.
(155) Mozurkewich, M.; Calvert, J. G. *J. Geophys. Res.* **1988**, *93*, 15889.
(156) Worsnop, D. R.; Zahniser, M. S.; Kolb, C. E.; Gardner, J. A.; Watson, L. R.; van Doren, J. M.; Jayne, J. T.; Davidovits, P. *J. Phys. Chem.* **1989**, *93*, 1159.
(157) Sehmel, G. A. *Atmos. Environ.* **1980**, *14*, 983.
(158) Finlayson-Pitts, B. J.; Pitts, J. N. J. *Chem. Ind. (London)* **1993**, *20*, 796.
(159) Wu, P.-M.; Okada, K. *Atmos. Environ.* **1994**, *28*, 2053.
(160) Lee, S.-H.; Murphy, D. M.; Thomson, D. S.; Middlebrook, A. M. *J. Geophys. Res.* **2002**, *107*, 10.1029/2000JD000011.
(161) Zhuang, H.; Chan, C. K.; Fang, M.; Wexler, A. S. *Atmos. Environ.* **1999**, *33*, 4223.
(162) Pakkanen, T. A. *Atmos. Environ.* **1996**, *30*, 2475.
(163) Galy-Lacaux, C.; Carmichael, G. R.; Song, C. H. *J. Geophys. Res.* **2001**, *106*, 12559.
(164) Hanke, M.; Umann, B.; Uecker, J.; Arnold, F.; Bunz, H. *Atmos. Chem. Phys.* **2003**, *3*, 417.
(165) Mamane, Y.; Gottlieb, J. *Atmos. Environ.* **1992**, *26A*, 1763.
(166) Underwood, G. M.; Li, P.; Al-Abadleh, H.; Grassian, V. H. *J. Phys. Chem. A* **2001**, *105*, 6609.
(167) Golden, D. M.; Spokes, G. N.; Benson, S. W. *Angew. Chem.* **1973**, *85*, 602.
(168) Goodman, A. L.; Li, P.; Usher, C. R.; Grassian, V. H. *J. Phys. Chem. A* **2001**, *105*, 6109.
(169) Goodman, A. L.; Underwood, G. M.; Grassian, V. H. *J. Phys. Chem. A* **1999**, *103*, 7217.
(170) Goodman, A. L.; Underwood, G. M.; Grassian, V. H. *J. Geophys. Res.* **2000**, *105*, 29053.
(171) Hanisch, F.; Crowley, J. N. *J. Phys. Chem. A* **2001**, *105*, 3096.
(172) Hanisch, F.; Crowley, J. N. *Phys. Chem. Chem. Phys.* **2001**, *3*, 2474.
(173) Hanisch, F.; Crowley, J. N. *Atmos. Chem. Phys.* **2003**, *3*, 119.
(174) Hanisch, F.; Crowley, J. N. *Phys. Chem. Chem. Phys.* **2003**, *5*, 883.
(175) Li, P.; Perreau, K. A.; Covington, E.; Song, C. H.; Carmichael, G. R.; Grassian, V. H. *J. Geophys. Res.* **2001**, *106*, 5517.
(176) Michel, A. E.; Usher, C. R.; Grassian, V. H. *Geophys. Res. Lett.* **2002**, *29*, 10.1029/2002GL014896.
(177) Michel, A. E.; Usher, C. R.; Grassian, V. H. *Atmos. Environ.* **2003**, *37*, 3201.
(178) Underwood, G. M.; Li, P.; Usher, C. R.; Grassian, V. H. *J. Phys. Chem. A* **2000**, *104*, 819.
(179) Underwood, G. M.; Miller, T. M.; Grassian, V. H. *J. Phys. Chem. A* **1999**, *103*, 6184.
(180) Underwood, G. M.; Song, C. H.; Phadnis, M.; Carmichael, G. R.; Grassian, V. H. *J. Geophys. Res.* **2001**, *106*, 18055.
(181) Usher, C. R.; Al-Hosney, H.; Carlos-Cuellar, S.; Grassian, V. H. *J. Geophys. Res.* **2002**, *107*, 10.1029/2002JD002051.
(182) Usher, C. R.; Michel, A. E.; Stec, D.; Grassian, V. H. *Atmos. Environ.* **2003**, *37*, 5337.
(183) Börensen, C.; Kirchner, U.; Scheer, V.; Vogt, R.; Zellner, R. *J. Phys. Chem. A* **2000**, *104*, 5036.
(184) Goodman, A. L.; Bernard, E. T.; Grassian, V. H. *J. Phys. Chem. A* **2001**, *105*, 6443.
(185) Fenter, F. F.; Caloz, F.; Rossi, M. J. *Atmos. Environ.* **1995**, *29*, 3365.
(186) Krueger, B. J.; Grassian, V. H.; Laskin, A.; Cowin, J. P. *Geophys. Res. Lett.* **2003**, *30*, 10.1029/2002GL016563.
(187) Song, C. H.; Carmichael, G. R. *J. Atmos. Chem.* **2001**, *40*, 1.
(188) Talbot, R. W.; Dibb, J. E.; Loomis, M. B. *Geophys. Res. Lett.* **1998**, *102*, 1367.
(189) (a) Hoffman, R. C.; Gebel, M. E.; Fox, B. S.; Finlayson-Pitts, B. J. *Phys. Chem. Chem. Phys.* **2003**, *5*, 1780. (b) Hoffman, R. C.; Kaleuati, M. A.; Finlayson-Pitts, B. J. *J. Phys. Chem. A* **2003**, *107*, 7818.
(190) John, W.; Wall, S. M.; Ondo, J. L.; Winklmayr, W. *Atmos. Environ.* **1990**, *24A*, 2349.
(191) Dassios, K. G.; Pandis, S. N. *Atmos. Environ.* **1999**, *33*, 2993.
(192) Noble, C. A.; Prather, K. A. *Environ. Sci. Technol.* **1996**, *30*, 2667.
(193) Martin, S. T. *Chem. Rev.* **2000**, *100*, 3403.
(194) Han, J.-H.; Hung, H.-M.; Martin, S. T. *J. Geophys. Res.* **2002**, *107*, 10.1029/2001JD001054.
(195) Judeikis, H. S.; Wren, A. G. *Atmos. Environ.* **1978**, *12*, 2315.
(196) Mamane, Y.; Gottlieb, J. *J. Aerosol Sci.* **1989**, *20*, 303.
(197) Goodman, A. L.; Miller, T. M.; Grassian, V. H. *J. Vac. Sci. Technol.* **1998**, *16*, 2585.
(198) Miller, T. M.; Grassian, V. H. *Geophys. Res. Lett.* **1998**, *25*, 3835.
(199) Alicke, B.; Platt, U.; Stutz, J. *J. Geophys. Res.* **2002**, *107*, 10.1029/2000JD000075.
(200) Calvert, J. G.; Yarwood, G.; Dunker, A. *Res. Chem. Intermed.* **1994**, *20*, 463.
(201) Kaiser, E. W.; Wu, C. H. *J. Phys. Chem.* **1977**, *81*, 1701.
(202) Sakamaki, F.; Hatakeyama, S.; Akimoto, H. *Int. J. Chem. Kinet.* **1983**, *15*, 1013.
(203) Pitts, J. N. J.; Sanhueza, E.; Atkinson, R.; Carter, W. P. L.; Winer, A. M.; Harris, G. W.; Plum, C. N. *Int. J. Chem. Kinet.* **1984**, *16*, 919.
(204) Svensson, R.; Ljungström, E.; Lindqvist, O. *Atmos. Environ.* **1987**, *21*, 1529.
(205) Jenkin, M. E.; Cox, R. A.; Williams, D. J. *Atmos. Environ.* **1988**, *22*, 487.
(206) Lammel, G.; Cape, J. N. *Chem. Soc. Rev.* **1996**, *25*, 361.
(207) Junkermann, W.; Ibusuki, T. *Atmos. Environ.* **1992**, *26A*, 3099.
(208) Notholt, J.; Hjorth, J.; Raes, F. *Atmos. Environ.* **1992**, *26A*, 211.
(209) Becker, K.-H.; Kleffmann, J.; Kurtenbach, R.; Wiesen, P. *J. Phys. Chem.* **1996**, *100*, 14984.
(210) Harrison, R. M.; Peak, J. D.; Collins, G. M. *J. Geophys. Res.* **1996**, *101*, 14429.
(211) Kleffmann, J.; Becker, K.-H.; Wiesen, P. *Atmos. Environ.* **1998**, *32*, 2721.
(212) Finlayson-Pitts, B. J.; Pitts, J. N. J. *Atmospheric Chemistry: Fundamentals and Experimental Techniques*; Wiley: New York, 1986.
(213) Febo, A.; Perrino, C. *Atmos. Environ.* **1991**, *25A*, 1055.
(214) Reisinger, A. R. *Atmos. Environ.* **2000**, *34*, 3865.
(215) Shuhui, W.; Ackermann, R.; Spicer, C. W.; Fast, J. D.; Schmeling, M.; Stutz, J. *Geophys. Res. Lett.* **2003**, *30*, 10.1029/2003GL017014.
(216) Finlayson-Pitts, B. J.; Wingen, L. M.; Sumner, A. L.; Syomin, D.; Ramazan, K. A. *Phys. Chem. Chem. Phys.* **2003**, *5*, 223.

(217) Lammel, G. *Formation of Nitrous Acid: Parametrization and Comparison with Observations*; Max-Planck-Institut für Meteorologie: 1999.
(218) Mochida, M.; Finlayson-Pitts, B. J. *J. Phys. Chem. A* **2000**, *104*, 9705.
(219) Saliba, N. A.; Mochida, M.; Finlayson-Pitts, B. J. *Geophys. Res. Lett.* **2000**, *27*, 329.
(220) Saliba, N. A.; Yang, H.; Finlayson-Pitts, B. J. *J. Phys. Chem. A* **2001**, *105*, 10339.
(221) Rivera-Figueroa, A. M.; Sumner, A. L.; Finlayson-Pitts, B. J. *Environ. Sci. Technol.* **2003**, *37*, 548.
(222) Luria, M.; Sievering, H. *Atmos. Environ.* **1991**, *25A*, 1489.
(223) Kerminen, V.-M.; Pirjola, L.; Boy, M.; Eskola, A.; Teinilä, K.; Laakso, L.; Asmi, A.; Heinola, J.; Lauri, A.; Vainio, V.; Lehtinen, K.; Kulmala, M. *Atmos. Res.* **2000**, *54*, 41.
(224) Dlugi, R. *J. Aerosol Sci.* **1983**, *14*, 292.
(225) Saxena, P.; Seigneur, C. *Atmos. Environ.* **1987**, *21*, 807.
(226) Jayne, J. T.; Davidovits, P.; Worsnop, D. R.; Zahniser, M. S.; Kolb, C. E. *J. Phys. Chem.* **1990**, *94*, 6041.
(227) Martin, L. R.; Good, T. W. *Atmos. Environ.* **1991**, *25A*, 2395.
(228) Sievering, H.; Boatman, J.; Galloway, J.; Keene, W.; Kim, Y.; Luria, M.; Ray, J. *Atmos. Environ.* **1991**, *25A*, 1479.
(229) Sievering, H.; Boatman, J.; Gorman, E.; Kim, Y.; Anderson, L.; Ennis, G.; Luria, M.; Pandis, S. N. *Nature* **1992**, *360*, 571.
(230) Chameides, W. L.; Stelson, A. W. *J. Geophys. Res.* **1992**, *97*, 20565.
(231) Sievering, H.; Gorman, E.; Pszenny, A.; Springer-Young, M.; Boatman, J.; Kim, Y.; Nagamoto, C.; Wellman, D. *J. Geophys. Res.* **1995**, *100*, 23075.
(232) Suhre, K.; Andreae, M. O.; Rosset, R. *J. Geophys. Res.* **1995**, *91*, 11323.
(233) Keene, W. C.; Sander, R.; Pszenny, A. A. P. *J. Aerosol Sci.* **1998**, *29*, 339.
(234) Capaldo, K.; Corbett, J. J.; Kasibhatla, P.; Fischbeck, P.; Pandis, S. N. *Nature* **1999**, *400*, 743.
(235) Krischke, U.; Staubes, R.; Brauers, T.; Gautrois, M.; Burkert, J.; Stobener, D.; Jaeschke, W. *J. Geophys. Res.* **2000**, *105*, 14412.
(236) Maahs, H. G. *J. Geophys. Res.* **1983**, *88*, 10721.
(237) Maahs, H. G. *Atmos. Environ.* **1983**, *17*, 341.
(238) Faust, B. C.; Hoffman, M. R.; Bahnemann, D. W. *J. Phys. Chem.* **1989**, *93*, 6371.
(239) Siefert, R. L.; Webb, S. M.; Hoffman, M. R. *J. Geophys. Res.* **1996**, *101*, 14441.
(240) Hegg, D. A.; Majeed, R.; Yuen, P. F.; Baker, M. B.; Larson, T. V. *Geophys. Res. Lett.* **1996**, *23*, 2613.
(241) Lelieveld, J.; Heintzenberg, J. *Science* **1992**, *258*, 117.
(242) Chuang, C. C.; Penner, J. E.; Taylor, K. E.; Grossman, A. S.; Walton, J. J. *J. Geophys. Res.* **1997**, *102*, 3761.
(243) Judeikis, H. S.; Stewart, T. B.; Wren, A. G. *Atmos. Environ.* **1978**, *12*, 1633.
(244) Chun, K. C.; Quon, J. E. *Environ. Sci. Technol.* **1973**, *7*, 532.
(245) Deo, A. V.; Dalla Lana, I. G.; Habgood, H. W. *J. Catal.* **1971**, *21*, 270.
(246) Low, M. J. D.; Goodsel, A. J.; Takezawa, N. *Environ. Sci. Technol.* **1971**, *5*, 1191.
(247) Schoonheydt, R. A.; Lunsford, J. H. *J. Catal.* **1972**, *26*, 261.
(248) Goodsel, A. J.; Low, M. J. D.; Takezawa, N. *Environ. Sci. Technol.* **1972**, *6*, 268.
(249) Davis, S. M.; Lunsford, J. H. *J. Colloid Interface Sci.* **1978**, *65*, 352.
(250) Chang, C. C. *J. Catal.* **1978**, *53*, 374.
(251) Harrison, W. D.; Gill, J. B.; Goodall, D. C. *Polyhedron Lett.* **1983**, *23*, 153.
(252) Karge, H. G.; Dalla Lana, I. G. *J. Phys. Chem.* **1984**, *88*, 1538.
(253) Datta, A.; Cavell, R. G.; Tower, R. W.; George, Z. M. *J. Phys. Chem.* **1985**, *89*, 443.
(254) Saur, O.; Bensitel, M.; Mohammed Saad, A. B.; Lavalley, J. C.; Tripp, C. P.; Morrow, B. A. *J. Catal.* **1986**, *99*, 104.
(255) Mitchell, M. B.; Sheinkar, V. N.; White, M. G. *J. Phys. Chem.* **1996**, *100*, 7550.
(256) Allen, D.; Hayhurst, A. N. *J. Chem. Soc., Faraday Trans.* **1996**, *92*, 1227.
(257) Waqif, M.; Mohammed Saad, A. B.; Bensitel, M.; Bachelier, J.; Saur, O.; Lavalley, J. C. *J. Chem. Soc., Faraday Trans.* **1992**, *88*, 2931.
(258) Junge, C. E.; Ryan, T. G. *Q. J. R. Meteor. Soc.* **1958**, *84*, 46.
(259) van den Heuvel, A. R.; Mason, B. J. *Q. J. R. Meteorol. Soc.* **1963**, *89*, 271.
(260) Scott, W. D.; Hobbs, P. V. *J. Atmos. Sci.* **1967**, *24*, 54.
(261) Foster, P. M. *Atmos. Environ.* **1969**, *3*, 157.
(262) McKay, H. A. C. *Atmos. Environ.* **1971**, *5*, 7.
(263) Urone, P.; Lutsep, H.; Noyes, C. M.; Parcher, J. F. *Environ. Sci. Technol.* **1968**, *2*, 611.
(264) Smith, B. M.; Wagman, J.; Fish, B. R. *Environ. Sci. Technol.* **1969**, *6*, 552.
(265) Ullerstam, M.; Vogt, R.; Langer, S.; Ljungström, E. *Phys. Chem. Chem. Phys.* **2002**, *4*, 4694.
(266) Andreae, M. O.; Charlson, R. J.; Bruynseels, F.; Storms, H.; van Grieken, R.; Maenhaut, W. *Science* **1986**, *232*, 1620.
(267) Zhang, D.; Shi, G.-Y.; Iwasaka, Y.; Hu, M. *Atmos. Environ.* **2000**, *34*, 2669.
(268) Xu, L.; Okada, K.; Iwasaka, Y.; Hara, K.; Okuhara, Y.; Tsutsumi, Y.; Shi, G. *Atmos. Environ.* **2001**, *35*, 3145.
(269) Han, J.-H.; Martin, S. T. *J. Geophys. Res.* **1999**, *104*, 3543.
(270) Martin, S. T.; Schlenker, J.; Chelf, J. H.; Duckworth, O. W. *Environ. Sci. Technol.* **2001**, *35*, 1624.
(271) Martin, S. T.; Han, J.-H.; Hung, H.-M. *Geophys. Res. Lett.* **2001**, *28*, 2601.
(272) Martin, S. T.; Hung, H.-M.; Han, J.-H. Presented at the 6th International Aerosol Conference, Taipei, Taiwan, 2002.
(273) Onasch, T. B.; McGraw, R.; Imre, D. *J. Phys. Chem. A* **2000**, *104*, 10797.
(274) Turcsanyi, E.; Cardoso-Vilhena, J.; Daymond, J.; Gillespie, C.; Balaguer, L.; Ollerenshaw, J.; Barnes, J. In *Trace Gas Emissions and Plants*; Singh, S. N., Ed.; Kluwer: Dordrecht, The Netherlands, 2000.
(275) Mauzerall, D. L.; Wang, X. *Annu. Rev. Energy Environ.* **2001**, *26*, 237.
(276) Fuhrer, J. *Ozone-Sci. Eng.* **2002**, *24*, 69.
(277) Horvath, S. M.; McKee, D. J. In *Tropospheric Ozone*; McKee, D. J., Ed.; Lewis: Boca Raton, FL, 1994.
(278) Graham, J. A.; Overton, J.; Costa, D. L. *Stud. Environ. Sci.* **1998**, *72*, 465.
(279) Taylor, G. E., Jr. *Hum. Ecol. Risk Assess.* **2001**, *7*, 1183.
(280) Hauglustaine, D. A.; Brasseur, G. P. *J. Geophys. Res.* **2001**, *106*, 32337.
(281) Prather, M.; Gauss, M.; Berntsen, T.; Isaksen, I.; Sundet, J.; Bey, I.; Brasseur, G.; Dentener, F.; Derwent, R.; Stevenson, D.; Grenfell, L.; Hauglustaine, D.; Horowitz, L.; Jacob, D.; Mickley, L.; Lawrence, M.; von Kuhlmann, R.; Muller, J.-F.; Pitari, G.; Rogers, H.; Johnson, M.; Pyle, J.; Law, K.; van Weele, M.; Wild, O. *Geophys. Res. Lett.* **2003**, *30*, 10.1029/2002GL016285.
(282) Dhandapani, B.; Oyama, S. T. *Appl. Catal. B: Environ.* **1997**, *11*, 129.
(283) Oyama, S. T. *Catal. Rev.−Sci. Eng.* **2000**, *42*, 279.
(284) Zhang, Y.; Sunwoo, Y.; Kotamarthi, V.; Carmichael, G. R. *J. Appl. Meteorol.* **1994**, *33*.
(285) Prospero, J. M.; Schmitt, R.; Cuevas, E.; Savoie, D. L.; Graustein, W. C.; Turekian, K. K.; Volz-Thomas, A.; Diaz, A.; Oltmans, S. J.; Levy, H., II. *Geophys. Res. Lett.* **1995**, *22*, 2925.
(286) de Reus, M.; Dentener, F.; Thomas, A.; Borrmann, S.; Ström, J.; Lelieveld, J. *J. Geophys. Res.* **2000**, *105*, 15263.
(287) Zhang, Y.; Carmichael, G. R. *J. Appl. Meteorol.* **1999**, *38*, 353.
(288) Suzuki, S.; Hori, Y.; Osamu, K. *Bull. Chem. Soc. Jpn.* **1979**, *52*, 3103.
(289) Klimovskii, A. O.; Bavin, A. V.; Tkalich, V. S.; Lisachenko, A. A. *React. Kinet. Catal. Lett.* **1983**, *23*, 95.
(290) Golodets, G. I. *Heterogeneous Catalytic Reactions Involving Molecular Oxygen*; Elsevier: New York, 1983.
(291) Alebic-Juretic, A.; Cvitas, T.; Klasinc, L. *Ber. Bunsen-Ges. Phys. Chem.* **1992**, *96*, 493.
(292) Alebic-Juretic, A.; Cvitas, T.; Klasinc, L. *Environ. Monit. Assess.* **1997**, *44*, 241.
(293) Alebic-Juretic, A.; Cvitas, T.; Klasinc, L. *Chemosphere* **2000**, *41*, 667.
(294) Smith, D. M.; Chughtai, A. R. *J. Atmos. Chem.* **1997**, *26*, 77.
(295) Grøntoft, T. *Atmos. Environ.* **2002**, *36*, 5661.
(296) Hanning-Lee, M. A.; Brady, B. B.; Martin, L. R.; Syage, J. A. *Geophys. Res. Lett.* **1996**, *23*, 1961.
(297) Radhakrishnan, R.; Oyama, S. T. *J. Catal.* **2001**, *199*, 282.
(298) Li, W.; Oyama, S. T. *J. Am. Chem. Soc.* **1998**, *120*, 9047.
(299) Heisig, C.; Zhang, W.; Oyama, S. T. *Appl. Catal. B: Environ.* **1997**, *14*, 117.
(300) Bulanin, K. M.; Alexeev, A. V.; Bystrov, D. S.; Lavalley, J. C.; Tsyganenko, A. A. *J. Phys. Chem.* **1994**, *98*, 5100.
(301) Bulanin, K. M.; Lavalley, J. C.; Tsyganenko, A. A. *J. Phys. Chem.* **1995**, *99*, 10294.
(302) Bulanin, K. M.; Lavalley, J. C.; Tsyganenko, A. A. *Colloids Surf. A* **1995**, *101*, 153.
(303) Bulanin, K. M.; Lavalley, J. C.; Tsyganenko, A. A. *J. Phys. Chem. B* **1997**, *101*, 2917.
(304) Thomas, K.; Hoggan, P. E.; Mariey, L.; Lamotte, J.; Lavalley, J. C. *Catal. Lett.* **1997**, *46*, 77.
(305) Berlier, G.; Yamamoto, T.; Spoto, G.; Lamberti, C.; Gribov, E.; Zecchina, A. *Phys. Chem. Chem. Phys.* **2002**, *4*, 3872.
(306) Murphy, D. M.; Thomson, D. S.; Mahoney, M. J. *Science* **1998**, *282*, 1664.
(307) Thomas, E. R.; Frost, G. J.; Rudich, Y. *J. Geophys. Res.* **2001**, *106*, 3045.
(308) Moise, T.; Rudich, Y. *J. Phys. Chem. A* **2002**, *106*, 6469.
(309) Barger, W. R.; Garrett, W. D. *J. Geophys. Res.* **1970**, *75*, 4561.
(310) Bezdek, H. F.; Carlucci, A. F. *Limnol. Oceanogr.* **1974**, *19*, 126.
(311) Marty, J. C.; Saliot, A.; Buat-Menard, P.; Chesselet, R.; Hunter, K. A. *J. Geophys. Res.* **1979**, *84*, 5707.
(312) Ellison, G. B.; Tuck, A. F.; Vaida, V. *J. Geophys. Res.* **1999**, *104*, 11633.
(313) Dobson, C. M.; Ellison, G. B.; Tuck, A. F.; Vaida, V. *Proc. Natl. Acad. Sci. U.S.A.* **2000**, *97*, 11864.

(314) Ketseridis, G.; Hahn, J.; Jaenicke, R.; Junge, C. *Atmos. Environ.* **1976**, *10*, 603.
(315) Graedel, T. E.; Hawkins, D. T.; Claxton, L. D. *Atmospheric Chemical Compounds: Sources, Occurrences, and Bioassay*; Academic Press: Orlando, FL, 1986.
(316) Simoneit, B. R. T.; Mazurek, M. A. *Atmos. Environ.* **1982**, *16*, 2139.
(317) Simoneit, B. R. T. *J. Atmos. Chem.* **1989**, *8*, 251.
(318) Standley, L. J.; Simoneit, B. R. T. *Atmos. Environ.* **1990**, *24B*, 67.
(319) Rogge, W. F.; Hildemann, L. M.; Mazurek, M. A.; Cass, G. R.; Simoneit, B. R. T. *Environ. Sci. Technol.* **1991**, *25*, 1112.
(320) Rogge, W. F.; Hildemann, L. M.; Mazurek, M. A.; Cass, G. R.; Simoneit, B. R. T. *Environ. Sci. Technol.* **1993**, *27*, 2700.
(321) Fraser, M. P.; Cass, G. R.; Simoneit, B. R. T. *Atmos. Environ.* **1999**, *33*, 2715.
(322) Schauer, J. J.; Kleeman, M. J.; Cass, G. R.; Simoneit, B. R. T. *Environ. Sci. Technol.* **1999**, *33*, 1578.
(323) Morris, J. W.; Davidovits, P.; Jayne, J. T.; Jiminez, J. L.; Shi, Q.; Kolb, C. E.; Worsnop, D. R.; Barney, W. S.; Cass, G. *Geophys. Res. Lett.* **2002**, *29*, 10.1029/2002GL014692.
(324) Smith, G. D.; Woods, E. I.; DeForest, C. L.; Baer, T.; Miller, R. E. *J. Phys. Chem. A* **2002**, *106*, 8085.
(325) Moise, T.; Rudich, Y. *J. Geophys. Res.* **2000**, *105*, 14667.
(326) Hobert, H. *Vib. Spectrosc.* **1995**, *9*, 169.
(327) Russell, L. M.; Maria, S. F.; Myneni, S. C. B. *Geophys. Res. Lett.* **2002**, *29*, 10.1029/2002GL014874.
(328) Murphy, D. M.; Thomson, D. S.; Middlebrook, A. M.; Schein, M. E. *J. Geophys. Res.* **1998**, *103*, 16485.
(329) Pósfai, M.; Xu, H.; Anderson, J. R.; Buseck, P. R. *Geophys. Res. Lett.* **1998**, *25*, 1907.
(330) Zappoli, S.; Andracchio, A.; Fuzzi, S.; Facchini, M. C.; Gelencser, A.; Kiss, G.; Kirvacsy, Z.; Molnar, A.; Meszaros, E.; Hansson, H.-C.; Rosman, K.; Zebuhr, Y. *Atmos. Environ.* **1999**, *33*, 2733.
(331) Falkovich, A. H.; Rudich, Y. *Environ. Sci. Technol.* **2001**, *35*, 2326.
(332) Goss, K.-U.; Schwarzenbach, R. P. *Environ. Sci. Technol.* **1999**, *33*, 4073.
(333) Grosjean, E.; Grosjean, D.; Frazer, M.; Cass, G. *Environ. Sci. Technol.* **1996**, *30*, 2687.
(334) Tanner, R. L.; Zielinska, B.; Uberna, E.; Harshfield, G.; McNichol, A. P. *J. Geophys. Res.* **1996**, *101*, 28961.
(335) Ayers, G.; Gillett, R.; Granek, H.; de Serves, C.; Cox, R. A. *Geophys. Res. Lett.* **1997**, *24*, 401.
(336) Lee, Y. N.; Zhou, X.; Kleinman, L. I.; Nunnermacker, L. J.; Springston, S. R.; Daum, P. H.; Newman, L.; Keigley, W. G.; Holdren, M. W.; Spicer, C. W.; Young, V.; Fu, B.; Parrish, D. D.; Holloway, J.; Williams, J.; Roberts, J. M.; Ryerson, T. B.; Fehsenfeld, F. C. *J. Geophys. Res.* **1998**, *103*, 22449.
(337) Singh, H. B.; Ohara, D.; Herlth, D.; Sachse, G. W.; Blake, D. R.; Bradshaw, J. D.; Kanakidou, M.; Crutzen, P. J. *J. Geophys. Res.* **1994**, *99*, 1805.
(338) Singh, H. B.; Chen, Y.; Gregory, G. L.; Sachse, G. W.; Talbot, R.; Blake, D. R.; Kondo, Y.; Bradshaw, J. D.; Heikes, B.; Thornton, D. *Geophys. Res. Lett.* **1997**, *24*, 127.
(339) Arnold, F.; Burger, V.; Droste-Fanke, B.; Grimm, F.; Krieger, A.; Schneider, J.; Stilp, T. *Geophys. Res. Lett.* **1997**, *24*, 3017.
(340) Duncan, J. L.; Schindler, L. R.; Roberts, J. T. *J. Phys. Chem. B* **1999**, *103*, 7247.
(341) Iraci, L. T.; Tolbert, M. A. *J. Geophys. Res.* **1997**, *102*, 16099.
(342) Jayne, J. T.; Worsnop, D. R.; Kolb, C. E.; Swartz, E.; Davidovits, P. *J. Phys. Chem.* **1996**, *100*, 8015.
(343) Kane, S.; Timonen, R.; Leu, M. *J. Phys. Chem. B* **1999**, *103*, 9259.
(344) Duane, S. X.; Jayne, J. T.; Davidovits, P.; Worsnop, D. R.; Zahniser, M. S.; Kolb, C. E. *J. Phys. Chem.* **1993**, *97*, 2284.
(345) Klassen, J. K.; Lynton, J.; Golden, D. M.; Williams, L. R. *J. Geophys. Res.* **1999**, *104*, 26355.
(346) Jang, M.; Czoschke, N. M.; Lee, S.; Kamens, R. M. *Science* **2002**, *298*, 814.
(347) Hair, M. L. *Infrared Spectroscopy in Surface Chemistry*; Dekker: New York, 1967.
(348) Little, L. H. *Infrared Spectra of Adsorbed Species*; Academic: San Diego, CA, 1966.
(349) Pimentel, G. C.; McClellan, A. L. *The Hydrogen Bond*; W. H. Freeman: New York, 1960.
(350) Carlos-Cuellar, S.; Li, P.; Christensen, A. P.; Krueger, B. J.; Burrichter, C.; Grassian, V. H. *J. Phys. Chem. A* **2003**, *107*, 4250.
(351) Singh, H. B.; Chen, Y.; Tabazadeh, A.; Fukui, Y.; Bey, I.; Yantosca, R.; Jacob, D.; Arnold, F.; Wohlfrom, K.; Atlas, E. L.; Flocke, F.; Blake, D. R.; Blake, N.; Heikes, B.; Snow, J.; Talbot, R.; Gregory, G. L.; Sachse, G. W.; Vay, S.; Kondo, Y. *J. Geophys. Res.* **2000**, *105*, 3795.
(352) Holzinger, R.; Warneke, C.; Hansel, A.; Jordan, A.; Lindinger, W.; Scharffe, D. H.; Schade, G.; Crutzen, P. J. *Geophys. Res. Lett.* **1999**, *26*, 1161.
(353) Khare, P.; Kumar, K.; Kumari, K. M.; Srivastava, S. S. *Rev. Geophys.* **1999**, *37*, 227.
(354) Chebbi, A.; Carlier, P. *Atmos. Environ.* **1996**, *30*, 4233.
(355) Goss, K.-U. *Environ. Sci. Technol.* **1993**, *27*, 2127.
(356) Goss, K.-U. *Environ. Sci. Technol.* **1994**, *28*, 640.
(357) Goss, K.-U.; Eisenreich, S. J. *Environ. Sci. Technol.* **1996**, *30*, 2135.
(358) Goss, K.-U. *Environ. Sci. Technol.* **1997**, *31*, 3600.
(359) Jang, M.; Kamens, R. M. *Environ. Sci. Technol.* **1999**, *33*, 1825.
(360) Song, C. H.; Phadnis, M.; Carmichael, G. R.; Underwood, G. M.; Miller, T. M.; Balster, E. T.; Grassian, V. H. In *Air Pollution*; WIT Press: Boston, MA, 1999; Vol. VII.
(361) Liao, H.; Adams, P. J.; Chung, S. H.; Seinfeld, J. H.; Mickley, L. J.; Jacob, D. J. *J. Geophys. Res.* **2003**, *108*, 10.1029/2001JD001260.
(362) Bian, H.; Zender, C. S. *J. Geophys. Res.* **2003**, in press.
(363) Martin, R. V.; Jacob, D. J.; Yantosca, R. M.; Chin, M.; Ginoux, P. *J. Geophys. Res.* **2003**, *108*, 10.1029/2002JD002622.
(364) Tabazadeh, A.; Turco, R. P. *J. Geophys. Res.* **1993**, *98*, 12727.
(365) Ammann, M.; Pöschl, U.; Rudich, Y. *Phys. Chem. Chem. Phys.* **2003**, *5*, 351.
(366) Mozurkewich, M. *Geophys. Res. Lett.* **1993**, *20*, 355.
(367) Al-Abadleh, H. A.; Grassian, V. H. *Chem. Commun.* **2003**, 2796.
(368) Li, P.; Al-Abadleh, H. A.; Grassian, V. H. *J. Phys. Chem. A* **2002**, *106*, 1210.
(369) Guazzotti, S. A.; Sodeman, D. A.; Prather, K. A. *J. Geophys. Res.* **2003**, submitted for publication.

CR020657Y